NASA CR-66487

FINAL REPORT

A STOP-START STUDY OF SOLID PROPELLANTS

P. L. Micheli

Prepared under Contract NAS 1-6600 by
Aerojet-General Corporation
Propellant Research and Development Division
Sacramento, California

For

NATIONAL AERONAUTICS AND SPACE ADMINISTRATION

TABLE OF CONTENTS

LIST OF FIGURES

LIST OF FIGURES (cont.)

LIST OF FIGURES (cont.)

ABSTRACT

The role of thermal properties and chemical kinetics of the solid phase in the combustion process of propellants was determined both analytically and experimentally. New techniques were developed to measure these properties under conditions of steady-state and transient deflagration. Contributions of solid phase reactions and radiation, which in the past have been considered to be negligible, have been shown to be of particular importance in determining the extinguishability of solid propellants as well as the steady-state burning process.

SUMMARY

Temperature profiles and surface temperature measurements were taken during steady-state and transient burning of solid propellants. The rate of chemical reaction in the solid was measured from these profiles and found to correlate with DTA patterns of the propellant. The surface temperature as measured by infra-red emission and thermocouple corroborated each other. Radiation penetration was measured by observing through the regressing grain using infra-red, and verified by thermocouple measurements.

The increased ignitability of the propellant after extinguishment was determined to be due to an increased reactivity by the solid phase, probably from ClO_3^- contaminants.

A transient burning rate model was developed which at least qualitatively describes the effect of depressurization. Measurements of the temperature profile during rapid depressurization were made and provide valuable insight into the response mechanism of the solid phase.

I. INTRODUCTION

A. PURPOSE OF REPORT

The purpose of the work covered in this report is to determine the extent to which the solid phase contributes to the combustion mechanism of ammonium perchlorate propellants during steady-state and transient pressure conditions. The role of the solid phase is often spoken of as being purely thermal, however the work presented clearly shows that chemical reactions do occur and contribute significantly to the overall deflagration process. In addition, the propellants tested have been found to be highly transmissive to radiation and hence the thermal role is more complex than is generally considered.

B. METHOD OF APPROACH

In Section II, analyses have been performed to develop a model of the combustion process during steady-state and transient burning. The model has been programmed to include the effect of chemical reactions, from which the temperature profile can be determined and compared to experimental data. The transient model which has been developed reveals that the response of the profile during depressurization can lead to an oscillatory surface regression and this has been verified by experimental data. In addition, the role of radiation and erosive burning on the combustion process are considered.

Section III is concerned with the experimental portion of the program. New techniques have been developed to measure the thermo-chemical contribution of the solid phase. The role of chemical reactions before and after extinguishment is considered in terms of laboratory techniques such

I,B, Method of Approach (cont.)

as DTA (Differential Thermal Analysis), DSC (Differential Scanning Calorimeter), and TGA (Thermogravimetric Analysis). A new and extremely precise method of measuring thermal diffusivity is derived. Thermocouple measurements of the temperature profile during steady-state and depressurization were made, with concurrent film coverage of some of these tests. The role of the solid phase during ignition was investigated using thermocouples and infra-red emission simultaneously. Finally, infra-red emission was used to determine the role of the surface temperature during steady-state and transient burning as well as to determine the radiative penetration during combustion.

The results of the theoretical and experimental findings are used to determine criteria which would allow an evaluation of the extinguishability characteristics of propellants. Several of the most extinguishable propellants are evaluated in light of these criteria in Reference (24).

C. CONCLUSIONS

In order to match the actual temperature profiles with the model it was found necessary to incorporate both solid phase chemical reactions and radiative heating. The transient model predicts that a complete interruption of the burning rate is unlikely to occur but rather that the solid phase will respond in a pulse-like regression when subjected to extremely high rates of depressurization.

Thermocouple and infra-red emission measurements of the temperature profile show corroborating results. The response of the surface temperature during depressurization was found to be extremely slow. The temperature

I,C, Conclusions (cont.)

profiles at low pressure revealed an inherently different mode of combustion than at higher pressures, indicating a mechanism shift from a semi-stable to stable burning as pressure increased. Radiation penetration measurements showed that the AP propellants transmitted at infra-red wavelengths and that small amounts of aluminum considerably reduced the penetration. Ignition of the AP propellants using an arc illuminator source demonstrated that the solid phase reactions predominate in the ignition process at ambient pressures. Work still remains to define the role of chemical reactions in the region of the lower pressure ignition regime.

II. DEVELOPMENT OF BURNING RATE MODEL

A. INTRODUCTION

One of the chief objectives of this program is to develop a model of the combustion process of a solid propellant which can be used to determine those characteristics which will improve the extinguishability of the propellant. The method of approach is to define those physico-chemical parameters which are of critical importance in determining the steady-state burning rate. With these parameters established, the steady-state model is then simplified by allowing the chemical reactions to vary with temperature in a mathematically tractable fashion.

The role of radiative penetration is next considered. It is shown that measured radiation penetration is relatively greater at low pressures and leads to adverse extinguishability conditions.

B. STEADY-STATE MODEL

The effect of solid phase reactions is generally neglected in describing a burning rate model. This assumption is likely to be true at high pressures because the surface temperature is sufficiently high that the solid phase can supply all the reactants required in a form suitable for combustion in the gas phase. However, at low pressures, the solid phase should control since the gas phase reactions can exist only to the extent that reactant species produced by the solid decomposition are made available. It is interesting to note that the Russian literature (e.g. Fur) assume solid phase decomposition to be rate determining.

Let us first examine the chemical kinetics of AP deflagration. The effect of pressure on ammonium perchlorate and propellant decomposition has been recently determined by Wenograd[20] and Schmidt[15]. These data lead to the result that solid phase reactions are significant and possibly controlling to pressures around 500 psia. Schmidt[15] concludes that with catalyzed AP propellants, the pressure range is extended. The low temperature decomposition of AP (even catalyzed) does not accelerate the burning rate over the higher pressure range of 300-3000 psia. Deflagration results only when AP is in the cubic state, and the decomposition in the high temperature decomposition mode involves $HClO_4$. In an AP propellant the high temperature decomposition is competitive with sublimation, their relative contributions depending on pressure, heat flux and catalyst, the sublimation contribution decreasing with increases in pressure and addition of catalyst.

II,B, Steady-State Model (cont.)

At low pressures and moderate heat fluxes, perchloric acid is involved in the decomposition. Without catalysts, the decomposition rate is controlled by sublimation; with catalyzed systems, heterogeneous decomposition of the acid occurs at the surface. In that case the fuel can interact at points of contact of the decomposing AP. These effects would similarly be found at higher heat flux levels.

The role of the AP decomposition can be further considered by examination of DTA[15] and DSC[19] patterns. Here one finds that not until subatmospheric conditions of less than 400 mm Hg does the heat of decomposition of AP markedly decrease, becoming eventually endothermic as pressure is decreased implying a change in products of reactions. When AP is endothermic (<5 psia), the lower limit of ignition should be reached. The rate of heat liberation by AP appears to follow an Arrhenius expression[19] with an activation energy of 62.5 kcal/mole. At low pressures, Powling[12] has shown that the burning rate of propellants using AP has an activation energy of just hslf this value. As Wenograd[20] has shown, this implies that the solid phase completely dominates the burning rate. Of interest is that the laboratory techniques of DTA and DSC show a change in the pattern of heat evolution with particle size, the smaller particles resulting in greater exothermicity at lower temperatures. As pressure in increased, these patterns show an accompanying decrease in the deflagration temperature until a lower limit is reached. At this point the deflagration exotherm more closely resembles an Arrhenius type reaction rate dependency on temperature.

II,B, Steady-State Model (cont.)

Prior to this, i.e. at lower pressures, the exothermicity is clearly not Arrhenius, but appears to be composed of several competing reactions. The thermocouple data to be presented tend to substantiate thse results. The solid phase decomposition rate therefore appears to be dependent on the extent of reaction, which implies an order of reactions in the solid phase.

During the course of this program, DTA patterns were used in an attempt to correlate the observed exothermic pattern with the model. Using the DTA, the heat of reaction of the solid phase decomposition, ΔH, can be obtained only if the reactions goes to completion in the solid phase, however, for the final exotherm leading to deflagration, the process is completed in the gas phase, and estimates of ΔH were generally too low when compared to literature values. Secondly, estimates of an activation energy from the DTA resulted in data scatter from which it was not possible to obtain meaningful quantitative results. The DTA therefore appears useful as a qualitative instrument only.

It is frequently argued that if solid phase reactions existed, gas evolution from below the surface should be observed. This is not necessary, however. Using TGA traces, it has been shown that the weight loss prior to deflagration decreases substantially with an increase in heating rate. Extrapolation of these data to propellant combustion conditions indicates that no appreciable gasification from the solid phase reactions need occur. Since the weight loss rate should be proportional to the extent of overall reaction, ξ, it is easily shown that when the reaction rate is solely temperature dependent, $\xi \sim f(T)$,

II,B, Steady-State Model (cont.)

$$\xi\phi = \int f(T)dT, \text{ a function only of temperature}$$

where ϕ is the heating rate. Using data for AP decomposition as shown in Figure 1, the rate of overall reaction, $\dot{\xi}$, is plotted in Figure 2 from which one sees that apparently two separate mechanisms are involved, a low temperature decomposition involving some 30% weight loss up to $\sim$ 400°C and a high temperature decomposition with activation energies of about 10 and 37 kcal/mole °K, respectively.

The equations* for the steady-state burning rate model are derived in Appendix I; we shall simply discuss the computer results here. In the solid phase, the dominant mode of heat transfer has been assumed to be conductive. Experimental data indicate the heat transfer to be radiative also and so the role of radiation is discussed separately in Section III.B.3. For the solid phase assuming that the heat of reaction is generated at a rate dependent on the extent, ξ, and a function of temperature, f(T), the burning rate, r, then depends primarily on the surface temperature, T_s.

$$r^2 = \frac{\alpha Z'(1-\xi_s)^n \int_{T_o}^{T_s} f(T)\, dT}{\xi_s \{.95\, T_s - T_o - \frac{Q\xi_s}{2C_s}\}} \qquad (1)$$

Note the inverse relationship between the burning rate and the extent of the reaction. For an Arrhenius reaction, f(T) = exp -E/RT, and generally since E/RT >> 1, the burning rate for the solid phase is governed by the surface

* Nomenclature defined in Glossary.

II,B, Steady-State Model (cont.)

temperature.

The model predicts that the burning rate for a material with a higher themal diffusivity resulting from a metal additive would cause a higher burning rate because the amount of heat penetration would be increased and reactions would begin sooner. This has been experimentally verified by Wenograd[20]. The model also predicts that the burning rate measured as a function of surface temperature should provide an activation energy half of that of the actual governing process. Thus for several propellants using AP, Powling[12] has obtained values of $\sim$ 30 kcal/mole, and the mechanism governing deflagration must have an E $\sim$ 60 kcal/mole. This value is not appropriate to the three major mechanisms hypothesized by Powling, namely sublimation, high temperature, or low temperature decomposition. This value is, however, appropriate to AP decomposition governed by the total decomposition process as measured by Waesche[19] (62.5 kcal) using a Differential Scanning Calorimeter and by Saunders and Pellette[14], who noted that two separate mechanisms appear to exist in the AP deflagration. This would mean that the burning rate is governed by the sum effect of the sequence of reactions because these (exothermic) reactions raise the temperature inside the grain and permit the surface temperature to be reached more rapidly.

Using the computer solution to the heat conduction equation with Arrhenius reactions, several typical profiles are shown in Figure 3. The depth below the surface at which the reactions become negligible is of the order of 0.3 α/r for the cases shown and is inversely proportional to the activation energy.

II,B, Steady-State Model (cont.)

As we see, when the heat of reaction is small ($QR/C_sE = .025$) but the surface temperature is high, ($Q/C_sT_s = .5$) the profile is indistinguishable from the case where no chemical reactions occur. Even for the case of a high heat of reaction ($QR/C_sE = .08$) and low surface temperatures ($Q/C_sT_s = 1.6$), the solutions are not appreciably different. This is because with Arrhenius type reactions, the reactions drop off rapidly with grain depth. Only when the extent of reaction at the surface is extremely high will a profile occur whose form is discernibly different from the exponential. Furthermore, except for the case of a significant extent of reaction in the solid ($\xi_s = .5$) and high surface temperatures, the temperature becomes essentially ambient at depths of $yr/\alpha \doteq 3$. Experimental evidence will be presented in Section III.2 which demonstrates that the experimental temperature profile is significantly greater than allowable by the thermal diffusivity and hence that conduction cannot be the sole heat transfer mechanism. Finally, since the profiles with and without chemical reactions are so similar, the presence of significant chemical reactions must be experimentally evaluated by a more sensitive method than plotting T(x). This method is detailed in Section III.2.

The reactant products evolved by the solid phase may be influenced by purely surface type reactions, involving an enthalpy change. The surface reactions may be pressure dependent as well as involving vaporization processes. In any event, when the gas phase adjoins the solid- (or liquid-) surface-interface, the transition is assumed to be describable by the same moving boundary heat conduction equation

$$r\rho_s \frac{dTC_p}{dy} - k \frac{d^2Tk}{dy^2} = L J_s$$

where L represents the heat liberated by the "interface" reactions

J_s is the reaction rate

Since the equation applies across a discontinuous medium, integration must be in the Stieltjes-Lebesgue sense, i.e.,

$$r\rho_s [C_p T_s - C_s T_s] + (-k \frac{\partial T}{\partial y}\Big|_g) - (-k \frac{\partial T}{\partial y}\Big|_s) = L\, r\rho_s$$

As is shown in Appendix I, this integration leads to the conclusion that the gradient of the extent of reaction at the surface must vanish, i.e. $\frac{d\xi}{dy}\Big|_s = 0$, and basically assumes a continuity of the reaction scheme in going from the solid to gas phase. Experimentally we have found that the deflagration exotherm goes through a maximum below the surface and the slope of the temperature profile then levels off. This would be in agreement with the vanishing ξ gradient. Hirschfelder and Curtiss[8] also make this assumption in their description of the flame structure of a combusting material. Integration of the heat conduction equation in the solid phase permits the gradient in the solid phase to be determined.

The heat flux from the gas phase then becomes for $C_p \doteq C_s$

$$k \frac{\partial T}{\partial y}\Big|_g = r\rho_s C_s (T_s - T_o) \left[1 - \frac{L + Q\xi_s}{C_s (T_s - T_o)}\right] \qquad (1.A)$$

II,B, Steady-State Model (cont.)

The bracket term is essentially a lag factor, λ, which shows that solid phase and interface reactions, L, reduce the heat flux required of the gas phase to promote a given burning rate. When these exist and the flux is reduced by depressurization, the solid phase can respond more rapidly because the reactions provide a more rapid transition in establishing the new profile. Although L is difficult to measure directly, indirect measurements of unstable combustion may provide reasonable estimates for use in a steady-state burning rate model.

Let us now turn our attention to the gas phase. The solution for the burning rate which satisfies the gas phase is derived in Appendix I from the Zeldovich equations.

$$(r\rho_s)^2 = \frac{.5(\alpha\rho)\ Z'\left(\frac{pC_p^n\ T_f}{QEe}\right)^n \left\{e^{-E/RT_f} - e^{-E/RT_s}\right\}}{(1-\xi_s)^2\left[T_m - T_f + \frac{Q(1-\xi_s)}{2\ C_p}\right]\frac{R}{E}} \qquad (2)$$

where $\alpha\rho$ has been assumed to be relatively independent of temperature. T_m is the temperature at which the reaction rate is a maximum, namely

$$T_m = \frac{T_f}{1+n\frac{RT_f}{E}}$$

The effect of changing the surface temperature or activation energy is shown in Figure 3a. When RT_s/E is reduced from .1 to .05, the profile is extended but the profile for $RT/E > .1$ remains almost identical and results in almost the same dimensionless burning rate, B, when the flame

II,B, Steady-State Model (cont.)

temperatures are kept the same. Thus the effect of surface temperature changes does not affect the burning rate calculated for the gas phase. This is in agreement with Corner's[3] results. The effect of diffusion can be shown to shift the extent of reaction closer to the surface as Le is decreased. When solid phase reactions exist ξ_s limits the amount of heat released in the gas phase, Q. As Q increases, the extent of reaction ξ_s increases and the reactions must extend over a greater distance.

Separation of the burning rate equations into a solid and gas phase component now requires that the unique value of the rate be related through the reaction extent at the surface, ξ_s. Such a solution is easily obtained if we assume ξ_s is small. Eliminating ξ_s between Eq. (1) and (2), the burning rate becomes

$$r = \frac{2A^2 e^{-E/RT_s}}{-Bp^{n/2} + \sqrt{B^2 p^n + 4A^2 e^{-E/RT_s}}} \qquad (3)$$

The burning rate is uniquely defined only when $p(T_s)$ is known. At low pressures, Equation (3) is completely dominated by the solid phase while at high pressures, the burning rate is governed by the gas phase decomposition rate. If, as an example, $p(T_s) \sim e^{-E'/RT_s}$, then the burning rate will be essentially a linear function of p^m, $m \neq n/2$, i.e. the measured burning rate exponent differs from the usually assumed value (n/2). Because of this r(p) can actually go through a maximum. In general, it is difficult to explain observed burning rate exponents resulting in platonic or even negative burning

II,B, Steady-State Model (cont.)

rate exponents, since zero order gas phase reactions are not probable. This model, however, makes such exponents possible if we assume that the surface temperature is sensitive to pressure, low E'. When E' is effectively negative (a decrease in surface temperature with pressure as observed by Powling[12]), we could reasonably expect burning rate exponents even in excess of unity. As $p \to 0$, a finite burning rate is still possible. Therefore, a loss mechanism not stated in the conductive equations must be involved to cause extinguishment. Such a mechanism is radiative heat transfer. Before turning our attention to the effect of transients, let us determine the effect of grain temperature on burning rate. Using Equation (3) and assuming that the surface temperature is not changed by changes in grain temperature, differentiation of $\ell n\ r$ yields

$$\pi_r = \left(\frac{\partial\ \ell n\ r}{\partial\ T_o}\right)_p = \frac{\left(n + \frac{E}{RT_f}\right)}{2T_f\sqrt{1+\lambda}} + \frac{\lambda}{(T_s - T_o - Q_s/2C_s)}\quad (1 + \lambda + \sqrt{1+\lambda})$$

where $\lambda = rA^2\, e^{-E/RT_s}/B^2 p^n$ and $C_s/C_p \approx 1$

At high pressures, $\lambda << 1$

$$\pi_r \approx \frac{1}{2T_f}\left(n + \frac{E}{RT_f}\right) \approx .1\%/°C$$

At low pressures, $\lambda >> 1$

$$\pi_r \approx \frac{1}{T_s - T_o} \approx .2\%/°C$$

II,B, Steady-State Model (cont.)

Thus we see again further evidence that at low pressures the deflagration process is dominated by solid phase decomposition, while at high pressures, the process should be gas phase controlled. The above estimates utilize nominal values to give reasonable values for π_r. The latter, higher value is more typical of solid rocket motor propellants. The coupling effect at intermediate pressures would tend to weight the burning rate sensitivity to lower values. Thus for $\lambda = 1$, $\pi_r \approx 0.13\%/°C$. Measurements of π_r as a function of pressure would therefore appear to offer a method of evaluating the relative effects of the solid and gas phase.

C. EXTINGUISHMENT MODEL

Under transient conditions, the partial differential equations describing the burning rate are sufficiently complex that only numerical solutions are possible. In order to gain meaningful insight into the extinguishment process we will relax the desirable criterion of an exact solution by simplifying the effect of chemical reactions, and allowing the instantaneous burning rate to take on a time averaged value during the depressurization. Thus the transient form of the heat conduction equation with chemical reactions takes on the following form, as can be derived from Appendix I.

$$\frac{\partial v}{\partial t} = \alpha \frac{\partial^2 v}{\partial y^2} - r \frac{\partial v}{\partial y} \tag{4}$$

where $$v = \frac{T - T_o - Q_s \xi / C_s}{T_{so} - T_o - Q_s \xi_s / C_s}$$

II,C, Extinguishment Model (cont.)

If we now define a flux function, F, by

$$F = \partial v/\partial y$$

and assuming $F_{yt} = T_{ty}$, we obtain, using Equation (4), the transient flux equation

$$\alpha \frac{d^2F}{dy^2} - \bar{r} \frac{dF}{dy} \tag{5}$$

where $\bar{r}$ is a time averaged burning rate.

Thus the flux, or temperature gradient, is governed by the same partial differential equation as the temperature itself, even if the burning rate changes with time. This approach is necessary since the flux at the grain surface is the quantity which is actually specified during depressurization. An initial condition and two boundary conditions are required to complete the evaluation.

These are given in Appendix I by

(1) $F(t=0) = \frac{r_o}{\alpha} \exp \frac{r_o y}{\alpha}$

the steady-state solution

(2) $F(y=0) = F_o \exp -Kt \qquad t > 0$

an imposed flux by which $\dot{p}/p \doteq$ constant

(3) $F(-\infty, t) = 0$

To solve Equation (5), we make use of the Laplace transform, defined by

$$f(y,s) = \int_o^\infty e^{-st} F(y,t)\, dt$$

The solution of the inverse Laplacian transform equation then becomes

II,C, Extinguishment Model (cont.)

$$\frac{F}{F_o} = \exp\left[\frac{r_o y}{\alpha} - \frac{\bar{r}\, r_o - r_o^2}{\alpha}\, t\right]$$

$$+ \frac{e^{-Kt}}{2}\left[e^{\frac{\bar{r}y}{2\alpha}\sqrt{1-\frac{4K\alpha}{\bar{r}^2}}}\ \mathrm{erfc}\left(\frac{y}{2\sqrt{\alpha t}} + \frac{\bar{r}}{2}\sqrt{\frac{t}{\alpha}\left(1-\frac{4K\alpha}{\bar{r}^2}\right)}\right)\right.$$

$$\left. + e^{\frac{\bar{r}y}{2\alpha}\sqrt{1-\frac{4K\alpha}{\bar{r}^2}}}\ \mathrm{erfc}\left(\frac{y}{2\sqrt{\alpha t}} - \frac{\bar{r}}{2}\sqrt{\frac{t}{\alpha}\left(1-\frac{4K\alpha}{\bar{r}^2}\right)}\right)\right]$$

$$- \frac{e^{-\left(\frac{\bar{r}\, r_o - r_o^2}{\alpha}\right)t + \frac{\bar{r}y}{2\alpha}}}{2}\left[e^{\frac{yr_o}{\alpha}\left(1-\frac{\bar{r}}{2r_o}\right)}\ \mathrm{erfc}\left(\frac{y}{2\sqrt{\alpha t}} + r_o\left(1-\frac{\bar{r}}{2r_o}\right)\sqrt{\frac{t}{\alpha}}\right)\right.$$

$$\left. + e^{-\frac{yr_o}{\alpha}\left(1-\frac{\bar{r}}{2r_o}\right)}\ \mathrm{erfc}\left(\frac{y}{2\sqrt{\alpha t}} - r_o\left(1-\frac{\bar{r}}{2r_o}\right)\sqrt{\frac{t}{\alpha}}\right)\right] \qquad (6)$$

We can see that from this equation that the exact solution of the equation involving the true reaction kinetics and flux, which must be even more formidible, prevents any simple description of the burning rate response during transient conditions. However, there are several aspects of the solution which provide deep insight into the response mechanism during depressurization. First, as burning rate, $\bar{r}$, decreases, the gradient at the surface of the grain changes from a simple exponential to a sinusoidal response because the term $\left(1 - \frac{4K\alpha}{\bar{r}^2}\right)$ becomes negative. The imaginary complementary error functions have been tabulated so that Equation (6) could

II,C, Extinguishment Model (cont.)

be numerically evaluated. The second boundary condition, $F \to 0$ as $y \to \infty$ is automatically obeyed by Equation (6). For points near the surface ($y \approx 0$), the first and third terms on the right hand side cancel each other and the gradient is effectively governed by the second term. In order to reduce Equation (6) to its most fundamental description and yet maintain the general nature of the response, we will use the response of the system near the surface. In addition, the complementary error functions for short times reduce to unity, so that in essence the solution to the flux equation reduces to the form

$$\frac{F}{F_o} = \exp\left(- Kt + \frac{\bar{r}y}{2\alpha}(1 + \Gamma)\right)$$

where $$\Gamma = \sqrt{1 - \frac{4K\alpha}{\bar{r}^2}}$$

Although this form is admittedly a very simplified version of the actual solution, it incorporates the two most salient features, the shift to a cyclic burning as $\bar{r} \to 0$, and the effect of the transient flux. Experimental evidence is provided in the next chapter to show that the cyclic burning occurs, and the frequency involved is associated with the depth of the zone, i.e. when the temperature has been reduced to essentially ambient conditions. This occurs when

$$\frac{y^2}{4\alpha t} \approx 3 = \frac{r^2}{4\alpha f}$$

The frequency is then

$$f \approx \frac{r^2}{12\alpha} \approx 15 \text{ cps}$$

II,C, Extinguishment Model (cont.)

which is approximately the level observed. Equation (7) obeys the boundary conditions and the initial condition, as well as the Fourier equation itself if $\bar{r}$ is interpreted as a constant. If $\bar{r}$ is used as the instantaneous value, the solution is shown to still be valid for values sufficiently close to the surface so that

$$y << 2\alpha/r$$

which, as previously mentioned, therefore defines the major portion of the profile for conductive heat transfer.

Using Equation (7) the temperature distribution can be determined by integration and yields

$$v = \int_{-\infty}^{y} F \, dy = \frac{2r_o}{\bar{r}\,(1+\Gamma)} \exp\left[-Kt + \frac{\bar{r}y\,(1+\Gamma)}{2\alpha}\right] \qquad (8)$$

In order that the temperature eventually goes down to the ambient conditions it is obviously necessary that the numerator must be less than the denominator, i.e. that the burning rate may actually exceed the steady-state burning rate, which is $r_o \exp(-Kt)$. We will now use the results of the above equations in a way so as to minimize the effects of the simplifying assumptions made. This is done by directly integrating Equations (4) and (7) which yields

$$\bar{r}\, v_s = \left(\frac{\partial v}{\partial y}\right)_s - \frac{\partial}{\partial t}\int_{-\infty}^{o} v \, dy = F_o \alpha \, e^{-Kt} - \frac{\partial}{\partial t} \frac{F_o \, e^{-Kt} \, 4\alpha}{[\bar{r}\,(1+\Gamma)]^2} \qquad (9)$$

Since the associated steady-state burning rate is given by

$$r_{ss} = r_o \exp(-Kt)$$

II,C, Extinguishment Model (cont.)

we obtain the more generalized solution

$$\overline{r}v_s = r_{ss} - 4\alpha \frac{d}{dt} \frac{r_{ss}}{\overline{r}^2 (1+\Gamma)^2} \lambda$$

It is of interest to note that if we were to assume at this point that the depressurization is small, so that $\Gamma \doteq 1$, and hence that $r_{ss} \doteq \overline{r}$, we obtain the solution originally derived by Paul[11]:

$$\overline{r} = r_{ss} + \frac{K \alpha}{r_{ss}}$$

The transient equation has been approximately considered by various authors. Paul[11] considered T_s to remain constant. Empirically, Lovine[9] has shown that the Paul[11] equation can be correlated using a lag factor, λ, such that

$$\lambda = \left(\frac{p}{p_e}\right) \left[1 + \left(\frac{p}{p_e}\right)^{2n}\right]$$

Typically λ has values from .3 to .5.

$$r = r_{ss} - \frac{\lambda \alpha n \dot{p}}{r_{ss} p}$$

This λ factor Marxman[10] has attributed to surface coupling reactions preventing solid phase response. Rather than assuming T_s as constant, Marxman[10] attacks the response problem by direct integration of the transient heat conduction equation as was done in obtaining Equation (9). Marxman assumes that the temperature profile is not able to respond, so that the steady-state profile can be used to evaluate the integral, and so

II,C, Extinguishment Model (cont.)

$$r = r_{ss} \frac{T_{so} - T_o}{T_s - T_o} - \frac{\alpha}{r_o} \frac{d \ln T_s - T_o}{dt}$$

The major problem therefore requires an empirical determination of the temperature profile during depressurization. This question will be considered in Section III where pertinent data are presented. As will be shown, the response is actually cyclic in nature, and therefore a theoretical description must be obtained which reflects this type of response. Marxman's approach is not substantiated by the data because the profile responds as well as the surface temperature.

D. THE EFFECT OF CHEMICAL KINETICS ON EROSIVE BURNING

Before examining the experimental data on extinguishment let us consider the effect of chemical kinetics on erosive burning. When gases flow over a surface, a boundary layer of stagnant gases is built up which increases in thickness as the friction tends to stagnate the flow more and more, so that the velocity profile bends close to the surface. If gases are discharged from the surface, the velocity profile is thickened and therefore prevents turbulent eddies entering into the gas layer adjacent to the surface. Equations for the momentum boundary layer with blowing must be considered in order to obtain the friction velocity, V_*, with mass addition. However, using the analogy between heat flux and friction velocity, the turbulent conductivity can be related to the turbulent eddy viscosity. The temperature profile is divided into two zones, a heating zone and a chemical reaction zone, for which the profiles with and without erosive burning can be compared, and

II,D, The Effect of Chemical Kinetics on Erosive Burning (cont.)

therefrom the turbulent and non-erosive burning rates, r_t and r. Such an analysis is carried out in Appendix II and leads to the result

$$\left(\frac{r_t}{r}\right)^2 = \left\{\frac{T_1-T_{s,t}}{T_1-T_s}\left(\frac{T_s-T_o'}{T_{s,t}-T_o'}\right)^2\right\} + \left\{\ell n\left(\frac{T_1-T_o'}{T_{s,t}-T_o'}\right)^2\right\}\left\{\frac{r\rho_s}{V_*\rho} P\sqrt{1+\nu/\nu_T}\int_o^{x_1}\frac{dx v^*/\nu}{1+{}_T/\nu}\right\}^{-2}$$

$$= \exp -\frac{E}{R}\left(\frac{1}{T_{s,t}} - \frac{1}{T_s}\right) \qquad (10)$$

This augmented rate applies only to the region where the flux is increased by the flow. From the boundary layer equation this point occurs when

$$V_*^2 > U\left(\frac{r\rho_s}{\rho}\right)$$

As an example of a typical motor

$$\left(\frac{V_*}{U}\right)^2 = .02\ R_x^{-.2} \approx .002$$

giving a minimum velocity of some 600 ft/sec before any appreciable erosive effect was actually noted.

Examination of Equation (10) shows that for high burning rate propellants which would be associated with a small activation energy, that a change in surface temperature would not as markedly affect the burning rate as for a slow burning propellant. That is, erosive burning should primarily affect slow burning rate propellants. Secondly, the effect of exothermic surface reaction and subsurface reaction (+L) is to decrease the turublent

II,D, The Effect of Chemical Kinetics on Erosive Burning (cont.)

rate through the first T_o' term. Third, if aluminized propellant is used where the exothermicity appears farther from the grain, T_1 will increase, hence the erosive effect will increase. Finally, if $T_{s,t}$ increases sufficiently, the chemical reaction temperature, T_1, is approached and the flame in the gas phase can no longer be sustained. Just prior to this, a maximum erosive rate must therefore exist. The general nature of the erosive burning effect should therefore be as sketched below:

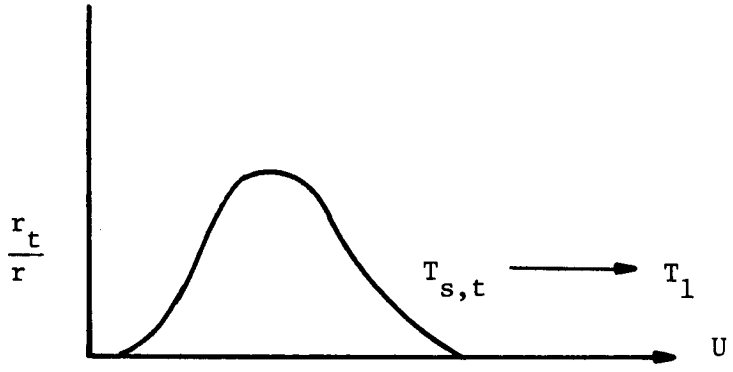

III. EXPERIMENTS CONCERNING THE STEADY AND TRANSIENT STATES OF COMBUSTION OF SOLID PROPELLANTS

A. INTRODUCTION

During the course of this program measurements were carried out which were aimed at clarifying some of the features of the combustion process of a solid propellant. Such questions regarding steady-state combustion as determining the contribution of solid phase reactions and the effect of radiation were raised. In addition, questions regarding the actual response of the temperature profile and quenching of chemical reactions during extinguishment needed experimental clarification. The experiments which were carried out to determine these effects involve several new techniques; therefore an interpretation of the data must be made in light of the measurement problems involved and an evaluation of these techniques is given.

B. STEADY-STATE BURNING RATE MEASUREMENTS

1. Thermal Diffusivity

The model has supposed that chemical reactions in the solid phase exist and contribute a significant heat release. The theoretical calculations of the model indicated that the presence of chemical reactions might well be difficult to determine from the temperature profile. Selzer[16] using polarized light to show the AP transition plane, calculated an excess of energy under the temperature profile due to chemical reactions. However, the thermal diffusivity at high temperatures must also be accurately known. Measurements of α were carried out using several techniques, all giving very similar results, and not indicating a significant change of α with temperature. Before returning to the question of solid phase reactions, let us therefore examine the results of thermal diffusivity measurements. Data from self-heating

III,B, Steady-State Burning Rate Measurements (cont.)

experiments were used to determine α, and for a test propellant composed of 16% Al, the value obtained was $1.8 \cdot 10^{-4}$ in^2/sec. The second method utilized the increase in internal energy by hydrostatic compression to produce a transient heat flow as the specimen relaxes toward thermal equilibrium following rapid depressurization. A typical decay plot is shown in Fig. 5. The heat transfer coefficient of the system can be determined by calibration and the diffusivity is obtained utilizing the analysis of Carslaw and Jaeger[2], and Chung.[4]

$$\alpha = - \frac{r \, d \, \ell nT/dt}{\chi_1^2}$$

where χ_1 is the smallest root of the transcendental equation satisfying the surface heat transfer response, tabulated for various geometries by Wiegand[23]. The value obtained was $1.85 \cdot 10^{-4}$ in^2/sec.

This method is especially appealing from the point of view that it provides a method of determining α from a small temperature differential, about .1°C, hence the value of α is at ($T \pm .1°C$). The usual methods require α measurements over a much larger temperature range. Although $\alpha(T)$ at high temperatures were not made, this method provides an experimental possibility of determining α into the temperature range of decomposition. Since Schmidt[15] and others have shown that in the presence of an ammonia atmosphere the solid phase decomposition process is retarded until temperatures of $\sim$ 400°C are reached, measurements in an NH_3 atmosphere where the pressure is rapidly dropped could be used to determine $\alpha(T)$ for AP propellants.

III,B, Steady-State Burning Rate Measurements (cont.)

Similar measurements for the binder can be made. Finally, composites of AP binder and even aluminum could be made to determine the interaction.

In utilizing a thermocouple to measure the temperature profile, the voltage output at low temperatures was separately amplified in order to provide a more accurate definition of T(x); the slope of the $\ell n\ T-T_o$ vs x curve provides the thermal diffusivity. Under actual burning conditions the value of α tended to be greater than five times as high as measured by the standard technique at the low temperatures. In order to better show this effect the temperature profile was electronically amplified and the chart speed run at 50 ips; the results are shown in Fig. 6. The explanation for the higher diffusivity is hypothesized as being due to radiative transfer, which will be considered in Section III.3.

2. Solid Phase Reactions

Theoretical calculations showed that the existence of solid phase reactions was unlikely to be answerable by measurement only of the temperature profile. One could integrate over the entire temperature profile, as Selzer[16] did, and of course with chemical reactions there would be an excess of energy, yet an inflection point indicating appreciable solid phase energy release would be difficult to find. These uncertainties arise because the temperature is an integration of the rates of heat release and fluxes.

However, if we consider that for a constant burning rate, the heat conduction equation can be written

$$-\frac{\alpha}{r^2}\frac{d^2T}{dt^2}+\frac{dT}{dt}=\dot{Q}_s=\left[\frac{Q}{C_s}\ z'(1-\xi)^n\ \exp\ -\ E/RT\right]$$

III,B, Steady-State Burning Rate Measurements (cont.)

We see that by differentiating the temperature profile trace, the chemical reactions become immediately available. The most direct method of doing this is to electronically differentiate the voltage signal. The problem is to match the frequency response characteristics of the circuit to the major frequencies of the event. This problem has been solved and the circuitry is discussed in detail in Appendix III. The theories all provide that dT/dt and dp/dt be known; rather than calculating these from the data of T(t) and p(t), the circuitry allows the measurement of the transients directly.

The use of thermocouples to measure the solid and gas phase profiles is subject to various sources of error, and hence misinterpretation. First, the leads must be brought in below the plane of the thermocouple to avoid premature heating of the TC leads. This and other sources of error are discussed in Strittmater[17]. Despite various precautions taken by Strittmater, temperature profiles were obtained which indicated that the thermal diffusivity measured in the grain depths is high by an order of magnitude, indicating that a heat flux other than purely conductive is forcing the temperature to increase deep into the grain. Similar results indicating a higher value of α at low temperatures have been obtained by Summerfield[18] using thermocouples. These data indicate that the surface temperature rises with pressure until somewhere between 500-1000 psi, depending on the propellant type, the surface temperature decreases.

To avoid such problems as heat losses in the thermocouple junction leads, a new technique has been developed in which the leads are

III, B, Steady-State Burning Rate Measurements (cont.)

in the plane of the junction. Secondly, to minimize the disturbing effect of the TC's presence on the normal temperature distribution in the propellant, the thickness has been reduced to a degree which improves on all presently available techniques by electroplating thin films and adhering these onto the propellant surface. The first thermocouples made were about 0.1 $in.^2$ area and about 10μ thick, but the thinness possible is limited only by the metal required to produce adequate thermoelectric effect. The electromotive power (24μ V/°C) is about 90% of that achievable for bulk thermocouples, with a sensitivity of better than 0.1°C. Results of T(t) on semi-log plots show a behavior typical of propellants, and shows the solid phase reactions at the higher temperatures. We also investigated vapor deposition which appears quite satisfactory as a means of forming thermocouples directly on the propellant surface. Finally, small TC beads were compressed under high pressures to obtain a planar thermocouple (∿5μ to 10μ thick and ∿50μ diameter). Results were essentially the same as in the previous two methods, and since these can be made up more readily, this latter method was used in the tests. However, it is anticipated that the vapor deposited thermocouples may provide insight into the gas phase profile since their response capability can be improved an order of magnitude. Measurements using cast in place and cementing TC's produced comparable results. The planar TC sheets formed provide an averaging process over the temperature front which can progress at different rates depending on whether or not the immediate front is an oxidizer crystal, binder, or metal particle.

III,B, Steady-State Burning Rate Measurements (cont.)

Using the thermocouples described above in conjunction with the differentiating circuitry, traces of T(t) and $\dot{T}(t)$ are given in Figures 7 through 10 for a typical PBD-AP-Al propellant. The temperature profiles are as expected relatively smooth, however, the derivative shows the presence of exothermicity. It is instructive to compare the $\dot{T}$ trace with the DTA (Fig. 48) for this propellant burned at 15 psia. We see that there is a high correlation with the AP endotherm clearly visible at 242°C, and the pre-deflagration exotherm-endotherm at ∿350°C. The deflagration exotherm leading up to a peak of ∿470°C cannot be completely revealed by the DTA, however, a comparison of $\dot{T}(t)$ with DSC thermograms may markedly clarify the relationship of the exotherms and the combustion process in the propellant. Two important points should further be noted about the temperature profiles. The first point is the leveling off of the profile after the ∿470°C exotherm. This result was noted for most of the propellants when burned at ambient conditions. As the pressure is raised the effect diminishes, completely disappearing at pressures in the 400 psia regime. Above 500 psia the 470°C exotherm has essentially vanished. This pressure level is also one at which the propellant deflagration exotherm as measured by DTA has shifted to its lower value, as noted previously in the section dealing with combustion kinetics.

The leveling off of the profile at ambient conditions leads one to believe that at the lower pressures a type of irregular surface condition may exist. The low burning rate allows the planar thermocouple more time to integrate over an irregular surface, while at higher burning rates the

III,B, Steady-State Burning Rate Measurements (cont.)

thermocouple will respond to the dominant surface characteristic. The fact that a thermal diffusivity calculated from the temperature gradient and measured in the same temperature regime as by standard techniques yields a value which is too high and changes with pressure indicates that the heating mode changes with pressure. This effect can also be noted in Summerfield's data, shown in Fig. 11, where the apparent conductivity changes with burning rate. It is difficult to separate the solid phase reactions from the radiative heating but we can be assured that convective heating plays only a partial role in the deflagration process at low pressures. Since α shifts to level values with increasing pressure, at higher pressures we might anticipate that convection is the dominant mode. Using microatomized AP ($\sim$10μ), the thermal diffusivity decreased to values comparable to the true value, indicating a secondary role for radiative heat transfer when microatomized AP is used. At low temperatures the profile shows thermal penetration to depths unexplainable except in terms of radiative preheating. Using microatomized AP ($\sim$6μ) - PU, the thermal diffusivity decreased to values several times the true value, as shown in Fig. 6a. The thermal diffusivity would be expected to be close to normal if the small particles act to scatter incident radiation. Furthermore, with the small particles the averaging effect of the planar thermocouple would be to see several localized regions of AP combustion which should produce a $\dot{T}(t)$ trace which is less regular, the endotherms and exotherms being mixed together. As is shown by Fig. 13, this is indeed the case. The scattering effect of radiation by small particles leads to a very significant

III,B, Steady-State Burning Rate Measurements (cont.)

conclusion regarding extinguishment. Thus, although the small particles give higher burning rates and should make extinguishment more difficult, small particle AP actually produces an easier to extinguish propellant. This result is unexpected in terms of gas phase combustion modeling, and can best be explained as caused by radiation. One final comment regarding use of microatomized AP. We have found that when Al and more AP but of larger particle size ($\sim$70μ) is added to a binder-micro AP matrix so that the flame temperature is increased but the solids loading remains constant there is no change in burning rate; the Al and large AP matrix deflagration appears to be the important parameter in controlling the burning rate. Since the mean particle size is reduced and the flame temperature increased we would expect from Summerfield's model some compensatory effects on burning rate. That the burning rates should be identical over a large pressure range and solids loading however indicates that more than coincidental compensating effects are involved.

Since the exothermicities as derived from the $\dot{T}(t)$ trace are qualitatively different for microatomized AP, this indicates that the solid phase decomposition is particle size dependent. The deflagration exotherm appears to be reasonably reproducible, namely $\sim$4500°C/sec. Using $\sim$470°C for the surface temperature it is interesting to note that $\dot{T}$ (at 470°C) varies with the square of the burning rate, as seen by the table given below for the PBD propellant.

III,B, Steady-State Burning Rate Measurements (cont.)

P	r	$\dot{T}(t)$	$\dot{T}(t)/r^2$
15 psi	.15 ips	4500°C/sec	$2.0 \cdot 10^5$
200 "	.33 "	15000°C/sec	$1.5 \cdot 10^5$
400 "	.40 "	30000°C/sec	$1.8 \cdot 10^5$

Since the value of $\dot{T}/r$ just below the surface is proportional to the gradient or is a measure of the flux, we have the relationship that the burning rate is proportional to the flux. The value of the thermal conductivity term as measured is small compared to the gradient term, so that the heat conduction equation reduces to

$$\frac{1}{r}\frac{dT}{dx} = \frac{\dot{Q}_s}{r^2} = \text{const.}$$

i.e. the burning rate is determined by the solid phase heat generation rate. The measured result that $d^2T/dt^2 = 0$ through the deflagration exotherm can be explained only by solid phase reactions, i.e. the conditions just below the surface appear to be governed by solid phase reactions.

Because of its importance to the combustion process we shall devote the next section to a discussion of the effects of radiation.

3. Radiation Heat Transfer

As was noted by the TC measurements, an appreciable radiation heat flux appeared present. To further check this result, the implications to deriving an accurate burning rate being quite significant, many different types of tests were carried out. We will first discuss these test results, all confirming radiative transfer, and then describe the theoretical implications.

III,B, Steady-State Burning Rate Measurements (cont.)

The first test used two thermocouples in the same plane; the first TC was located immediately below a large AP crystal. The temperature trace for this shown in Figure 12 shows a marked increase in temperature deep inside the grain with the typical leveling off effect at ∿500°C. The second test utilized microatomized and high speed AP; if radiation does penetrate deep inside the grain, the smaller AP particles should scatter the radiant energy so that the effective α would decrease. As shown in Figure 6a, the small AP particle propellant did indeed demonstrate a highly reduced thermal diffusivity, closer to that of the propellant's diffusivity when measured by standard techniques. When a small grain was burned in an internal burner configuration with a calorimeter attached to the burnout surface, heat flux was perceived by the calorimeter at about 650μ below the surface. Again this depth was much too great to be accounted for by simple conduction.

By implication, the fact that a calorimeter could perceive sufficient thermal effects through the grain led us to believe that a radiative profile could be obtained using not only a photocell but also a monochromator. Typical results of such a test at 1.45μ and 4μ are shown in Fig. 14. The photocell and monochromator profiles are different because the monochromator responds to essentially only the preset wavelength. Secondly, the monochromator response is not quite as rapid as the photocell. As shown in Fig. 15, when the wavelength is changed, the maximum transmission is strongly altered. For the propellant tested at 15 psia the peak transmission occurs at about ∿1.3μ. A propellant with 16% Al, however, showed a vastly reduced level of emitted

III,B, Steady-State Burning Rate Measurements (cont.)

energy through the grain. The transmission or radiation "profile" is due to the composite of several separate effects, namely, the radiant energy flux from the gas phase and the transmissivity of the propellant which are wavelength dependent, and secondly as the grain depth decreases the higher grain temperatures become more important. These two effects have been separated by measurements of the transmissivity of the propellant (at ambient conditions). The AP is essentially as transmissive at 4μ as at 2μ, an absorption band existing at 3μ. Therefore it appears most likely that the reduced radiative flux noted by the monochromator is due to a decreased flux from the gas phase at 4μ. In terms of a blackbody radiative source, the peak at 1.3μ would correspond to 2300°K, which can be compared to the flame temperature for this propellant of ∿2500°K. In Section III.4 it will be shown that the monochromator voltage, V, varies logarithmically with the temperature, i.e., $\ell n\ V \sim -1/T$. The "radiation profile", i.e. V(x) in the grain as measured is nearly exponential, and assuming that the radiative flux varies logarithmically with the temperature, yields a "radiation" temperature profile of the form

$$\frac{1}{T} - \frac{1}{T_s} = Ax$$

where A was measured from the profile data to be $.5 \cdot 10^{-6} \mu^{-1} {}^{\circ}C^{-1}$. Essenhigh[5] has shown that the "radiation" temperature through a solid without conduction should have the form

$$T^4 = T_s{}^4 - KBx$$

III,B, Steady-State Burning Rate Measurements (cont.)

where K is the transmissivity coefficient defined by

$$\tau_\lambda = (1-\rho_\lambda) \exp -Kx$$

and

$$B = \frac{1}{2} \left\{ T_f^4 \alpha_g - \varepsilon_s T_s^4 - \alpha_s T_s^4 e^{-KL} \right\}$$

which can be assumed dominated by the flame temperature. Measured values of K (see below) indicated that the depth of the profile should only be about 30μ, even for α_g as low as .5. Since the measured depths are much greater, this requires that the effective emissivity of the gas could be relatively low (less than .1), or that the radiant driving temperature be nearly that of the surface temperature. Few measurements of propellant gas emissivities are available; one from Adams[1] gives emissivity values which are not in conflict with these results. (See Fig. 16).

Of the incident radiation falling on a surface, a fraction, α_λ, is absorbed, a fraction, ρ_λ, is reflected, and a fraction is transmitted, τ_λ. Absorption by liquids and solids is generally limited to the region near the surface. For good electric insulators (propellant), the depth is generally of the order of 1000μ.[7] Hence, for a propellant with a conductive temperature profile governed by the burning rate and of the order of ∿200μ, the depth or penetration by radiation can be considered to be greater than the conductive profile.

In an actual burning propellant, the temperature profile drops rapidly and hence the emissivity for a thin layer close to the surface obeys

III,B, Steady-State Burning Rate Measurements (cont.)

Kirchhoff's Law, namely

$$\varepsilon_\lambda = (1-r_\lambda)(1 - \exp -\alpha_\lambda y)$$

The optimum wavelength for measuring the surface temperature therefore is one for which ρ_λ is small and α_λ is high. Powling[12] has shown that for AP the absorbing wavelengths are in the 3, 7 and 9μ regions. It is interesting to note that in the 2.5μ and 4-5μ regions AP transmits some 80% of the incident radiation even to a 80μ depth. Thus radiant emission from the gas into the propellant at these wavelengths must be considered to be deep when the radiation impinges on an AP crystal. Generally the transmissivity follows an exponential decay as shown in Fig. 17. Since these results depend on the value of the transmissivity, K, we have calculated one from the measured value of A and compared to the theoretical isothermal radiation profile, i.e. for temperature close to the surface, and $\alpha_g \approx .1$

$$X = \frac{1}{A}\left(\frac{1}{T} - \frac{1}{T_s}\right) \doteq \frac{\left(T_s^4 - T^4\right)}{\frac{K}{2} T_f^4 \alpha_g}$$

or

$$K \doteq \frac{2A}{\alpha_g}\left\{\frac{4\ T_s^5}{T_f^4}\right\} = 10^{-3}\ \mu^{-1}$$

This is in reasonably good agreement with Powling's value from AP that we feel until more complete transmissivity data on the sprecific propellants are available, values of about 1-3 x 10^{-3} μ^{-1} can be used as an approximate figure for

III,B, Steady-State Burning Rate Measurements (cont.)

purposes of discussion. From this the transmitted energy deep into the grain can be estimated. It can be seen that the radiant depth of penetration can be significant even at 1000μ, and that large (∿200 μ AP crystals would transmit from such a source some 60% of the incident radiation. Assuming a gaseous radiation source of 3000°K of which 99% is absorbed through the gases so that ∿1 cal/cm^{2}sec impinges at the surface and using the transmittance, K, determined from Fig. 17, this amounts to about .6 cal/cm^{2}sec radiant flux transmitted from the surface to the 200μ depth. If we compare this to an estimated heat flux at 200μ from conduction alone along the temperature gradient, namely for a rate at higher pressures of .7 cm/sec

$$\dot{q}\ (200\mu) = C_s \rho r\ (T_s - T_o)\ \exp - \frac{ry}{\alpha} \approx 1.8\ \text{cal/cm}^2\text{sec} \qquad (1\text{-A})$$

and lower pressures of .25 cm/sec, $\dot{q}$ (200μ) ≈ 6.5 cal/cm^{2}sec, we see that the radiant contribution in depth can be a significant contribution. At greater depths the flux is essentially radiative. Therefore, radiant penetration at least through large AP crystals must be considered to contribute to the thermal rise deep into the grain.

A consequence of assuming that radiant penetration is significant would be to effect the temperature sensitivity of the propellant, π_r. Studies of the effect of radiation on π_r are needed. These studies should include an evaluation of dyes which may preferentially absorb radiation at various wavelengths. It may also be possible that simply coating large AP crystals with a non-transmitting material such as Viton would decrease the depth of radiant transfer and therefore lead to a reduced temperature

III,B, Steady-State Burning Rate Measurement (cont.)

sensitivity. Radiant transfer might also explain why a change in grain temperature shows essentially no effect on extinguishability. Thus the grain is heated by radiation to appreciable depths ahead of the flame front and thereby causes heats of solid phase reactions to be generated which must be removed during extinguishment. Because these are extensive in depth, the extinguishment process is then effectively governed by the depth of the chemical reaction profile produced by the radiation.

The conductive heat flux decays with distance into the grain by r/α while the radiantly transmitted heat flux decays by a factor K_λ. The radiant energy reaching the source from the gas phase will decay with the pressure as

$$(1-e^{-\alpha px})$$

where α is an absorption coefficient, depending on wavelength

p is the pressure

x is the beam length

At first it would appear that at high pressures most of the radiant energy in the flame is absorbed before reaching the surface and hence at high pressures little radiant energy would impinge on the grain surface. Let us examine this closely. At nominal pressures, the reaction zone thickness is essentially inversely proportional to pressure, i.e. the gas temperature in the reaction zone is a unique function of px. Hence, if $(1-e^{-\alpha px})$ of the radiant energy emitted at the point x is absorbed by the gases and radiates at a temperature T(x), then the flux transmitted to the surface is approximately

III,B, Steady-State Burning Rate Measurement (cont.)

$e^{-\alpha px}T^4(px)$. From Fig. 17, of the radiant flux transmitted to the surface, the depth y will receive a fraction exp (-Ky). The radiant flux into the grain is then

$$q_r \sim \frac{1}{p} \int e^{-\alpha px}\, T^4(px)\, dpx \cdot e^{-Ky}$$

The integral itself is insensitive to pressure since the flame zone thickness varies inversely with pressure. Neglecting the change of α with pressure, the radiant energy impinging on the grain surface is then inversely proportional to pressure. The conductive flux deep into the grain depends on the burning rate through Eq. (1-A) and diminishes rapidly with pressure. The ratio of radiant to convective heat flux is

$$\frac{q_r}{q} \sim \frac{e^{ry/\alpha - Ky}}{pr}$$

Differentiation shows that as the pressure decreases the contribution of radiative to convective heat transfer will go through a minimum, and any further decrease in pressure will result in a proportionately greater radiative contribution. In other words, at low pressures for those wavelengths which are transmitted, the radiative heat transfer penetrates relatively deeper into the grain, and probably via the largest AP crystals. Therefore extinguishment should be enhanced if the large AP crystals were coated with a material which prevented transmittance, and if the AP particle sizes are decreased.

It is interesting to note some further consequences of the effect of radiation. The conductive profile has a relaxation time given by

III,B, Steady-State Burning Rate Measurement (cont.)

the unsteady heat conduction equation, namely

$$\tau_c \sim y^2/\alpha$$

Although the radiative flux which enters the grain establishes itself rapidly (speed of light through the medium) that portion which is absorbed in thin sections goes into raising the temperature and requires a finite time to raise the grain temperature. The relaxation time for this process is given by[5]

$$\tau_r = \frac{\rho C\ T_s}{K\sigma T_s^4}$$

At various grain depths, an effective thermal diffusivity, α_r, can therefore be defined which would be measured by the gradient of the ℓn T vs x profile, since this more basically measures the thermal relaxation time during combustion. Using the typical value of K,

$$\alpha_r \equiv \frac{x^2 K\sigma\ T_s^3}{\rho C} \approx 5\cdot 10^{-4} \left[\frac{in^2}{sec}\right] \left(\frac{x(\mu)}{2000}\right)^2$$

From this we see that values of α as measured from the temperature profile during burning of AP propellants could be several times "normal" at depths of 2000μ and greater, because the profile is more rapidly established by radiation at these depths. This penetration is further not only a function of the transmissivity but sensitive to the surface temperature, as well as the entire temperature profile. Measurements of the latter are given in the

III,B, Steady-State Burning Rate Measurement (cont.)

following section. When similar boundary conditions are applied, Essenhigh[5] has shown that an effective thermal conductivity can be defined, from which the diffusivity will be

$$\alpha_r = \frac{\sigma T_s^3}{K\rho C} N$$

where $N \approx 8$ at the surface

$N \approx 4$ deep into the grain

Typically for propellant α_r will be from 2-4 times the actual value, again showing good agreement between theory and measurement of the radiation effect. Substantially higher values indicate possible photochemical effects. Prior to considering these measurements one further point about radiation must be considered, namely the measured propellant emissivity, since this can be altered by radiation.

In defining emissivity as the ratio of emitted intensity compared to a blackbody at the same temperature, the propellant must be maintained at a uniform temperature. During burning the profile is not in equilibrium with respect to the steady-state radiation profile, and even more acutely, during extinguishment the radiation profile will establish itself more rapidly. Since at low pressures, this profile is relatively deeper, the effect of radiation is to lead the profile into the grain hence creating a response lag to extinguishment. Thus in the transient burning rate equations the thermal diffusivity plays the role of allowing the heat to escape through the surface. The equivalent thermal diffusivity from radiation cannot be viewed in this

III,B, Steady-State Burning Rate Measurement (cont.)

manner since it plays a directional role, i.e. always deeper into the grain as the pressure decreases.

In Appendix IV, it is shown that the radiative heat conduction equation requires solution of an integro-differential equation. As a first approximation, the radiation can be shown to act as a space dependent heat source, and this case is solved in the appendix. From this the temperature profile with radiation is given by

$$r\rho C\left[T-T_o\right] = \dot{q}_c\, e^{-\frac{rx}{\alpha}} + \frac{\alpha_f \sigma T_f^4}{1-\frac{\alpha K}{r}}\left[e^{-\frac{rx}{\alpha}} - e^{-Kx}\right]$$

Generally, $\frac{r}{\alpha} > K$, so that deep into the profile, the term e^{-Kx} dominates, the relative contribution of radiation changing with pressure and the effective thermal diffusivity is given by $\alpha' = \frac{r}{K} \approx 2\cdot 10^{-3}\ in^2/sec$ which corresponds in order of magnitude to measured values. Appendix IV also shows that the propellant surface emissivity is affected by the burning rate through the temperature gradient. Finally, radiation affects primarily the grain "in depth" and hence when radiation effects burning rate it must do so by acting to "preheat" the grain temperature, effectively a π_r effect.

4. Surface Temperature Measurement Using Infrared

The measurement of the surface temperature of a burning propellant using infrared (1-10μ) wavelength was first performed by Powling[12]. This technique is fraught with several problems, and a discussion of these is necessary in order that the data may be viewed in perspective. The technique

III,B, Steady-State Burning Rate Measurement (cont.)

used to measure the surface temperature rests on a comparison of the radiation emitted from the propellant surface compared to a blackbody. The comparison must be based on the fact that the specimen is at the same uniform temperature as the propellant. This uniformity was verified by using a thermocouple embedded in the propellant. Powling's procedure was to test using equidistant mirrors to guarantee that the optical paths were identical. Our purpose was to determine if the surface temperature response could be measured during rapid depressurization. In addition a procedure to determine the surface response to an externally variable radiant heat flux was required. To do this, a window bomb was constructed in which the surface could be viewed through a first-surface reflecting mirror. In order to allow measurement at various wavelengths, the reflected rays were passed through a sodium chloride window in the bomb wall and then into the monochromator. A purge system of N_2 was used to decrease the obstruction by the particulated gases generated by the various propellants. A schematic drawing of the apparatus is shown in Fig. 18, with photographs of the set-up in Fig. 19 and Fig. 20. For simplicity the blackbody output was calibrated against a light source and this source was used in situ in the bomb in the propellant location. A comparison with the blackbody then gave an effective beam length through the bomb's lens system which was used as the standard calibration distance of the blackbody. The first surface mirror and NaCl window did not result in any significant loss in intensity. After firing, the light source was again used to determine if the production of corrosive gases had produced any significant deterioration

III,B, Steady-State Burning Rate Measurement (cont.)

of the mirror or window and loss in intensity. Generally, the losses were small or negligible. Once in a while, however, the mirror would be sufficiently corroded to void the test results. The corrosion was found to depend primarily on the degree of purge used, and a stronger purge was then used to correct the problem of smoke or corrosion of the mirror. The light beam (at wavelength λ) emitted from the propellant surface at the temperature T is reflected by the first surface mirror and passes through a sodium chloride window into the monochromator which measures the temperature. The voltage output from the monochromator is compared to the voltage output of a blackbody source at the same wavelength and known temperature T_B. Since the propellant itself may emit less radiation than the blackbody at the same temperature, the temperature T can be determined only if the ratio of the emissive intensities between propellant and blackbody are known.

In order to determine the propellant emissivity, a reference blackbody radiation source is required. The blackbody used is an Electro Optical Industries Model 143 with an EO Model 215B Temperature Controller (all solid state). If greater precision is required, the blackbody source is equipped with a platinum resistance thermometer to be coupled into a bridge for temperature measurement of the source. The cavity emissivity is 99 $\pm$ 1%. The blackbody source has a .50 in. diameter cavity and can operate over a temperature range of 50°C to 600°C, the controller providing $\pm$ 1°C accuracy and .1°C stability. Several aperatures of nominal diameters (.200", .100", .050", .025") are available.

III,B, Steady-State Burning Rate Measurement (cont.)

a. Calibration Technique

In order to show how the temperature measurement is made, let us examine some simple principles of radiative heat transfer. For an ideal blackbody, the emissive intensity follows Planck's Law:

$$E_{\lambda B} = \frac{C_1 \lambda^{-5}}{\exp \frac{C_2}{\lambda T} - 1}$$

where $C_1 = 268$ cal μ^4/sec cm^2

$C_2 = 14{,}380\ \mu°K$

λ = wavelength in micron, $1\mu = 10^{-4}$ cm

At low wavelength readings, Wien's Law where the exponential term in (1) dominates, is used. In that case the temperatures of two bodies can be compared at the same wavelength by

$$\frac{1}{T} = \frac{1}{T_o} - \frac{\lambda}{C_2} \ln \frac{E_{\lambda B}(T)}{E_{\lambda B}(T_o)} \qquad (2)$$

Therefore we need to compare the emissive intensity, E_B, with the actual voltage reading, V_λ. Differentiating Eq. (1) at constant temperature, the maximum emissive intensity ($E_{\lambda B_{max}}$) occurs when

$$\lambda_m(\mu)\ T_m(°K) = 2898 \qquad (3)$$

Measurements at different blackbody temperatures of the wavelength at peak voltage were made, to determine if Eq. (3) was being obeyed. The result is

III,B, Steady-State Burning Rate Measurement (cont.)

shown in Fig. 21. There is an apparent shift in the peak wavelength from ideal as the temperature increases. In Fig. 22, the emissive characteristics of the blackbody are shown as well as for reference the ideal blackbody normalized for the same peak voltage and calculated from Planck's Law. Not only at 190°C, but also at other temperatures there appears to be a plateau in the 7-8μ region. Because of absorption through the atmosphere, the spectral intensity varies with distance, example measurements of the intensity at beam lengths of six and eight inches from the slit are shown in Fig. 23. If the constant C_2 were increased, the emissive spectrum would result in a narrower profile more closely duplicating the actual spectrum, but shifting the peak toward higher values of λ_m. Therefore we see that in using Planck's Law a measurement of the change in voltage with temperature must be made in order to utilize Eq. (2). Since the voltage does not follow E_λ linearly, the relationship of $V_\lambda(T_B)$ must be evaluated at the wavelength of interest.

The final characteristic of the blackbody to be considered is the exponent of λ in Eq. (1). Differentiation of Eq. (1) shows that $d \ln E_{\lambda m}/d \ln T_m = 5$. A plot of the $\ln V_{\lambda m}$ vs $\ln T_m$ in Fig. 24 shows a slope of 5.88, indicating that the emission would drop off more abruptly than an ideal blackbody at high values of λ, which is experimentally verified by Fig. 22. This higher slope accounts for the shift in peak emission to lower values of λ, as also shown in Fig. 21.

Therefore, a modification of Eq. (2) is in order. A plot of Eq. (2) in Fig. 25 using the voltage instead of the emissive intensity shows the relation (2) is usable in the form

III,B, Steady-State Burning Rate Measurement (cont.)

$$\frac{1}{T} = \frac{1}{T_o} - \frac{\lambda}{C'_2} \ln \frac{V_B(T)}{V_B(T_o)} \tag{2.1}$$

if the constant C_2 is replaced by the experimental value 16,000 μ°K for measurements at 4μ. At a wavelength of 2.2μ, C_2 is 13,700 μ°K, in good agreement with theoretical.

Finally, as was pointed out before, the emissive intensity at the same wavelength of the propellant compared to that of the blackbody will differ; the ratio is called the emissivity, ε_λ, defined by

$$\varepsilon_\lambda = \frac{E_\lambda}{E_{\lambda B}} \tag{4}$$

In order to measure the emissivity of the propellant under test, a black holder, with an aperture equal to that of the blackbody, is heated in a stream of hot nitrogen or air, and the voltage output is measured. A sample of the propellant is then placed in the hot nitrogen stream, the sample size being large enough to cover the aperture. The sample is allowed to heat up to the stream temperature, and the temperature of the sample is measured by an iron-constantan thermocouple. When temperature equilibrium is established, the voltage is again measured. The difference in voltage output is assumed due to the emission of the propellant. Comparing this voltage to that of the blackbody at the same temperature gives the emissivity, i.e.

$$\varepsilon_\lambda = \frac{V_\lambda(T)}{V_{\lambda B}(T)} \tag{4.1}$$

III,B, Steady-State Burning Rate Measurement (cont.)

Equation (2.1) using the emissivity then becomes

$$\frac{1}{T} = \frac{1}{T_o} - \frac{\lambda}{C'_2} \ln \frac{V_\lambda(T)}{V_{\lambda B}(T_o)\varepsilon_\lambda} \tag{2.2}$$

Since the propellant cannot be heated to the actual surface temperature existing during deflagration, it must be assumed that ε_λ is not a strong function of temperature. Comparative measurements over a range of 200°C did not show any significant change in emissivity. The emissivity of several propellants was determined and are shown in Fig. 27, 26a, b, c. In addition the emissivity of pure AP as measured by Powling is shown for comparison. Because of low transmissivity of AP at $\sim 3\mu$, one would expect a high emissivity at this wavelength. This is found for thin sections of pressed AP by Powling. However, the high emissivity of AP at 3μ does not appear to exist in the propellants tested. Since it is desirable to make surface temperature measurements in a region where the emissivity does not change appreciably, the region above 5μ is indicated. On the other hand the error in surface temperature measurement is reduced when lower wavelengths are used, as given by Equation (2.2). The temperature sensitivity is immediately derivable from Equation (2.2) by differentiation, namely at 237°C and $\lambda = 6\mu$.

$$\frac{\Delta V_\lambda}{T} = \frac{C'_2 V_\lambda}{\lambda T^2} = \frac{1.78 \times 10^4 \times .3}{6 \times 510^2} = .0034 \ \mu v/°K$$

It should be pointed out that the temperature as measured by Eq. (2.2) is relatively insensitive to the actual emissivity and the voltage reading

III,B, Steady-State Burning Rate Measurement (cont.)

because of the logarithmic relationship. Thus if the emissivity were .9 and unity were assumed, at $\lambda = 6\mu$, the error in the temperature would be about 20°C, or roughly 2-1/2%. If a wavelength of 2μ were used, the error would be about 7°C, which corresponds to an error in voltage reading of approximately .02 μv. This latter is close to the measured limiting voltage deflection reading of .015 μv, hence we can assume that the primary errors in surface temperature measurement will not be associated with emissivity measurements but rather with other factors, such as the accurate interpretation of the emissive intensity.

The emission at 2.2μ of a PU-AP propellant at higher temperatures was tested by slowly heating the propellant, allowing some 5 minutes for thermal equilibrium to be established between each temperature change. The results are shown in Fig. 25 and compared to the blackbody calibration curve. Samples of the propellant were removed at different temperatures for microscopic examination. Although the propellant changed from an ochre -brown - black material as the temperature was increased to the ignition threshold, there was only a slight upward shift in the relative emissive intensity. After the emissivity measurement was completed, samples were cut for microscopic examination. White speckels of porous AP were found to exist in a matrix of charred binder (black).

In addition, as is shown in Appendix IV, the actual emissivity will be somewhat different in the combustion state because of a non-uniform temperature distribution below the surface. The best check on

III,B, Steady-State Burning Rate Measurement (cont.)

the emissivity is therefore to determine if the surface temperature within reasonable agreement with the thermocouple data. This was found to be the case. Before examining the results of the surface temperature measurement, let us consider the layer of hot gases above the propellant surface during combustion.

b. Problem of Optical Measurement of T_s

Probably the most severe criticism that can be leveled against the optical procedure of measuring the surface temperature is that one must look through the layer of hot gases which envelopes the propellant and itself emits radiation. Since the emissivity decays rapidly with beam depth through the flame zone, the gas emission can be restricted by removal of the gaseous products from the surface. Powling[12] did this by sweeping the flame away from the surface with a N_2 purge. If radiation substantially affects the regression rate the temperature may be reduced considerably at higher pressures; this could possibly explain why Powling obtained a decreasing T_s with pressure. Optimally, the surface temperature should be measured at values of λ where gaseous absorption is nominal. Our measurements showed that substantially the same "surface" temperature was obtained at 2.2 and 4μ and these are wavelengths from Powling's absorption date which should be highly transmissive to radiation in depth. To further test this hypothesis grains were burned on their sides so that the flame was viewed on edge. These results showed an emissive intensity for the propellants tested of about 10-20% which would reduce the surface temperatures measured through the flame

III,B, Steady-State Burning Rate Measurement (con.)

by about 100°C. However, even on edge the propellant is hot and so some of the emission seen "on edge" would be due to the solid and not the flame. A comparison of the surface temperature as measured by the monochromator and TC is given in Fig. 28 wherefrom we conclude that the surface temperature is possibly 50°C lower because of the flame. Another proof is the response of the surface temperature, since if it were the gas phase emission, the response to depressurization should be very rapid. As is shown later, the surface temperature dramatically lags and so it would appear we are measuring the surface temperature response. Several other "gas phase" tests such as changing sample size were conducted and these also gave similar results, namely some but not an apparent overriding contribution from the gas phase.

If a solid material is highly absorptive at a given wavelength, then the radiative penetration is low and the emissivity is high. Powling (Fig. 27) noted that AP has three major absorption bands at 3, 7 and 9 and the AP emissivity was high at 3μ (absorption in the 3-4 region is due to NH, OH and CH bonds). His temperature measurements were therefore made at the wavelengths of the three major absorption bands. The relative transmissability of the PU-microatomized AP propellant shown in Fig. 49 however did not particularly correlate with the emissivity measurements (Fig. 26b); it was decided then to make measurements at wavelengths where the measured emissivity levels were higher - generally 2.2 or 4μ.

The PU-AP propellant was selected for scanning through the wavelength range of 1-6.4 μ See Fig. 29. All the temperatures calculated

III,B, Steady-State Burning Rate Measurement (cont.)

at the various wavelengths yielded reasonably identical temperatures except between 3 and ∿3.8 where a significantly lower surface temperature was obtained (∿200°C difference). This coincides with the regime where the PU-AP propellant is highly absorptive rather than transmissive. The increase in temperature due to the inclusion of the lower emissivity value is about 100°C, thus it appears that during burning the relative transmissabilities may be strongly altered. It is also possible that sufficient NH, OH and CH bonds exist in the gas phase during combustion which absorb in the ∿3μ range to substantially further reduce the energy emitted from the solid. It is not too clear at this time how the effective emissivity at different wavelengths is being altered, nor the relationship of the "isothermal" transmissivity to the actual surface energy emitted.

c. Steady-State Surface Temperatures

Three propellants were tested to determine the surface temperature as a function of pressure. These are labelled

A)	PU-AP	ΔE = 9.7 kcal/m°K
B)	PBD-AP	= 13.2 "
C)	PU-AP-2% A - catalyzed	= 14.7 "

The surface temperature as a function of pressure for these is shown in Fig. 30. The measured values are plotted in such a way as to derive an activation energy, the values being those given above. For PBD the data scatter was appreciable, however. These values are quite low, indicating a strong sensitivity to pressure. This is probably a valid judgement since

III,B, Steady-State Burning Rate Measurement (cont.)

the propellants tested were all of high burning rate slope as is usual of extinguishment propellants. These values also indicate that if extrapolated to pressures of ∿2000 psia the surface temperatures would be unreasonably high, hence that a mechanism change would occur between ∿200 psia and ∿2000 psia. However, at the higher pressures the NaCℓ crystal window is structually too weak to allow verification of this. Furthermore, at higher pressures the gas phase absorption would dominate over the emission from the surface.

A typical trace of a firing to determine $T_s(p)$ is given in Fig. 31. There appear to be fluctuations at lower pressures which tend to disappear at the higher pressures, supplementing results obtained using the TC, and indicating a less stable surface temperature than at higher pressures. There is also some decay in the intensity as the firing progresses which was accounted for by the regression of the grain away from the monochromator slit, during combustion. Just before burnout there is an unmistakable increase in the intensity, and was encountered in most of the firings. This is probably caused by the effectively higher average temperature of the profile near burnout. The durations, typically 80 msec at 15 psia for this event, correspond to ∿200 μ, i.e. the depth of the convective profile. Such an argument however, requires that the "surface" include emission from below the surface. As was shown in the previous section, significant emission can be measured through the grain.

Let us now turn our attention from the steady-state measurements to those occuring during depressurization.

C. TRANSIENT STATE MEASUREMENTS

1. Surface Temperature Response

The three propellants were tested to determine their surface temperature response during rapid depressurization. Typical traces for these are shown in Fig. 32 through 34. In every case of the many firings made, the response was sufficiently slow that the surface can be said to lag equilibrium conditions by times bordering on .5 second.

A comparison between the steady-state temperature readings and the instantaneous values are shown in Fig. 35 to 37; we note that the surface temperature remains almost constant during the initial response but settles down to the equilibrium value after some five seconds. Subsequent to these results it was deemed necessary to determine if the response capabilities of the pressure and infrared recording systems could be improved. A high response pressure transducer with a Visicorder recording at 50 in/sec showed that the pressure response was actually much faster during the initial .2 sec, but that the previous values could be used as average values. The response of the infrared could not be improved, but an estimate of the response time was obtained, and the "actual" temperature calculated therefrom. These values are shown in the graphs by dotted lines, and indicate that the beforementioned results are valid. The surface temperature measurements at ambient pressures using the planar thermocouple indicated the presence of a locally irregular surface regression. This would then be compatible with the cyclic surface temperature measurements using infra-red. During depressurization low frequency surface temperature oscillations ($\sim$20 cps) were noted as seen in Fig. 32-34, being more pronounced at 15 psia. It would therefore appear

III,C, Transient State Measurements (cont.)

plausible that the nature of the surface regression during depressurization is pulsating rather than steadily decreasing. Such an irregular regression has been visually observed by Lovine[9], and a typical case is shown in Fig. 39, where the instantaneous and steady state burning rates are shown. The surface temperature response of the three propellants has been plotted as $T_s(p)$ in Fig. 35-37 for some of the typical cases to better emphasize the temperature lag characteristics. From such data, a simple correlation between the rate at which the surface temperature responds to the average depressurization rate was obtained and is shown in Fig. 38. Note here that the aluminized propellant (with catalyst) responds slowest, polybutadiene next and the polyurethane most readily. Insufficient data are available to say that this is due solely to the binder, however polyurethane in general has been found to be more readily extinguishable which is in agreement with these results. Furthermore, there appears to be a leveling off of $\dot{T}_s$ vs $\dot{p}$ at higher depressurization rates indicating a decreasing capacity of the surface temperature to respond. It is difficult to extrapolate the curves to rates of depressurization beyond several hundred psia/sec, but at these higher levels the differences between the binder systems is probably not as important as at the lower depressurization rates. Therefore, the binder differences may show up more in terms of affecting low pressure extinguishment through curtailing p_{DL}.

III,C, Transient State Measurements (cont.)

2. Propellant Temperature Profile Response

In addition to determining the propellant's capability to respond to surface temperature changes, it was felt that a knowledge of the response capability of the entire profile would be desirable. This can be obtained only by thermocouple measurements. The problem is obvious; since the duration of the profile is only several tenths of a second, depressurization must be initiated during the time that the thermocouple sees the profile passing. Since the response time of an operator is ∿.4 sec, an initial thermocouple ahead of a second recording TC was used to tell when the depressurization would be initiated; the second TC was located at ∿500μ behind the first, to allow for the .4 sec reaction time. Many such tests were run and often the TC broke in the gas phase, probably because of the depressurization shock. A few successful tests, however, were obtained. The results show that with more sophisticated automated instrumentation the temperature profiles during depressurization can be obtained, and these would give deep insight into the actual extinguishment mechanism. Such a test result is shown in Figure 40.

The initiating profile was completely normal and reproduced the result in Figure 27, where the TC broke because it was in the gas phase at the instant of depressurization. The profile during depressurization, as shown by Figures 27 and 40, is dramatically different. At initiation of depressurization, the TC was calculated from the initiating profile to be ∿50μ below the surface. Rather than continuing to rise, the temperature actually decreased and not until several tenths of a second did it again rise.

III,C, Transient State Measurements (cont.)

Photographic coverage of the test did not reveal any abnormal flame behavior, simply a lengthening of the flame zone. Because the profile decayed, it appeared as if the surface had stopped regressing. Calculations assuming a complete interruption of the burning front were carried out for two cases, zero flux, and 20% steady-state flux. These are compared to the actual profile in Figure 41. The similarity of profiles indicates that the burning rate was essentially interrupted and that the "flux" was some 20% of the steady-state value. These results indicate further that the profile at deeper portions of the grain actually respond which is in opposition to the model proposed by Marxman[10]. We can only hypothesize reasons for the profile responding at depth at this time, but it appears that radiation and solid phase reactions must be involved. The 20% steady-state flux rate was chosen because this would be approximately the reduced flux level predicted by the Paul model for the average depressurization rate.

D. IGNITABILITY OF SOLID PROPELLANTS

If a solid acts simply as an inert thermal carrier, the application of heat flux to the surface will produce a rate of change of temperature given by Carslaw and Jaeger[2]

$$T - T_o = 2 \frac{\sqrt{\alpha/\pi}}{k} \dot{q} \sqrt{t} \left\{ e^{-x^2/4\alpha t} - \frac{x\sqrt{\pi}}{2\alpha t} \operatorname{erfc} \frac{x}{2\sqrt{\alpha t}} \right\} \qquad (5)$$

The ignition time (when T(x=0) changes to a run-away condition) should then vary with flux so that

$$t_{ig} \sim \dot{q}^{-2}$$

Experimentally, however, the exponent is generally lower, say -1.3 to -1.8, departing more drastically at high flux levels as shown in Figure 42. Secondly, the effect of grain temperature would be to shift the ignition times by substantially lesser amounts than actually observed (Figure 42). These two effects can best be explained in terms of solid phase reactions. We then must solve the transient equation

$$\frac{\partial T}{\partial t} = \alpha \frac{\partial^2 T}{\partial y^2} + \frac{ZQ}{\rho C_s} (1 - \xi)^n \exp - \frac{E}{RT} \qquad (6)$$

$$- \frac{k \partial T}{\partial y}\bigg|_s = \dot{q}$$

Equation (6) was solved by Price and Bradley[21] for n = 0, who found that prior to any significant onset of the reaction term, the curve obeys (5). We have found that the time when the temperature increase is run-away can be

III,D, Ignitability of Solid Propellants (cont.)

determined by letting the surface temperature be governed by the first order quadrature solution (i.e. neglecting the reactive contribution).

$$\frac{dT_s}{dt} = \frac{\sqrt{\alpha/\pi}}{k} \dot{q}\, t^{-1/2} + \frac{ZQ}{C_s\rho} \exp - \frac{E}{RT_s} \qquad (7)$$

The reason for this is that the Arrhenius type reaction is negligible until T_s reaches a "critical" value. Figure 43 compares the results of Price, where the run-away condition $\left(\frac{d^2T_s}{dt^2} = 0\right)$ as calculated from Equation (7) is shown as block points. The heat generation term therefore behaves as an independent factor (i.e. a solid phase vs surface ignition model is not distinguishable by ignitability data) and hence could be considered to occur at the surface; thus measurements of T_s will not be a sensitive function of the temperature profile below the surface during ignition heating. Because of this, even a small net rise in temperature above what is expected from the case of an inert solid phase can be considered to demonstrate the existence of solid phase exothermicity. This measurement was made using a TC located 200μ below the surface and a monochromator to measure the surface temperature, and the results are shown in Figure 44. The heat flux was supplied by a carbon arc illuminator operating at low rates (∿2 cal/cm^2/sec). For the case of an AP propellant, the departure from the inert profile occurs well below the phase transition and is verified by the temperature profile of this propellant during burning (Figure 7). Similar results have recently also been obtained by Inami[22] at SRI who found that $KClO_4$ acted inertly while AP acted as a solid phase heat generating source. The reactions in depth may

III,D, Ignitability of Solid Propellants (cont.)

possibly be photochemical in nature, but this has not yet been verified. This can be determined by supplying radiative heating at different wavelengths. No effect of wavelength on time-to-ignition has been observed, hence it would appear unlikely that photochemical reactions are important.

The effect of solid phase reactions on ignition was next considered for the case of an extinguished propellant. Microtomed samples of an extinguished propellant were taken from three depths of the grain, 0-40μ, 40-80μ, and 80-120μ. The DTA thermograms of these samples are shown in Figure 45 and show the presence of the first "chlorate" exotherm existing to grain depths of at least 120μ. The microtomed samples did not show any physical traces of departure from normality. An extinguished propellant therefore is not only more readily ignited but should show a higher burning rate after ignition, to depths of several hundred microns.

Two samples of AP were each taken up to 438°C, below the deflagration temperature, where some weight loss as shown by TGA has occurred. Allowing these samples to cool and reheating produced the DTA thermograms shown in Figures 46 and 46-a. The small "chlorate" exotherm initially at 320°C was shifted to a lower temperature and more energetic exotherm, the exothermicity increased strongly with heating rate. These results indicate that heat treated AP decomposition goes by at least three different mechanisms. The first exotherm is probably associated with some "chlorate" impurities, and this reaction can be driven to completion prior to deflagration. It is possibly also generated by pre-heating through radiation during the burning phase. The

III,D, Ignitability of Solid Propellants (cont.)

other two mechanisms were discussed and behave as untreated AP. Reheating a PBD-AP propellant produced similar results (Figure 46-b), but it should be noted that an exotherm appears to exist prior to the 242°C endotherm.

Let us suppose that an interruption of the burning rate has occurred during depressurization. The propellant now can be reignited more readily and in a motor where heat flux can continue even after extinguishment, reignition is likely to ensure. The effect of heat flux and pressure on ignition are shown in Figure 47 for a typical extinguishable propellant. At normal operating conditions during extinguishment, the time to ignite a subsequent layer which might have been (temporarily) extinguished, is from .5 to .1 the original ignition time. These shorter times to ignition are available to the propellant since depressurization rates are generally not high enough in a motor to completely vent the system. The data presented in Figure 47 show that the chemical induction time of the solid phase (t_o) has been changed by depressurization, but not the gas phase lower ignitability pressure; this is again further evidence of solid phase reactions controlling the decomposition process leading to ignition and then burning. The slope of t_{ig} vs $\dot{q}$ is reduced to a -1.3 relationship indicating a large departure from the "inert" case. Motor extinguishment tests therefore would appear to be as much a measure of reignitability as of extinguishability.

Permanent extinguishment then requires that the depth of the reaction profile must be extended into the grain sufficiently that reignition is prevented, making sustained extinguishment at high pressures generally impossible.

DISCUSSION OF RESULTS

The experimental data taken during the course of this program strongly suggest that the solid phase is not a chemically inert material nor acts as a simple thermal conductor of energy. Rather it is a highly reactive substance and is transmissive to radiation. Sufficient solid phase exothermicity appears to be available to actually determine the burning rate, at least at low pressures, while the radiant transmission is to such depths as to substantially preheat the propellant. Because these conclusions are in conflict with the generally accepted gas phase theory, it would be amiss not to comment further.

Primary evidence for ruling out the solid phase comes from thermocouple measurements; for a chemically inert, conductive substance $\ell n\ (T-T_o)$ vs. x would be linear. Calculations and closer scrutiny of data (in the lieterature as well as our own), however show several discrepancies with the inert model. There would be no reason for the diffusivity to change with pressure, as has been found to be the case, nor to account for high diffusivities deep into the grain. Furthermore, thermocouple data always have slight undulations in them - previously explained in terms of propellant heterogeneity. These undulations now are correlated with DTA, and we feel that the differentiated temperature traces too closely resemble the DTA traces to be purely coincidental. If we then consider that the thermal diffusivity is effectively a measure of radiative and conductive heat flux and therefore depends on pressure through reaction rate and emissivity, the superimposition of radiation on solid phase reactions

Discussion of Results (cont.)

becomes more plausible.

By radiative superimposition we do not mean to imply that convective heat flux is not important, but rather that the radiative flux is substantially greater than has generally been believed. The radiative role will be especially pronounced at low pressures because the gradient will be shallow and the emissivity will be high, thus leading to increased heat losses from the surface to the gases and finally extinguishment. Poorer combustion should also be anticipated. Temperature profile and $\dot{T}(t)$ measurements near the lower pressure deflagration limit should result in a better understanding of the factors governing P_{DL}. To demonstrate the radiative role, we have used carbon black in the PBD propellant and been able to drastically decrease the burning rate and slope. Carbon black is however catalytic so that the radiation hypothesis is not completely verified by this preliminary test. The use of ZrC, which is inert, and decreases radiation, should clarify this point.

The transient response of the profile at depth indicates an unexpectedly fast response mechanism; certainly the response is faster than would be indicated by a conductive wave. The radiative wave has been shown to be capable of establishing itself an order of magnitude faster than the conductive wave and would result in a shallower profile during depressurization leading to higher emissivity and radiative heat losses. Therefore it appears possible that radiation may play a key role in extinguishment, something which is correlated with the fact that propellants compsed of small AP particles extinguish easier. However, more data are necessary to more clearly define this effe t.

Discussion of Results (cont.)

The transient response measurements show that the surface temperature lags equilibrium for a significant duration during depressurization and that this inability to react and reach equilibrium increases as the depressurization rate is increased. This would mean that the Paul model is more realistic. The data indicate that PU is a faster responding binder material than PBD and would explain why the former is generally more easily extinguishable.

The increased ignitability of solid propellants following extinguishment has been traced to solid phase reactions of greater exothermicity, changing the time-to-ignition vs flux to a more sensitive functional relationship.

We conclude by noting that solid phase reactions and radiation give a propellant a dynamic quality in which the ballistic properties are affected by the thermal history of the propellant, as evidenced by increased reignitability of a surface following extinguishment and by the changing emissivity produced by changes in the temperature gradient. This dynamic quality will result in the burning rate of a propellant being different under ostensibly similar ambient conditions. A propellant which has been extinguished will thus burn at a higher rate when reignited. Casting against different surfaces, changes in the igniter induced thermal flux pattern, and changes in the radiative flux induced by motor geometry (especially at low pressures) will be some of the specific factors altering the motor burning rate.

APPENDIX I

DERIVATION OF STEADY-STATE AND TRANSIENT BURNING RATE MODEL

A. STEADY-STATE

The steady-state model presented below examines the flame structure in the gas phase and the related thermal structure allowing chemical reactions in the solid phase. The results are discussed in the text. The boundary conditions are stipulated by which the separate solid-gas phase descriptions are related to yield a unique burning rate.

Zeldovich Equations

The heat flux and enthalpy leaving a section is equal to the flux and enthalpy into the section plus the heat liberated by chemical reactions, i.e., for steady-state combustion

$$\frac{d}{dy}\left[r\rho_s(C_pT) + \dot{q}\right] = QJ$$

where J is the rate of reaction. In the solid phase, we assume

$$J = Z(1-\xi)^n\, e^{-E/RT}$$

while in the gas phase, the reaction rate requires a density dependence

$$J = Z'\rho^n\,(1-\xi)^n\, e^{-E/RT}$$

Similarly, the extent of the reaction is governed by the mass flow due to convection and diffusion, so that

$$\frac{d}{dy}\left[r\rho_s\xi - D\rho\,\frac{d\xi}{dy}\right] = J$$

In the solid phase, D is negligible.

Now the heat flux, $\dot{q}$, is assumed governed by Fourier's law, i.e., for conduction alone

$$\dot{q} = -k \frac{dT}{dy}$$

The above statements can be derived in terms of several simultaneous reactions and the relative diffusion of all the species; see Hirschfelder and Curtiss[9]. However, our purpose here is to determine a general structure, and the extent of the reaction, ξ, defined as usual in Irreversible Thermodynamics (see Prigogine[13]) allows for this. Similarly, the properties, C_p,k,D... are themselves pressure and temperature sensitive. These changes would have a secondary influence on the preliminary results desired, hence will be assumed constant here. However, the relative value of D to α called the Lewis Number, Le, is important and is considered.

Using the nomenclature defined in the glossary, the mass and energy balances reduce to the following:

Solid Phase $\qquad -\infty \leq y < 0$

$$r\rho_s \frac{d\xi}{dy} = \rho_s Z(1-\xi)^n e^{-E/RT} \tag{1.1}$$

$$r\rho_s \frac{dT}{dy} - \alpha\rho_s \frac{d^2T}{dy^2} = \frac{Q\rho_s Z}{C_s} (1-\xi)^n e^{-E/RT} \tag{1.2}$$

Z [=] $\sec^{-1}$

Gas Phase

$$G = \xi - \frac{D\rho}{r\rho_s} \frac{d\xi}{dy} \qquad 0 < y \leq +\infty \tag{2.1}$$

$$r\rho_s \frac{dG}{dy} = r\rho_s \frac{d}{dy} - D\rho \frac{d^2\xi}{dy^2} = Z'\rho^n (1-\xi)^n e^{-E/RT} \tag{2.2}$$

$$r\rho_s \frac{dT}{dy} - \alpha\rho \frac{d^2T}{dy^2} = \frac{Q}{C_p} Z' \rho^n (1-\xi)^n e^{-E/RT} \qquad (2.3)$$

$$Z' \ [=] \ \sec^{-1} \left[\frac{gm}{cc}\right]^{-(n-1)}$$

In a gas, $\alpha\rho$ is mainly temperature dependent, however for our purposes it suffices to use an average value.

Boundary Conditions

The boundary conditions at the edges of the combustion zone by definition require no transport of energy and completion of the reaction, i.e.,

$$y \longrightarrow -\infty \qquad \left.\begin{array}{l} \frac{dT}{dy} \longrightarrow 0 \\ \xi \longrightarrow 0 \end{array}\right\}$$

$$T = T_o$$

$$y \longrightarrow +\infty \qquad \left.\begin{array}{l} \frac{dT}{dy} \longrightarrow 0 \\ \frac{dG}{dy} = \frac{d\xi}{dy} \longrightarrow 0 \end{array}\right\}$$

$$\xi = G \longrightarrow 1$$

$$T = T_f$$

At the hot edge ($+\infty$) of the combustion zone, an indeterminacy arises from the ratio of (2.2) to (2.1), namely

$$\frac{\frac{d}{dy}\left[T - \frac{\alpha\rho}{r\rho_p} T_y\right]}{\frac{d}{dy} G} = \frac{Q}{C_p}$$

However, for the simple case of the function of J used above, it can be shown that $J \longrightarrow 0$ sufficiently fast that dT/dG is uniquely defined.

The equations, (1) and (2), can be integrated when the functions are assumed continuous. At the gas-solid interface we assume a Stieltjes-Lebesgue integration is possible where the surface reactions (J) are allowed to generate heat. Equation (2.1) then becomes

$$r\rho_s [C_p T_s - C_s T_s] + \left(\frac{-k\ dT}{dy}\right)_g - \left(\frac{-k\ dT}{dy}\right)_s = Lr\rho_s \qquad (3)$$

where L now represents the heat liberated from all the possible types of surface reactions including vaporization and reactions which may be either pressure dependent or independent. Similarly, since no mass is created at the surface, (2.1) integrates to

$$r\rho_s G_s - r\rho_s \xi_s = 0 \qquad (4)$$

Equation (4) is that assumed by Hirschfelder and Curtiss[9]. It should be noted that (3) and (4) also follow from an overall mass and energy balance. Thus, integrating (1.1) and (1.2) from $-\infty$ to the surface

$$r\rho_s \xi_s = \int_{-\infty}^{o} Z(1-\xi)^n\ e^{-E/RT}\ dy = \frac{C_s}{Q}\left\{r\rho_s(T_s-T_o) - \alpha\rho_s\left[-\left|\frac{dT}{dy}\right|_s\right]\right\} \qquad (1.3)$$

and in the gas phase from the surface to $+\infty$,

$$r\rho_s(1-G_s) = \int_{o}^{\infty} Z'^{\,n}(1-\xi)^n\ e^{-E/RT}\ dy = \frac{C_p}{Q}\left\{r\rho_s[T_f-T_s] - \alpha\rho\left[-\frac{dT}{dy}\right]_s\right\} \qquad (2.4)$$

Using (1) and (2.4) in (3), and remembering that $k = \alpha\rho C$

$$\rho_s [C_p-C_s]\ T_s = \rho_s \left\{L + [Q\ (1-G_s) - C_p(T_f-T_s)]\ C_p + [\xi_s\ Q - C_s(T_s-T_o)]\right\}$$

or

$$L + Q(1-G_s) + Q\xi_s = C_p T_f - C_s T_o \qquad (5)$$

Since the RHS of (5) must equal the total enthalpy change, Q+L, we must again stipulate (4).

The burning rate can then be calculated if the following parameters are known: $Z,Z',n,E,T_f,T_o,T_s,\alpha,D,Q,\xi_s,C_p,C_s,L$. Obviously, the major difficulty lies in experimentally determining these values. As an example, the heat of reaction in the gas phase can only be estimated. Thus if we assume that the enthalpy content at some intermediate gas temperature ($T<T_f$) corresponds to the equilibrium composition at that enthalpy, the temperature can be determined. For instance, for pure AP, we have made thermodynamic calculations at 1 atmosphere which show that the composition does not change appreciably in the flame temperature range:

At	$1373°K = T_f$	1300°K
Mole fraction:	$[HCl] = .234$	.2345
	$[N_2] = .118$	.118
	$[H_2O] = .354$	.3535
	$[O_2] = .294$	.294
Enthalpy	370.6 cal/g	344.6 cal/g

Thus apparently, 26.0 cal/g are required to raise the temperature from 1300 to 1373°K. This is in reasonably good agreement with the enthalpy change $C_p(73) = 24.6$ cal/g required. A reasonable heat of reaction for the gas phase, considering a surface temperature of 475°C, therefore appears to be 220 cal/gm. This value is comparable to values determined for the solid phase decomposition of AP.

The latent heat, L, the extent of the reaction at the surface, ξ_s, and Z' and E for the gas are at this time beyond being measured or even

estimated. However, instability (combustion) measurements may eventually allow some reasonable estimated of L to be determined. The solid phase kinetics can be estimated using DSC. The order of reaction in the gas phase, n, is estimated as twice the burning rate slope; as will be shown later this is only an approximation. The various diffusivities can be measured and at least for the solid up to relatively high temperatures approximately estimated above that. Finally, the surface temperature can be measured, and these values will be used in the burning rate model. Thus we see that it is mainly the gas phase for which kinetic and thermodynamic data are not available. From Eq. (1.3) we obtain

$$\frac{Q}{C_s}\,\xi_s = T_s - T_o - \frac{\alpha}{r}\,T_{ys} \qquad (1.3.1)$$

If T_s and αT_{ys} can be reasonably measured from the temperature profile, $\frac{Q\xi_s}{C_s}$ can be evaluated. However, as we shall show in the following section, when Q/C_s is small, even large changes in Q do not change the burning rate appreciably, hence the inverse is true, the burning rate data do not provide a sensitive means of calculating Q. Since Q of the deflagration process cannot be obtained from DTA, it appears that use of another type of instrument such as a differential scanning calorimeter is required.

B. RESULTS OF COMPUTER CALCULATIONS

1. Solid Phase

The solid phase equations can be integrated by multiplying (1.1) by T_y and eliminating J between (1.1) and (1.2). Thus

$$r\,d\xi\left[T_y = \frac{r}{\alpha}\left(T - T_o - \frac{Q}{C_s}\xi\right)\right] = z'(1-\xi)^n \exp -\frac{E}{RT}\cdot dT \qquad (1.4)$$

Generally, only a small fraction of the total reaction is completed in the solid phase and ξ decreases to a negligible value for $T \approx .9\ T_s$. Therefore, we can integrate (1.4) directly to

$$r^2 = \frac{\alpha z'(1-\xi_s)^n \int_{T_o}^{T_s} \exp -E/RT\ dT}{\left[.95\ T_s - T_o - \frac{Q\ \xi_s}{2\ C_s}\right] \xi_s} \tag{1.5}$$

It is not difficult to show that for $E/RT \gg 1$, the integral is essentially $e^{-E/RT_s}\ RT_s^{\ 2}/E$. Comparison of (1.5) with the exact computer calculation shows that the burning rate so calculated is within a few percent of the exact value.

2. Gas Phase Calculations

When the Lewis number is unity, the gas phase equations can be combined to give

$$\frac{Q}{C_p} \frac{d}{dy} \left(\xi - \frac{\alpha\rho}{r\rho_s}\ \xi_y\right) = \frac{d}{dy} \left(T - \frac{\alpha\rho}{r\rho_s}\ T_y\right) \tag{2.5}$$

$$\xi = \xi_s + \frac{C_p(T-T_s)}{Q} \tag{2.6}$$

Using the second boundary condition

$$\xi_s = 1 - \frac{C_p}{Q} (T_f - T_s) \tag{2.7}$$

Thus only if $Q = C_p(T_f - T_s)$ can the gas phase reactions begin at a vanishingly small extent of reaction in the solid phase. In general, however, ξ should be finite to allow for solid phase reactions. More generally, when the Lewis number is not equal to unity, the general solution is

$$\xi = 1 - \frac{C_p}{Q}(T_f - T_s) + (\psi - \psi_\infty) \exp \frac{r\rho_s y}{\alpha\rho}$$

where $$\psi = \frac{Le-1}{Le} \int_0^\xi \exp \frac{-r\rho_s y}{\alpha\rho} d\xi; \quad \psi_\infty = \lim_{\xi \to 1} \psi$$

Thus the effect of diffusion is to shift the extent of the reaction closer to the surface as Le is decreased. However, the burning rate is essentially determined by the maximum reaction rate, J_m, and this value is not drastically altered by small deviations in Le away from unity, hence the burning rate is nearly that for the case of Le=1.

Just as in the case of solid phase reactions, Eqs. (2.2) and (2.3) can be combined to yield the temperature gradient

$$\frac{\alpha\rho}{r\rho_s} T_y = [T - T_f] + (1-G)\frac{Q}{C_p}$$

and the diffusion parameter is then given for Le=1

$$r\rho_s \frac{dG}{dT}\left\{T_y = \frac{r\rho_s}{\alpha\rho}\left[T - T_f + \frac{Q}{C_p}(1-G)\right]\right\} = z' \left(\frac{p}{E}\right)^n \left(\frac{1-\xi}{RT/E}\right)^n e^{-E/RT}$$

Hence
$$(r\rho_s)^2 = \frac{\alpha\rho z' \left(\frac{p}{E}\right)^n \int_{\theta_s}^{\theta_f} \left[\frac{C_p E}{Q R}\right]^n \left(\frac{\theta_f - \theta}{\theta}\right)^n e^{-1/\theta} d\theta}{\int_{G_s}^{1} (\theta - \theta_f)\, dG + \frac{QR}{C_p E}\left[\frac{1-G_s^2}{2}\right]} \qquad (2.8)$$

where $\theta = RT/E$

Now the integrals in the numerator and denominator are dominated by the maximum reaction rate, i.e., when

$$J = \left(\frac{\theta_f - \theta}{\theta}\right)^n e^{-1/\theta}$$

is a maximum. This occurs at a θ value of

$$\frac{RT_m}{E} = \theta_m = \frac{\theta_f}{1+n\,\theta_f}$$

for which $J_m = \left(\frac{n\theta_f}{e}\right)^n \exp -1/\theta_f$

Comparison with exact computer calculations shows that the integrals can be reasonably well approximated by $1/2\ J_m/(1-G_s)$ and $(\theta_m - \theta_f)(1-G_s)$ and Eq. (2.8) becomes

$$(r\rho_s)^2 = \frac{\frac{1}{2}\alpha\rho z' \left(\frac{pC_p nT_f}{QEe}\right)^n e^{-E/RT_f}}{(1-G_s)^2\left[\theta_m - \theta_f + \frac{QR}{C_p E}\frac{1-G_s}{2}\right]}$$

A more exact integration of Eq. (2.8) would include the lower limit of surface temperature, which would replace the activation energy term by $\left[\exp -E/RT_f - \exp -E/RT_s\right]$; the latter term is essentially negligible. Thus the gas phase burning rate is essentially independent of surface temperature until T_s approaches T_m, which has been verified by computer calculations. As $T_s \longrightarrow T_m$, the burning rate decreases sharply because the gas phase reactions cannot dispose of the reactant species coming from the solid.

Finally, it is necessary to point out how convergence of a solution is achieved. Two criteria must be fulfilled simultaneously, $\frac{dT}{dy} \longrightarrow 0$ and $\psi \longrightarrow \psi_\infty$ as $y \longrightarrow +\infty$. By reiteration a burning rate is selected and the calculations through the profile are carried out. As is

seen from Fig. 3-A, the solutions for too large or too small a burning rate are quite different and the burning rate can be accurately determined even if the convergence criteria are not precisely met. The burning rate equations can be rearranged into dimensionless groups to give

$$\frac{d\theta}{dy} = \theta - \theta_f + A(1-G)$$

$$\frac{dG}{d\theta} = \frac{\left(B\,\frac{1-\xi}{\theta}\right)^n e^{-1/\theta}}{\theta - G_f + A(1-G)}$$

$$\xi = 1 - \frac{\theta_f - \theta}{A} + (\psi - \psi_\infty)\, e^{y'}$$

where $y' = \frac{yr}{\alpha}$

$$B = \frac{z'\alpha\rho}{(r\rho_s)^2}\left(\frac{p}{E}\right)^n$$

$$A = \frac{QR}{C_p E}$$

C. TRANSIENT-STATE EQUATIONS

The complexity of the partial differential equations describing the burning rate under transient conditions requires that some simplifying statements be invoked. Although this prevents an exact mathematical description from being obtained, the most important features of the burning rate response to transient pressure conditions can be determined. The transient reaction and energy balances are given by

mass: $\frac{\partial \xi}{\partial t} - r\xi_y = \dot{\xi}$

energy: $\frac{\partial T}{\partial t} = \alpha\, T_{yy} - r(t)\, T_y - \frac{Q_s}{C_s}\dot{\xi}$

where $\dot{\xi} = z(1-\xi)^n \exp(-E/RT)$

Combining the aforementioned mass and energy balances

$$\frac{\partial}{\partial t}\left(T-T_o - \frac{Q_s\xi}{C_s}\right) = \alpha \frac{\partial^2}{\partial y^2}(T-T_o) - r\frac{\partial}{\partial y}\left(T-T_o - \frac{Q_s\xi}{C_s}\right) \qquad (6)$$

The reaction extent decays over such a small temperature differenct that the extent of the reaction can be assumed to vary almost linearly with temperature in the reaction profile of the grain. A negligible error is then incurred by including $\left(-\frac{Q_s\xi}{C_s}\right)$ in the second derivative term. With this addition, Equation (6) assumes the familiar Fourier heat transfer form.

Introducing the variable

$$V = \frac{T - T_o - Q_s\,\xi/C_s}{T_{s_o} - T_o - Q_s\,\xi_s/C_s}$$

the transient heat conduction equation can be written

$$\frac{\partial V}{\partial t} = \alpha \frac{\partial^2 V}{\partial y^2} - r\frac{\partial V}{\partial y} \qquad (7)$$

Let $F = \frac{\partial V}{\partial y}$ (8)

Differentiate (7) with respect to y

$$\frac{\partial^2 V}{\partial y \partial t} = \frac{\partial F}{\partial t} = \frac{\partial}{\partial y}\left[\alpha\frac{\partial F}{\partial y} - r\,F\right] \qquad (10)$$

The flux function, F, is governed by the same partial differential equation as the temperature.

The initial condition is given by the steady-state solution prior to onset of depressurization.

$$1. \quad v(t=0) = \exp \frac{r_o y}{\alpha}$$

$$\text{or } F(t=0) = \frac{r_o}{\alpha} \exp \frac{r_o y}{\alpha}$$

Since we desire to determine how the temperature profile responds to a change in flux, it is necessary to describe the flux during extinguishment in a realistic fashion, e.g., realistic in terms of motor conditions. Since the flux at the surface was shown to be proportional to p^n, and during depressurization $\dot{p}/p$ tends to remain essentially constant [9], we can let

$$F \sim p^n$$

$$\text{or } \dot{F} \sim n\dot{p}\, p^{n-1} = nF \frac{\dot{p}}{p}$$

This boundary condition simply stipulates that the gas generated by the propellant does not contribute sufficient mass to change the pressure. Integrating $F = F_o \exp \frac{n\dot{p}t}{p}$

Hence, the second boundary condition assumes an exponential decay:

$$2. \quad F(y=0) = F_o \exp(-Kt) \quad t \geq 0$$

Comparison of Equations (8) and (9) at $t = 0$ gives $F_o = r_o/\alpha$.

Finally, in steady-state, the burning rate can be assumed to depend on the surface temperature in a form given by Equation (1). Note that this form still allows chemical reactions in the solid phase to be controlling. Now as the surface temperature decreases with a decreasing flux, the steady-state burning rate will also decrease. It is obvious that the temperature decrease during depressurization precedes the reduction in burning rate.

3. The second and final boundary condition requires that as $y \longrightarrow -\infty$, the gradient must vanish, i.e.,

$$F(-\infty,t) = 0$$

To solve Equation (9), we use the Laplace transform which is defined by

$$f(y,s) = \int_o^\infty e^{-st} F(y,t)dt$$

Applying this to Equation (9), we obtain

$$sf - F(t=0) - \alpha \frac{d^2f}{dy^2} + \frac{d}{dy} \int_o^\infty e^{-st} F(y,t)\, r\, dt = 0$$

Since the burning rate as a function of time is the unknown desired to be determined, we use a Laplacian average burning rate, $\bar{r}$, so that we obtain finally

$$\alpha \frac{d^2f}{dy^2} - \bar{r} \frac{df}{dy} - sf = - F_o \exp \frac{r_o y}{\alpha}$$

The solution to Equation (10) has the form

$$f = A \exp my + B \exp \frac{r_o y}{\alpha} \qquad (10)$$

Applying the boundary condition, Equation (9), evaluation of the constants gives

$$\left.\begin{aligned} A &= \frac{F_o}{K+s} - \frac{F_o}{s + \dfrac{\bar{r}\, r_o - r_o^2}{\alpha}} \\ B &= \frac{F_o}{s + \dfrac{\bar{r}\, r_o - r_o^2}{\alpha}} \\ m &= \frac{\bar{r}}{2\alpha} - \frac{\bar{r}}{2\alpha}\sqrt{1 + \frac{4s\alpha}{\bar{r}^2}} \end{aligned}\right\} \qquad (11)$$

Inverting the Laplace transform of (10) using Equation (11) yields Equation (6) in the text.

APPENDIX II

EFFECT OF EROSIVE BURNING ON CHEMICAL REACTIONS

Many empirical descriptions of erosive burning are available in the literature, and models of the heat transfer mechanism, such as Corner[3], have been put forth. However, the contribution of chemical kinetic and thermodynamic variables on erosive burning has not been clearly defined.

The momentum boundary layer equation is given by Schlichting

$$U^2 \frac{d\theta}{dx} + \frac{11}{2} \theta U \frac{dU}{dx} = v_*^2 \qquad \text{(C-1)}$$

where $v_o = \frac{r\rho_s}{\rho}$

U is the mean stream velocity

v_* is the friction velocity

θ is the momentum boundary layer thickness

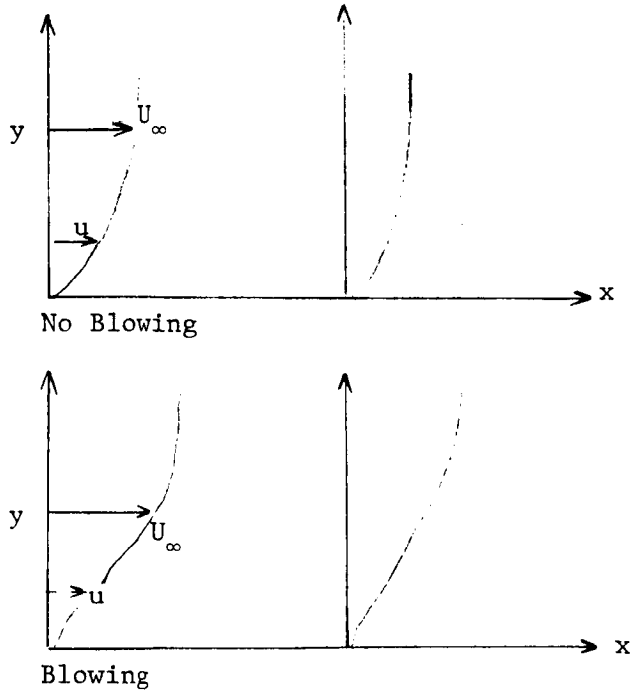

The heat flux to the surface is given by

$$q = -k \left(\frac{dT}{dy} \right)_s \tag{C-2}$$

Similarly, the friction velocity at the wall is given by

$$v_*^2 = \left(\frac{\partial u}{\partial y} \right)_s \tag{C-3}$$

It is beyond the scope of this analysis to determine the various possible friction velocities with mass addition, since these also depend on the bulk stream velocities and geometries. However, by analogy between (C-2) and (C-3), we see that if the thermal conductivity is replaced by an effective turbulent value, $(k + k_T)$, and if we assume that the conductivities are related to the turbulent kinematic viscosities by analogy of (2) and (3), i.e., $\frac{k_T}{k} = \frac{\nu T}{\nu}$, then the added heat flux augmenting burning rate can be solved if $v_*(U)$ is defined.

First of all, no appreciable augmentation in flux occurs until $v_*^2 >> v_o U$, since until then the boundary layer thickness does not grow appreciably. Hence, the burning rate would not be augmented until some threshold velocity, U, is reached. Empirical data generally correlate the burning rate in terms of an erosive constant, K_v, so that

$$\frac{r_t}{r} = 1 + R_v(U-U_o) \tag{C-4}$$

At low velocities, the turbulent core which displaces the temperature profile closer to the grain surface will not markedly change the temperature profile in the immediate gasification zone. Let us now consider the chemical kinetic factors entering into the erosive constant.

The augmentation in burning rate due to an increased heat flux at the surface caused by turbulence would result in an increase in surface temperature, so that from Appendix I,

$$\frac{r_t}{r} = \exp\left\{-\frac{E}{2R}\left[\frac{1}{T_{s,t}} - \frac{1}{T_s}\right]\right\} \tag{C-5}$$

where the subscript, t, refers to turbulent conditions.

Similarly, from the solid phase equation

$$\alpha_s \frac{d^2T}{dx^2} + r\frac{dT}{dx} = \frac{Q_r}{C_s}\frac{d\xi}{dx} \tag{C-6}$$

the flux at the solid interphase is

$$-k_s\left(\frac{dT}{dx}\right)_s = r\,\rho_s C_s\left(T_s - T_o - \frac{Q\xi_s}{C_s}\right) \tag{C-7}$$

which is related to the flux from the gas phase by

$$-k_s\left(\frac{dT}{dx}\right)_s = -k\left(\frac{dT}{dx}\right)_g + L\rho r \tag{C-8}$$

where L is the heat of reaction of surface reactions. Under turbulent conditions, the effective thermal conductivity, $k + k_t$, gives

$$r_t\rho_s C_s\left(T_{s,t} - T_o - \frac{Q\xi_s}{C_s} - \frac{L}{C_s}\right) = -(k + k_t)\left(\frac{dT}{dx}\right)_g \tag{C-9}$$

The turbulence changes the local heat flux throughout the gas temperature profile so that the energy balance is given by

$$-\frac{d}{dx}(k + k_T)\frac{dT}{dx} = C_p\rho\, r_t\frac{dT}{dx} - \dot{Q}_r \tag{C-10}$$

In order to solve Eq. (C-10), let us assume that the temperature profile consists of two zones, a heating zone and a chemical reaction zone. Although this technique is not useful in solving (10) exactly for r_t, we are interested only in comparing r_t to r and the errors introduced by creating two zones should be negligible.

In the chemical reaction zone (neglect dT/dx), so that integrating (1) up to the end of the reaction zone

$$- (k+k_T)^2 \left(\frac{dT}{dx}\right)_g^2 = 2 \int_{T_{s,t}}^{T_1} \dot{Q}(T)\, dT\, (k + k_T)$$

Calling $$T_o + \frac{Q\xi_s}{C_s} + \frac{L}{C_s} = T_o' \qquad \text{(C-11)}$$

$$\left[r_t \rho_s C_s (T_{s,t} - T_o')\right]^2 = 2\,(k+k_T) \int_{T_{s,t}}^{T_1} \dot{Q}(T)\, dT$$

Under non-erosive conditions

$$\left[r \rho_s C_s (T_{s_1} - T_o')\right]^2 = 2\, k \int_{T_s}^{T_1} \dot{Q}(T)\, dT$$

The major difference between the two integrals is due to the difference in surface temperatures, i.e., $\int \dot{Q}(T)\, dT \approx Q_g (T_1 - T_s)$; hence,

$$\left(\frac{r_t}{r}\right)^2 = \left(1 + \frac{k_T}{k}\right) \left\{ \frac{T_1 - T_{s,t}}{T_1 - T_s} \left(\frac{T_s - T_o'}{T_{s,t} - T_o'} \right)^2 \right\} \qquad \text{(C-12)}$$

The bracket term is of order of unity, since the surface temperature does not have to change appreciably in order to change the burning rate strongly.

In the heating zone, neglecting $\dot{Q}$, we have

$$\frac{d}{dx}(k + k_t)\frac{dT}{dx} = - r_t \rho_s C_p \frac{dT}{dx}$$

Integrating once, we get

$$\frac{dT}{dx} = \left(\frac{dT}{dx}\right)_g - \frac{r_t \rho_s C_p}{k+k_t}(T-T_{s,t})$$

Integrating a second time, we get

$$T-T_{s,t} = - \frac{r_t \rho_s C_p (T_{s,t}-T_o')}{k+k_t} \exp\left[- r_t \rho_s C_p \int \frac{dx}{k+k_t}\right] \int e^{r_t \rho_s C_p \int \frac{dx}{k+k_t}} dx$$

Although k_t is a function of x, the effect of the exponential is to cancel this dependency, hence to a close approximation

$$\frac{T-T_o'}{T_{s,t}-T_o'} = \exp - r_t \rho_s C_p \int \frac{dx}{k+k_t}$$

Using x in the negative direction, and integrating up to a point, x, where the temperature is T_1

$$\ell n \frac{T_1-T_o'}{T_{s,t}-T_o'} = r_t \rho_s C_p \int_o^{X_1} \frac{dx}{k+k_t}$$

Hence

$$\frac{r_t}{r} = \frac{\left(\int \frac{dx}{k+k_t}\right)^{-1}}{r \rho_s C_p} \ell n \frac{T_1-T_o}{T_{s,t}-T_o'} = \psi \qquad \text{(C-13)}$$

Using (12) and (13),

$$\left(\frac{r_t}{r}\right)^2 = F(T)\left[1 + \frac{k_t}{k}\right] = \psi^2$$

or

$$\left(\frac{r_t}{r}\right)^2 = F(T) + \frac{\frac{k_t}{k}\psi^2}{1 + k_t/k}$$

$$\left(\frac{r_t}{r}\right)^2 = \left\{\frac{T_1-T_{s,t}}{T_1-T_s}\left(\frac{T_s-T_o'}{T_{s,t}-T_o'}\right)^2\right\} + \frac{\left[\frac{1}{r\rho_s C_p}\,\ell n\left(\frac{T_1-T_o'}{T_{s,t}-T_o'}\right)\right]^2\left(\int_o^{x_1}\frac{dx}{k+k_t}\right)^{-2}}{1 + k/k_t}$$

$$= \exp -\frac{E}{R}\left(\frac{1}{T_{s,t}} - \frac{1}{T_s}\right) \qquad \text{(C-14)}$$

This second term on the right hand side can be reduced to a form involving the friction velocity, by introducing the turbulent viscosity, thus

$$r\rho_s C_p\left(\int\frac{dx}{k+k_t}\right)\sqrt{1+k/k_t} = \frac{r\rho_s}{v_*\rho}\,P\sqrt{1 + \nu/\nu_t}\int\frac{dx\ v^*/\nu}{1 + \nu_t/\nu}$$

where P is the Prandtl number, typically about unity.

APPENDIX III

DIFFERENTIATING CIRCUITRY

Figure A-1 shows the circuit design used to differentiate the voltage signal, e_1, except that the "bound" circuit was found to be unnecessary for the signals processed. Figure A-2 illustrates the voltage-gain vs frequency (log-log) for the typical circuitry. Ghe breakover frequency, w_c, should be chosen through proper selection of C_d, R_d, R_i, C_i, to be about one decade above the highest frequency signal to be processed. Even then some departure from ideal differentiation will occur, namely a decrease in ideal amplitude and a phase lag, respectively of 1% and -11.4°. Suppose that w_c is set at some typical value, and differentiation is without appreciable error. Any attempt to increase w_c will result in an increase of the voltage output of the intrinsic noise level of the circuit, until the output noise level is intolerable. At the other extreme, if w_c is made too small, higher frequencies in the input spectrum will be grossly distorted. For the present case of differentiating the thermocouple voltages, the following values were used:

R_d = 200,000 Ω

C_d = 0.15 mfd

R_i = 2,000 Ω

C_i = 4,000 pfd

DIFFERENTIATING CIRCUIT

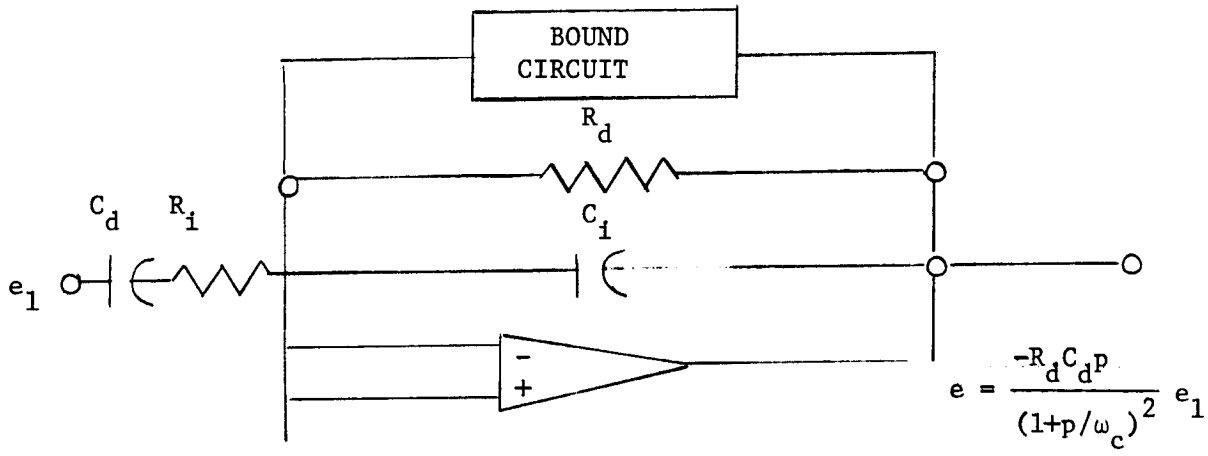

Figure A-1 $p(.) = \frac{d(.)}{dt}$

VOLTAGE GAIN VS FREQUENCY FOR DIFFERENTIATING CIRCUIT

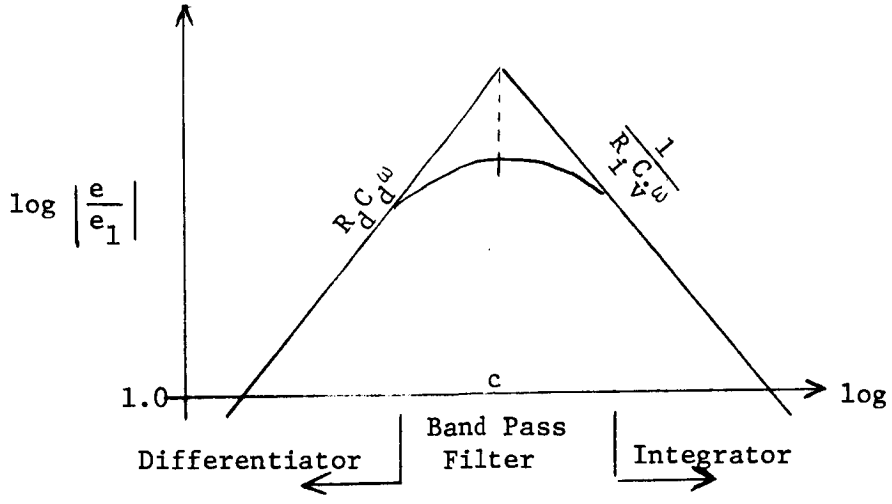

Figure A-2

APPENDIX IV

RADIATION EFFECT IN A BURNING PROPELLANT

Consider the temperature profile in Figure A-3 where a radiator source is superimposed on the convective gas profile.

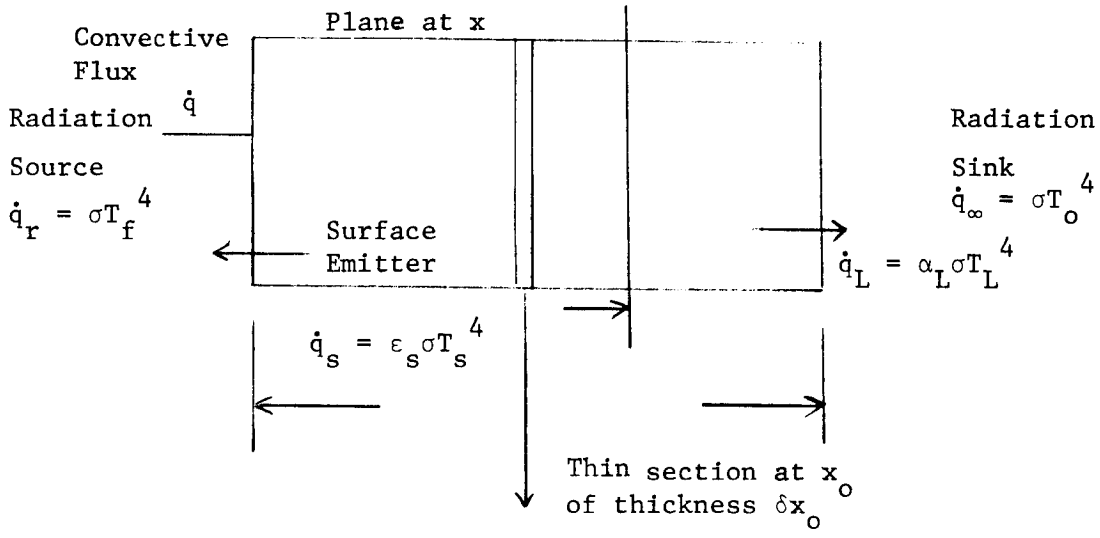

Figure A-3

The rate of change of energy in the slab at x if thickness δx is

$$\frac{d}{dt} C\rho T \, \delta x$$

This rate of change is due to the net conductive heat flux across the section

$$\dot{q}_x - \dot{q}_{x+\delta x} = - \delta x \frac{\partial \dot{q}}{\partial x}$$

plus the net heat effectively produced at x by radiation. The radiation flux is composed of that portion absorbed by the plane at x in the thin section δx minus the radiative loss from the section. At any arbitrary plane x_o and temperature T_o radiates from both faces of the section δx_o with an intensity

σT_o^4. However, this section absorbs per unit length with an absorbtivity K, which is also its emissivity, hence the irradiancy is $K\sigma T_o^4\ \delta x_o$. The radiation emitted from the section at x_o is attenuated as it travels to x so that the flux impinging at the section x is $K\sigma T_o^4\ \delta x_o \exp -K(x-x_o)$.

In addition, the source outside the propellant supplies a flux attenuated by the absorbtivity, $\alpha_f \sigma T_f^4 e^{-Kx}$. The sum impinging at x is therefore

$$\dot{q}_1 = \alpha_f \sigma T_f^4 e^{-Kx} + \int_o^x K\sigma T_o^4 \exp - K(x-x_o)\, dx_o$$

Similarly, the flux passing between $x_o > x$ and the end of the grain, L, is given by

$$\dot{q}_2 = \alpha_L \sigma T_L^4\ e^{-K(L-x)} + \int_L^x K\sigma T_o^4\ e^{-K(x_o-x)}\, dx_o$$

The fraction of energy absorbed by the thin section at x of all the radiation going from one end of the grain to the other, therefore, is

$$K\delta x(\dot{q}_1-\dot{q}_2)$$

and the radiation loss is $2K\sigma T^4\ \delta x$. Therefore, the net heat effectively produced at x by radiation is

$$\left\{K(\dot{q}_1-\dot{q}_2) - 2K\sigma T^4\right\} \delta x$$

The energy balance reduces to

$$C_\rho \frac{\partial T}{\partial t} = - \frac{\partial \dot{q}}{\partial x} + K(\dot{q}_1-\dot{q}_2) - 2K\sigma T^4$$

With a boundary moving at a rate r the energy carried across the section at x is $\frac{d}{dx}\, r\rho C(T-T_o)$. Assuming the conductive flux is related to the temperature by Fourier's Law, we have finally at steady-state

$$0 = k\,\frac{\partial^2 T}{\partial x^2} + r\rho C\,\frac{\partial T}{\partial x} + K\left\{\left[\alpha_f \sigma T_f^{\,4}\, e^{-Kx} + \int_o^x K\sigma T^4(x_o)\, \exp -K(x-x_o)\, dx_o\right.\right.$$

$$\left.\left. - \alpha_L \sigma T_o^{\,4}\, e^{-K(L-x)} - \int_o^x K\sigma T^4(x_o)\, \exp - K(x_o-x)\, dx_o - 2\sigma T^4\right\}\right.$$

This is an integro-differential equation whose solution may not be possible of an analytic solution. Near the surface and for significantly sized propellant webs, the bracket term, $\left\{\ \right\}$, can be assumed governed by the source flux. This simplifies the above to

$$0 = \alpha\,\frac{d^2 T}{dx^2} + r\,\frac{dT}{dx} + \frac{K}{\rho C}\,\left\{\alpha_f \sigma T_f^{\,4}\, e^{-Kx}\right\}$$

The radiative heat flux at the surface is generally described by an expression of the form

$$\dot{q}_r = \alpha_f \sigma T_f^{\,4} - \varepsilon_s \sigma T_s^{\,4} - \alpha_L \sigma T_L^{\,4}\, e^{-KL} \qquad \text{(A-1)}$$

In actuality, the flux into the grain is $\dot{q}_1$, while the flux going out of the grain is $-\dot{q}_2$, hence the net flux is $\dot{q}_1+\dot{q}_2$, or

$$\alpha_f \sigma T_f^{\,4}\, e^{-Kx} - \alpha_L T_s^{\,4}\, \sigma e^{-K(L-x)} + \int_o^x K\sigma T^4\, e^{-K(x-x_o)}\, dx_o - \int_x^L K\sigma T^4\, e^{-K(x_o-x)}\, dx_o$$

Comparison of the above two equations at the surface gives the emissivity

$$\varepsilon_s = \int_o^{KL} \left(\frac{T}{T_s}\right)^4 e^{-Kx_o}\, dKx_o$$

If T is assumed approximately exponential in x, say

$$\frac{T}{T_s} = e^{-\lambda x_o}$$

$$\varepsilon_s = \left\{1 + \frac{4\lambda}{K}\right\}^{-1} \left\{1 - e^{-KL(1 + \frac{4\lambda}{K})}\right\}$$

For deep grains this reduces to

$$\varepsilon_s = \frac{1}{1 + \frac{4\lambda}{K}} \qquad \text{(typically } \sim .2 \text{ at higher burning rates)}$$

Since λ will be proportional to the burning rate, we see that as the burning rate decreases, the emissivity will increase, i.e. less radiation will penetrate the grain, thereby leading to extinguishment at low pressures. As the burning rate increases, the emissivity will decrease and more radiant energy will be allowed to penetrate, hence augmenting radiation effects at higher pressures. The fact that the emissivity is burning rate dependent results from the temperature gradient behind the grain which requires a contribution of the solid such that the black body equivalent temperature is less than the surface temperature. The emissivity is therefore a dynamic property of the propellant and must be defined in terms of the total combustion process.

With the radiant flux now defined by (A-1), we have the temperature gradient at the surface

$$-kT_{xs} = \dot{q}_c + \dot{q}_r$$

The solution to the differential equation is

$$T - T_o = \frac{\dot{q}_c + \dot{q}_r + \alpha_f \sigma T_f^4 / \left|\frac{r}{\alpha K} - 1\right|}{r\rho C} \; e^{-\frac{rx}{\alpha}} - \frac{\alpha_f \sigma T_f^4}{r\rho C \left[1 - \frac{\alpha K}{r}\right]} e^{-Kx}$$

Hence at the surface

$$r\rho C\ (T_s - T_o) = \dot{q}_c + \dot{q}_r - \alpha_f \sigma T_f^4$$

$$= \dot{q}_c$$

Thus the surface temperature is basically dominated by the convective heat flux from the gas phase. Because the radiant transmission is an "in depth" effect, radiant energy influences the burning rate by a mechanism which alters the propellant properties beyond the convective profile, specifically the grain temperature. Therefore, the superposition of radiant energy affects the burning rate through π_r.

NOMENCLATURE

B	Thermal driving force by radiation	$°K^4$
C_s	Heat capacity	cal/gm °K
E	Activation energy	cal/mole
K	Radiative transmissivity	μ^{-1}
n	Order of reaction	-
p	Pressure	lb/in^2
Q	Heat of reaction	cal/cm
$\dot{q}$	Heat flux	cal/cm^2 sec
r	Burning rate	cm/sec
R	Gas constant	cal/mole °K
T	Temperature	°K
t	Time	sec
x,y	Distance from surface	cm
V	Voltage	μ volts
Z	Pre-exponential coefficient	sec^{-1} $(gm/cm^3)^{-n+1}$
α	Thermal diffusivity	cm^2/sec
ξ	Extent of reaction	-
μ	Micron	$1\mu = 10^{-4}$ cm
τ	Transmissivity	-
$\alpha_g, \alpha_s, \alpha_\lambda$	Gas solid phase absorptivity; absorptivity	-
ε_s	Emissivity	-
ρ_λ	Reflectivity	-
ρ	Density	gm/cm^3

NOMENCLATURE (cont.)

σ	Stefan-Boltzmann constant	$cal/cm^2\ sec\ °K^4$
λ	Wavelength	μ
ν	Kinematic Viscosity	cm^2/sec

Subscripts

s	Surface or interphase between solid and gas phase
o	Ambient condition ($y \to -\infty$)

BIBLIOGRAPHY

1. Adams, J., "Flame Temperature Measurements of Metalized Propellants", AF 04(611)-10545, Final Rep., AFRPL-TR-66-203, Sept. 1966.

2. Carslaw, H. S., and Jaeger, J. C., "Conductions of Heat in Solids", Oxford, (1959).

3. Corner, J., "Interior Ballistics of Guns", Wiley & Sons, London, (1950).

4. Chung, P. K., and Jackson, M. L., "Thermal Diffusivity of Low Conductivity Materials", Ind. Eng. Chem., Vol. 46, p 2563-2566, (Dec. 1954).

5. Essenghigh, R. H., (Penn. State), "On Radiative Heat Transfer to Solids", AIAA Thermophysics Specialist Conf., New Orleans, (Apr. 17-20, 1967).

6. Fur, Z. I., "The Basis of the Dependence of Burning Rate on Pressure in the Relaxation Theory of Propagation of Combustion", J. of Eng. Physics, Vol. 8, No. 4, pp 307-310, (Apr. 1965).

7. Giedt, W. H., Principles of Eng. Heat Transfer, D. van Nostrand Co., New York, (1957).

8. Hirschfelder and Curtiss, "Theory of Propagation of Flames", 3rd Symposium on Combustion and Flame, Williams and Wilkins Co., Balt. Md., (1949).

9. Lou, R. L., Landers, L. C., and Lovine, R. L., "Theoretical and Experimental Study of Extinguishable Propellants", Tech. Rep. No. AFRPL-TR-66-128, July 1966 (Conf.), (Quoted Material from Unclassified Portion.)

10. Marxman, G., "Model of Solid Propellant Response to Combustion Instability", 3rd Combustion Conference, CPIA, (Oct. 1962).

11. Paul, B. E., Lovine, R. L., and Fong, L. Y., "A Ballistic Explanation of the Ignition Pressure Peak", AIAA Preprint 64-121, 5th AIAA Solid Propellant Rocket Conf. (Palo Alto, Cal.), Jan. (1964).

12. Powling, J., "Combustion of AP-Based Composite Propellants", ERDE Rep. 15/R/65.

13. Prigogine, I., "Thermodynamics of Irreversible Processes", C. C. Thomas Publ., Springfield, Ill., (1955).

14. Saunders, A., and Pellette, G., "Mass Spectrometer Pyrolysis of AP at Low Pressures", 3rd Comb. Conf., CPIA, Oct. (1966).

BIBLIOGRAPHY (Cont.)

15. Schmidt, W., "The Effect of Solid Phase Reactions on the Ballistic Properties of Propellants", Cont. NAS 1-6323, AGC Rep. 1062-81Q-2, Dec. 27, 1966.

16. Selzer, H., Personal Communication.

17. Strittmater, R. C., "Measurement of Temperature Profiles in Solid Propellants", Memo. Rep. 1737, USAMC BRL, Mar. 1966.

18. Summerfield, M., Sabadell, A., and Wenograd, J., "The Measurement of the Temperature Profiles of Burning Solid Propellants by Microthermocouples", Contract NONR 1858(12) TR 23 Sept. 1963, Aero. Eng. Rep. No. 664. Also, thermocouple traces sent to J. H. Wiegand. Private communication.

19. Waesche and Wenograd, "Kinetics of Propellant Decomposition Reactions", United Aircraft Res. Lab. Rep. E 91047-6-3, Oct. 1966, and F 91047-6-6, Jan. 1967.

20. Wenograd, J., "Measurement of Temperature Profiles in Burning Solid Propellants using Microthermocouples", Tech. Rep. Princeton Univ., Aero. Eng. 664, Jan. 1962.

21. E. Price and H. Bradley, personal communication with J. H. Wiegand.

22. Inami, S. H., Rosser, W. A., Jr., and Wide, H., Heat-Release Kinetics of AP in the Presence of Catalysts and Fuel, Contract NONR-3415(00), Mar 1967.

23. Wiegand, J. H., "Simplified Unsteady-State Conduction Calculations", Ind. Eng. Chem., 48, p. 817-820 (1956).

24. Micheli, P. L., Final Report, "A Stop-Start Study of Solid Propellants", Section IV (Conf.), on Contract NAS 1-6600, Dec. 1967.

THERMOGRAVIMETRIC DECOMPOSITION OF AP (74 - 105μ) AT VARYING HEATING RATES

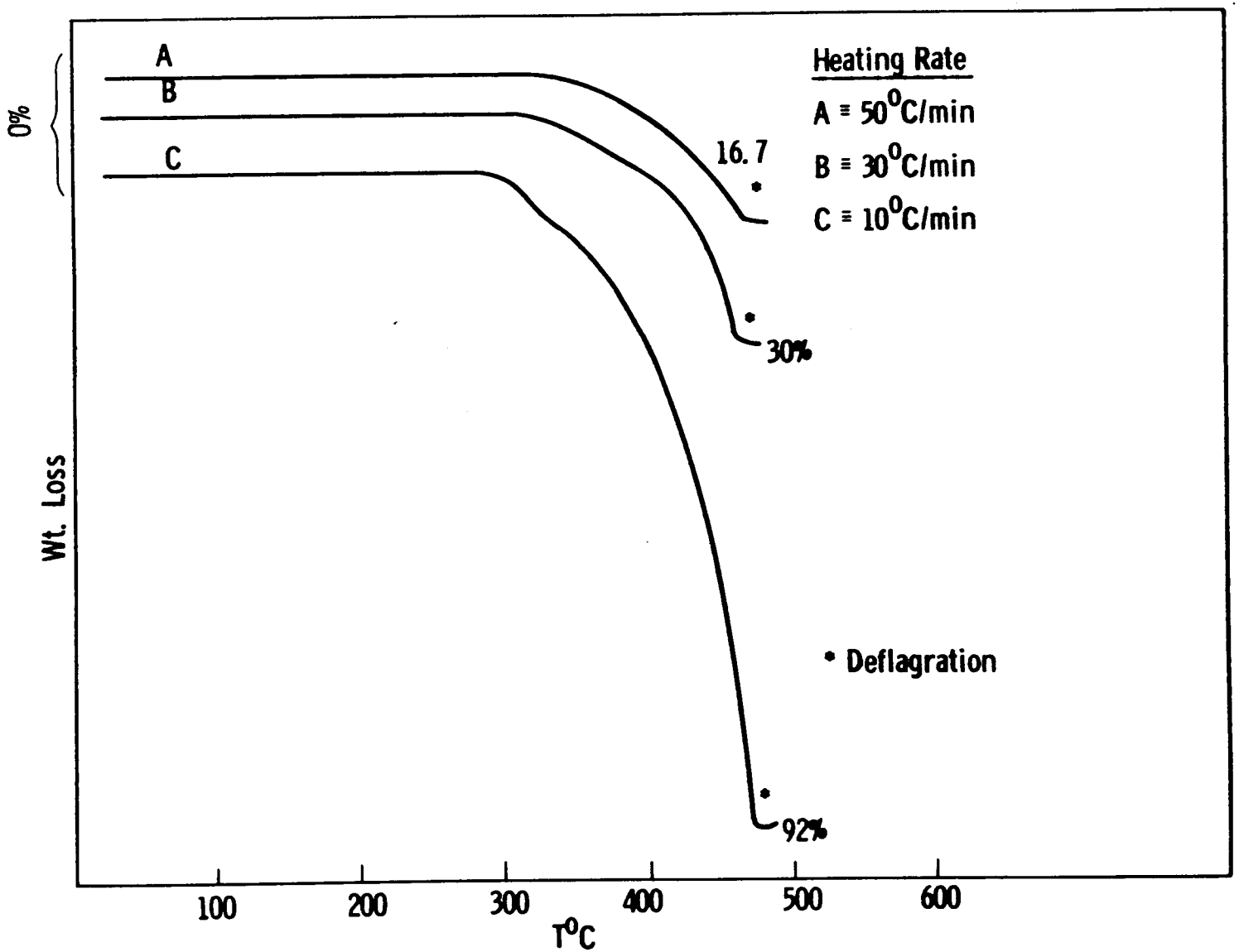

Figure 1

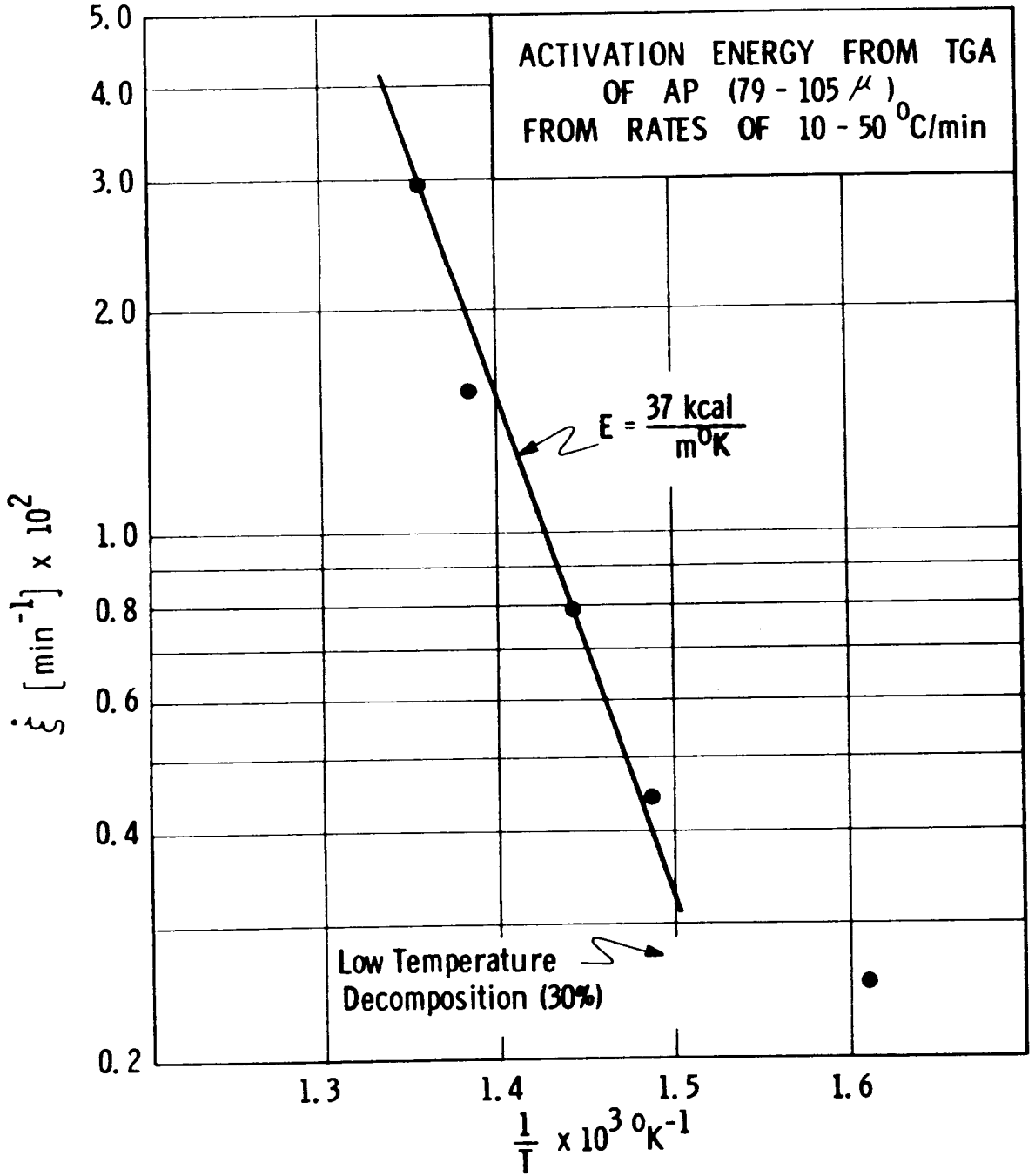
ACTIVATION ENERGY FROM TGA
OF AP (79 - 105 μ)
FROM RATES OF 10 - 50 °C/min
E = 37 kcal / m°K
Low Temperature
Decomposition (30%)
5.0
4.0
3.0
2.0
1.0
0.8
0.6
0.4
0.2
1.3
1.4
1.5
1.6
$\dot{\xi}$ [min^{-1}] x 10^2
$\frac{1}{T}$ x 10^3 °K^{-1}

Figure 2

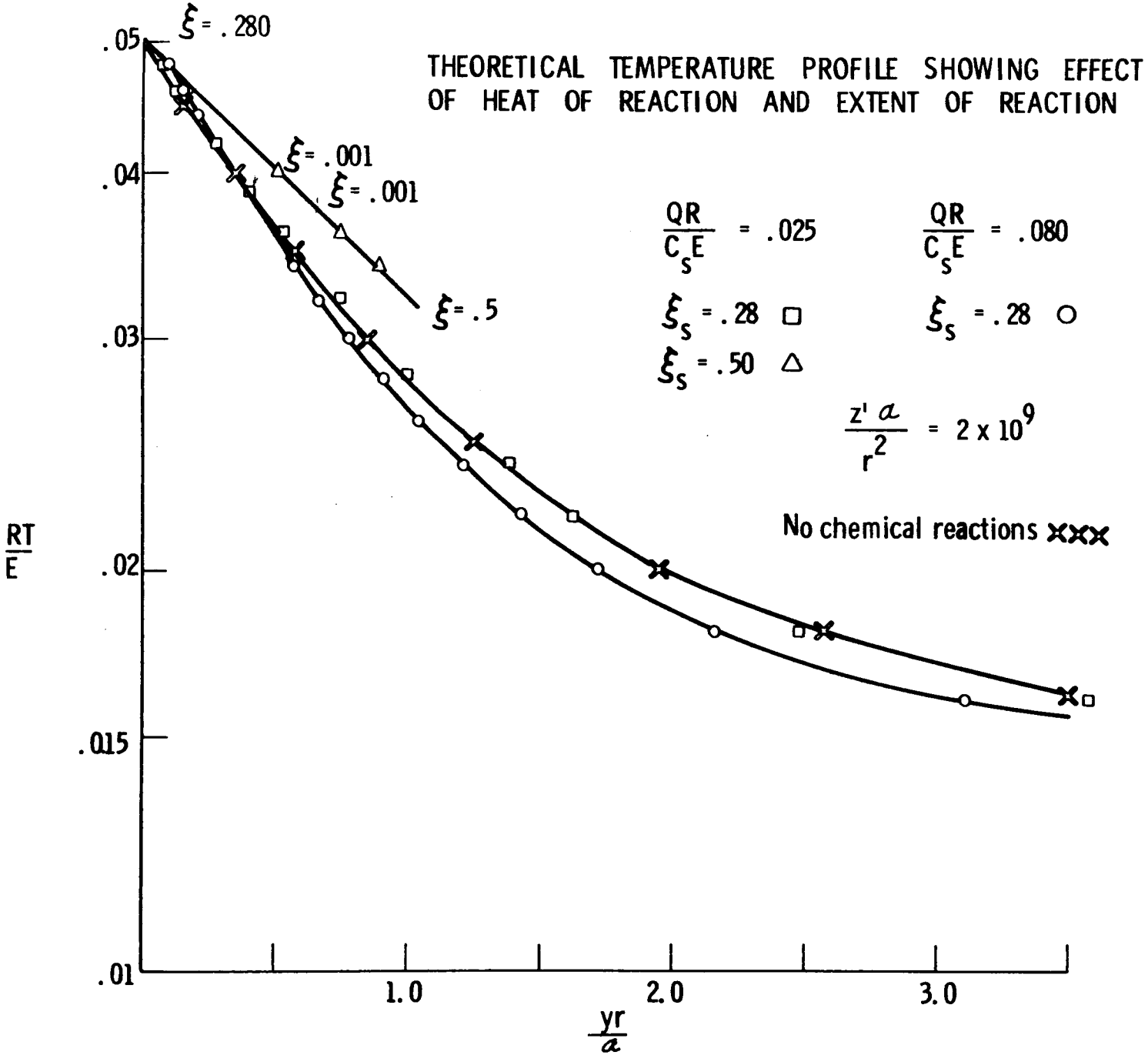
THEORETICAL TEMPERATURE PROFILE SHOWING EFFECT OF HEAT OF REACTION AND EXTENT OF REACTION
ξ = .280
ξ = .001
ξ = .001
ξ = .5
QR/CsE = .025
ξs = .28 □
ξs = .50 △
QR/CsE = .080
ξs = .28 ○
z' a/r² = 2 x 10⁹
No chemical reactions ×××
RT/E
.05
.04
.03
.02
.015
.01
1.0
2.0
3.0
yr/a

Figure 3

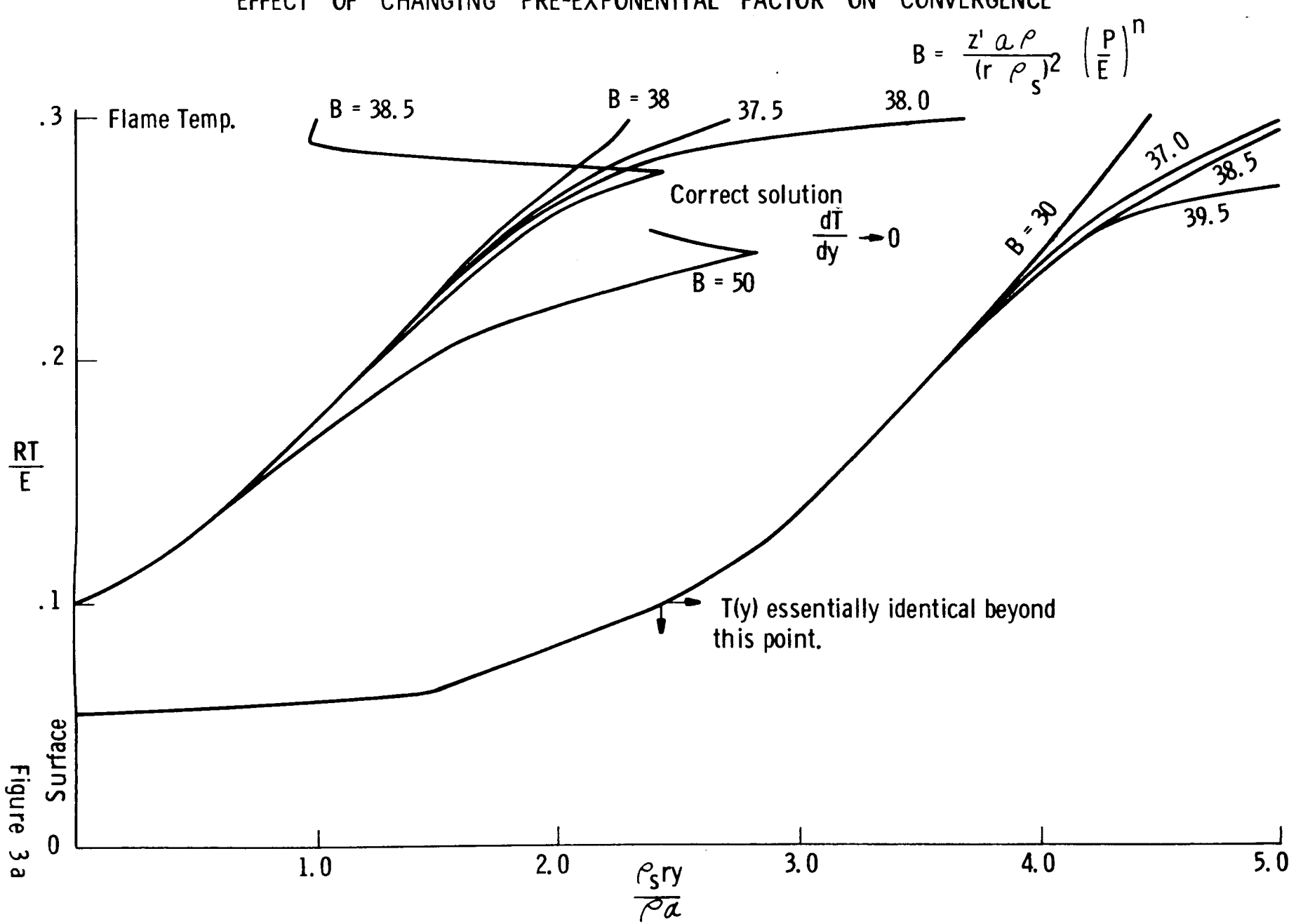
EFFECT OF CHANGING PRE-EXPONENTIAL FACTOR ON CONVERGENCE
$B = \frac{z' a \rho}{(r \rho_s)^2} \left(\frac{P}{E}\right)^n$
B = 38.5
B = 38
37.5
38.0
Correct solution
$\frac{dT}{dy} \to 0$
B = 50
B = 30
37.0
38.5
39.5
T(y) essentially identical beyond this point.
Flame Temp.
.3
.2
.1
0
Surface
$\frac{RT}{E}$
1.0
2.0
3.0
4.0
5.0
$\frac{\rho_s r y}{\rho a}$

Figure 3a

COMPARISON OF GAS PHASE PROFILES FOR VARIOUS VALUES OF BURNING RATE EXPONENT, n, AND SAME RATE, $r \rho_s y^*/a\rho = 1.0$

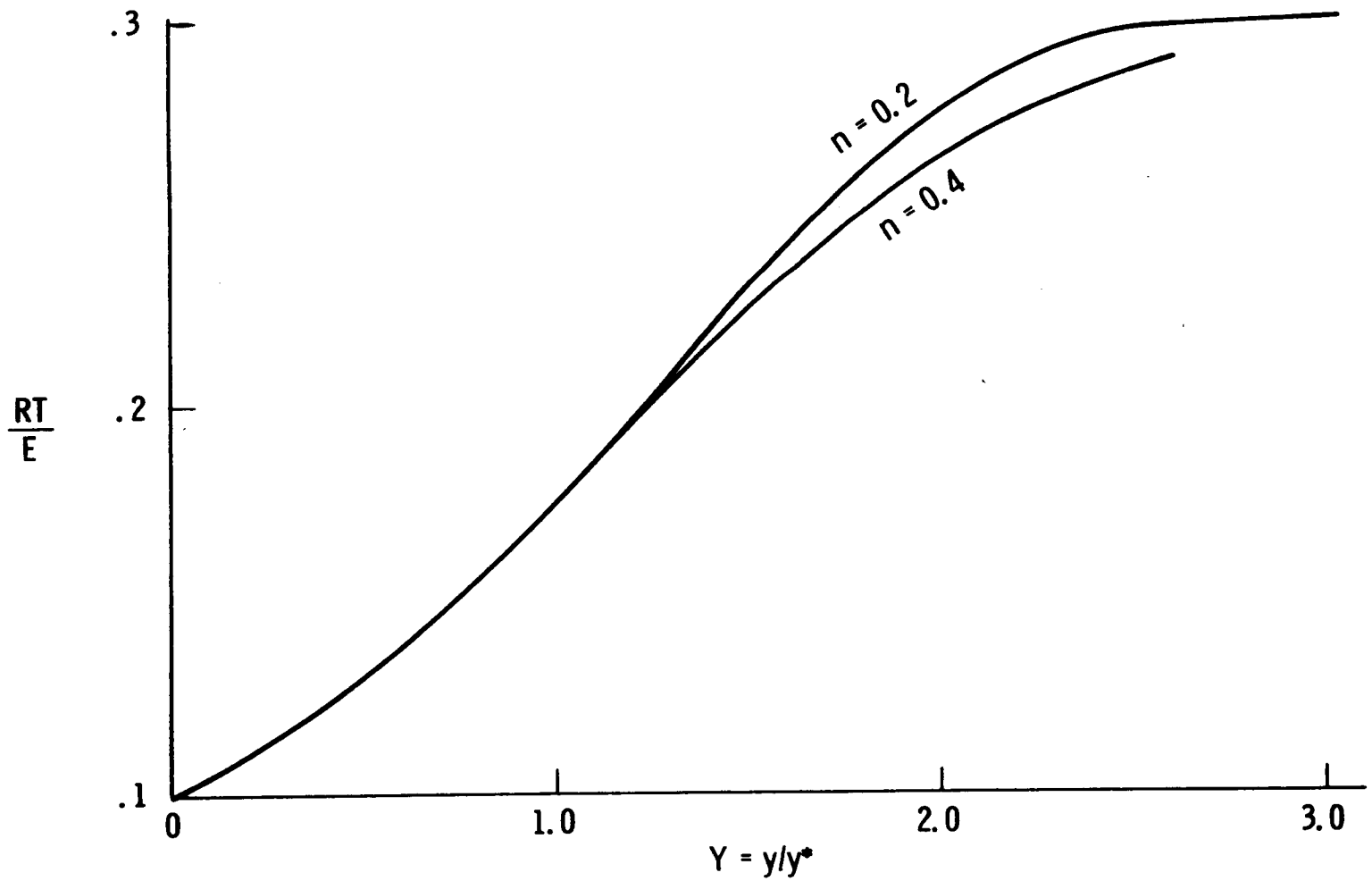

Figure 4

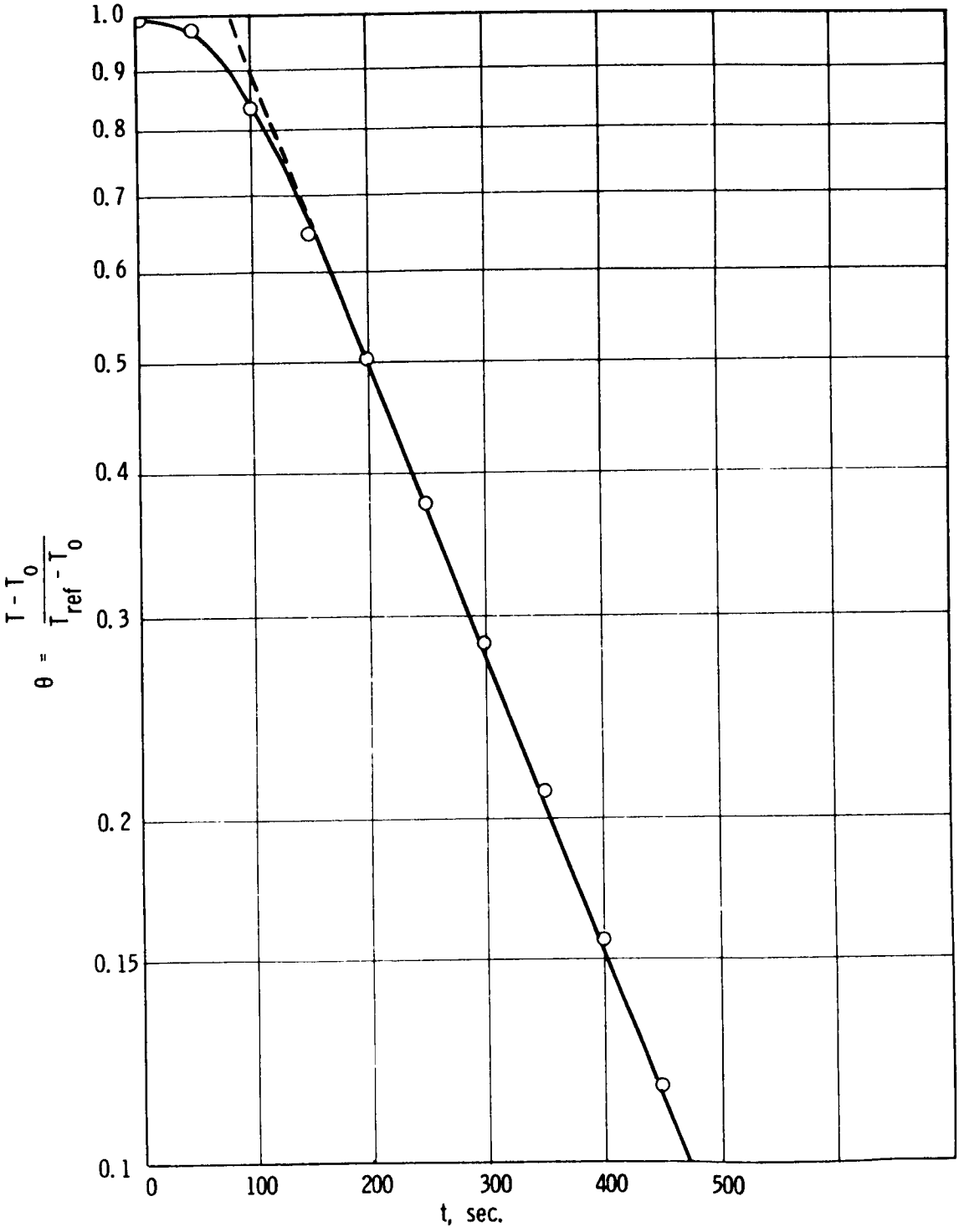

Graph of θ vs Time for the Temperature Change Following Depressurization

Figure 5

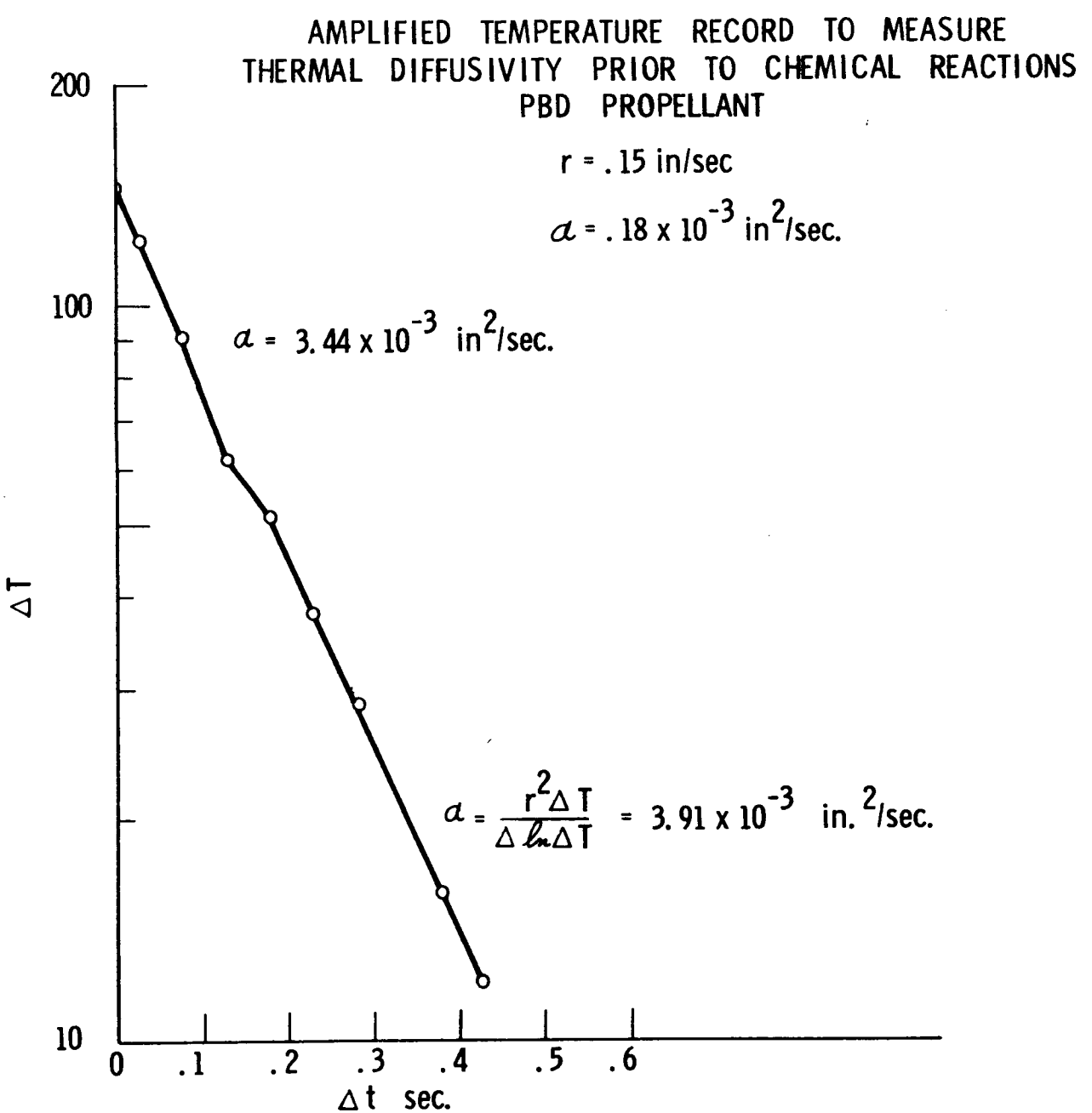
AMPLIFIED TEMPERATURE RECORD TO MEASURE
THERMAL DIFFUSIVITY PRIOR TO CHEMICAL REACTIONS
PBD PROPELLANT
r = .15 in/sec
$\alpha = .18 \times 10^{-3}$ in^2/sec.
$\alpha = 3.44 \times 10^{-3}$ in^2/sec.
$\alpha = \frac{r^2 \Delta T}{\Delta \ln \Delta T} = 3.91 \times 10^{-3}$ in.^{2}/sec.
200
100
10
ΔT
0
.1
.2
.3
.4
.5
.6
Δt sec.

Figure 6

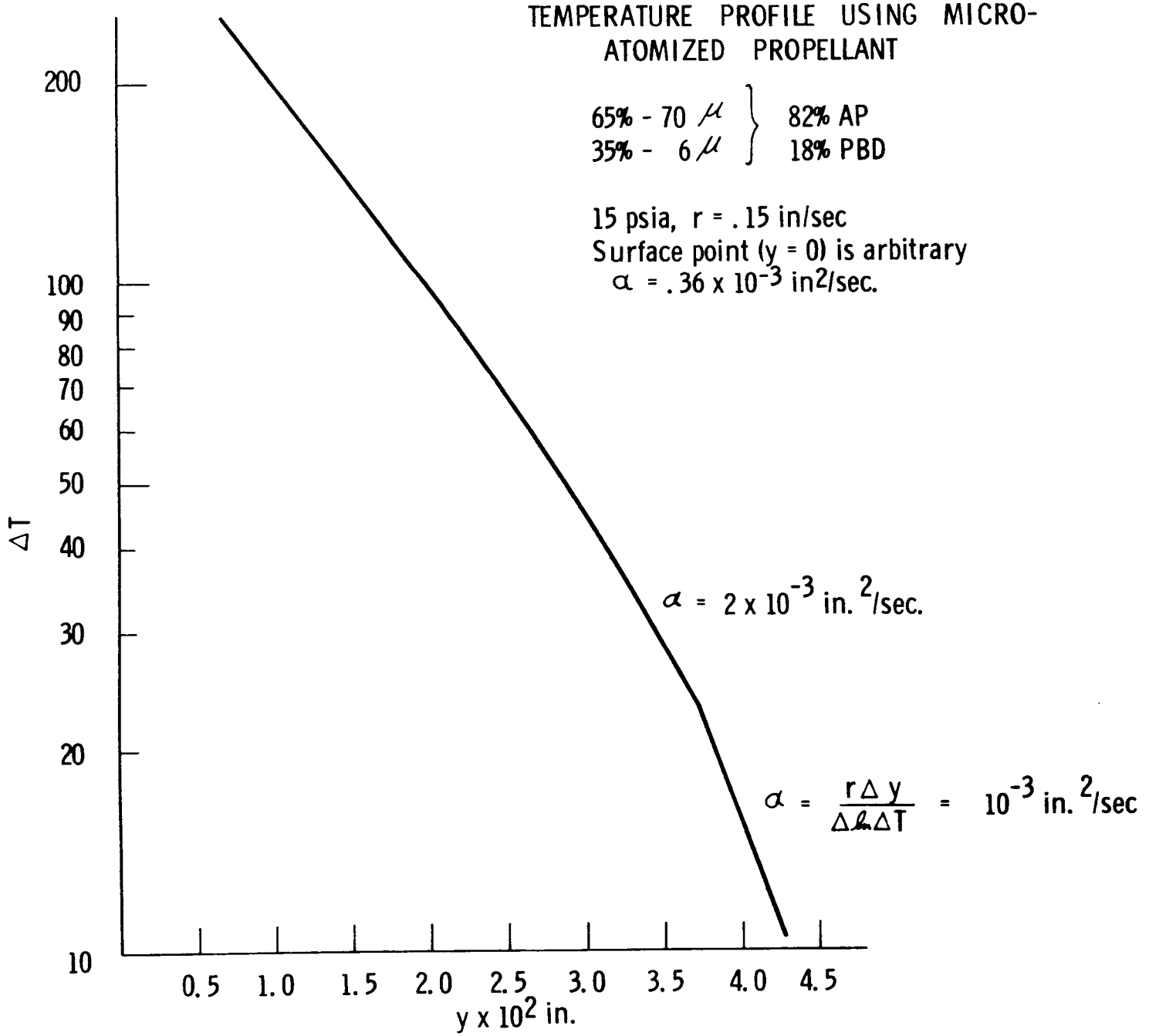
TEMPERATURE PROFILE USING MICRO-ATOMIZED PROPELLANT
65% - 70 μ
35% - 6 μ
82% AP
18% PBD
15 psia, r = .15 in/sec
Surface point (y = 0) is arbitrary
α = .36 x 10^-3 in^2/sec.
α = 2 x 10^-3 in.^2/sec.
α = rΔy/ΔhΔT = 10^-3 in.^2/sec
ΔT
200
100
90
80
70
60
50
40
30
20
10
0.5
1.0
1.5
2.0
2.5
3.0
3.5
4.0
4.5
y x 10^2 in.

Figure 6a

TEMPERATURE AND TRANSIENT OF PBD PROPELLANT

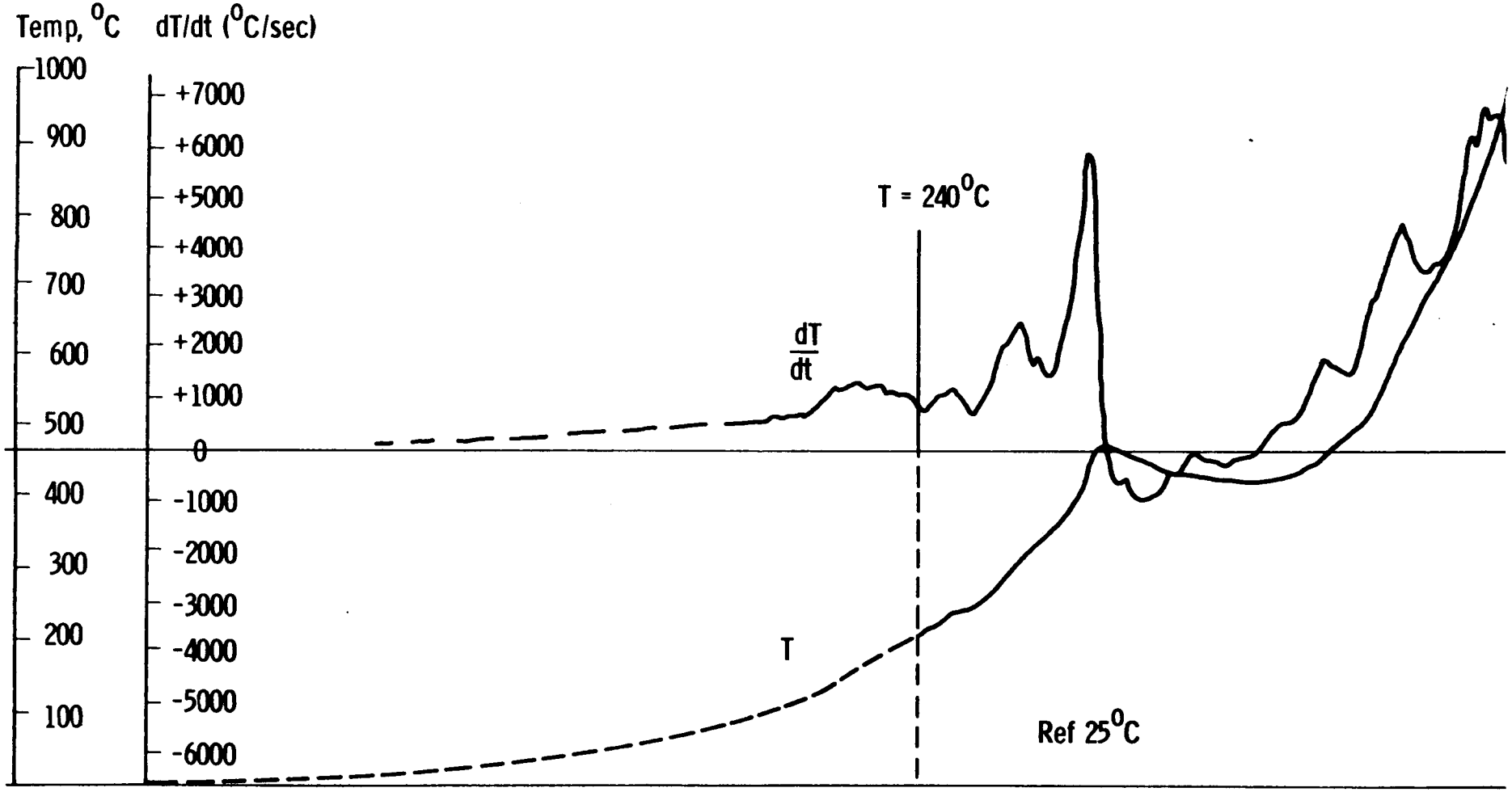

Figure 7

TEMPERATURE AND DERIVATIVE FOR PBD PROPELLANT

200 psi

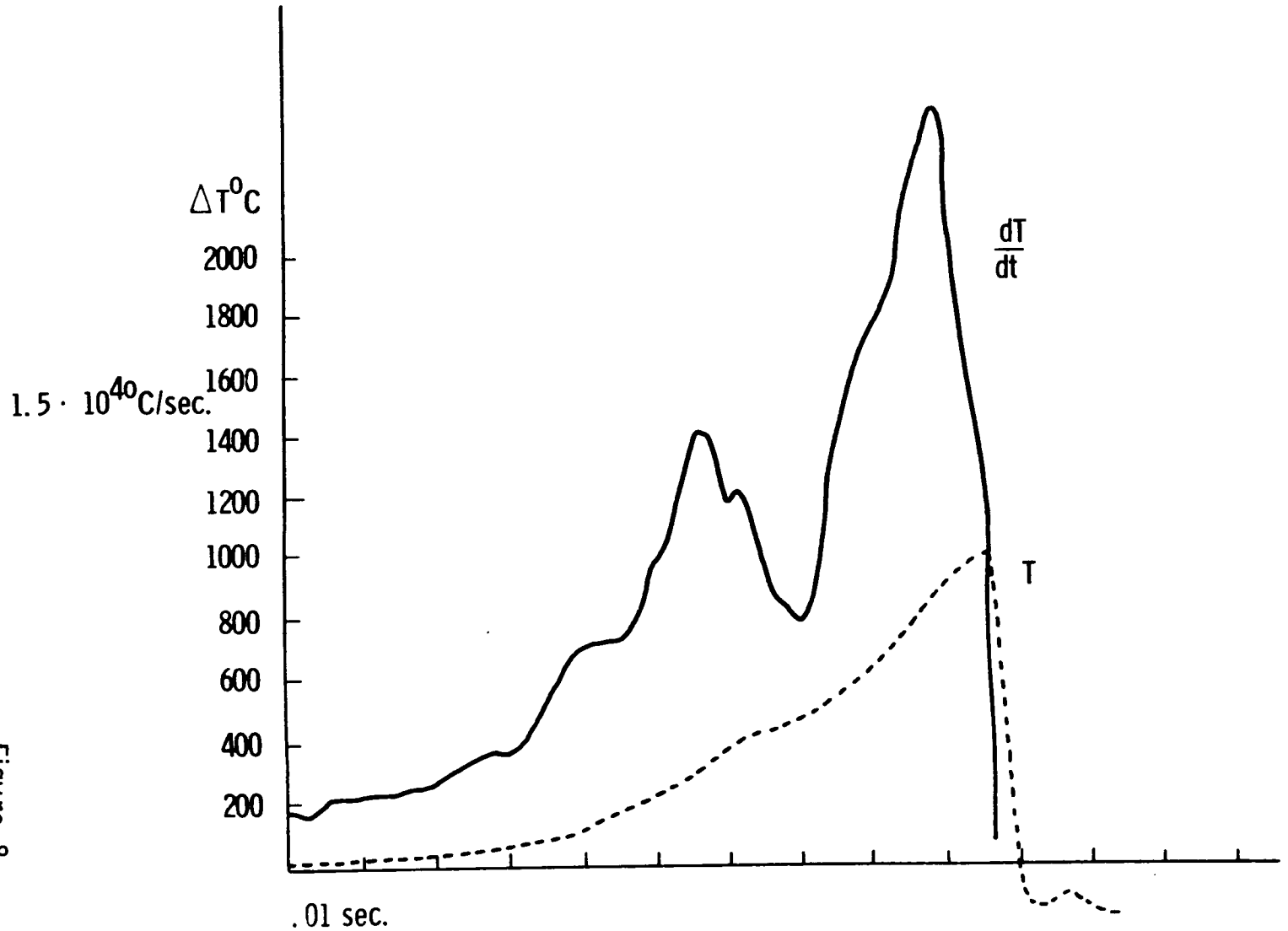

Figure 8

TEMPERATURE AND DERIVATIVE FOR PBD PROPELLANT
400 psi

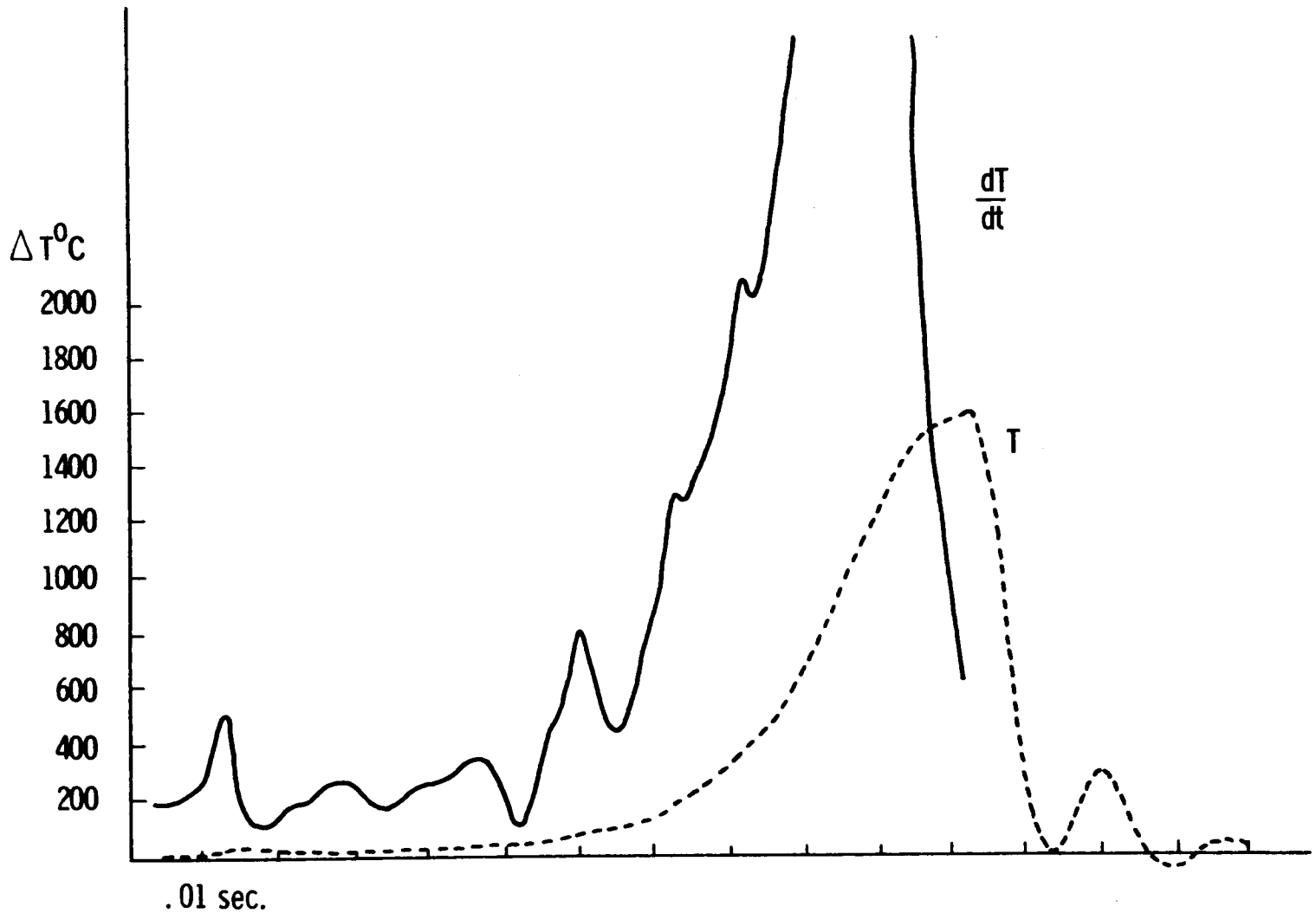

Figure 9

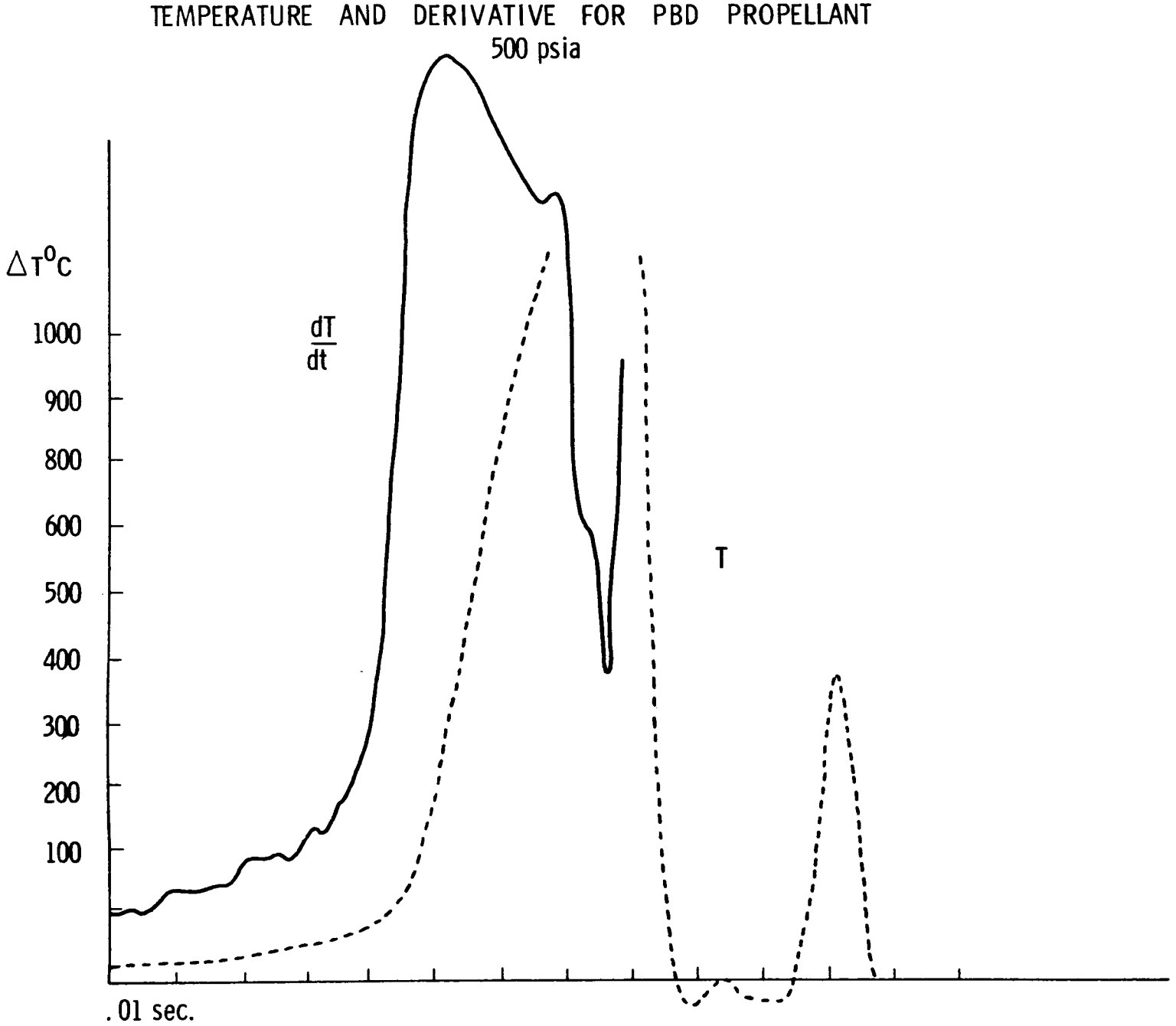
TEMPERATURE AND DERIVATIVE FOR PBD PROPELLANT
500 psia
ΔT°C
1000
900
800
600
500
400
300
200
100
dT/dt
T
.01 sec.

Figure 10

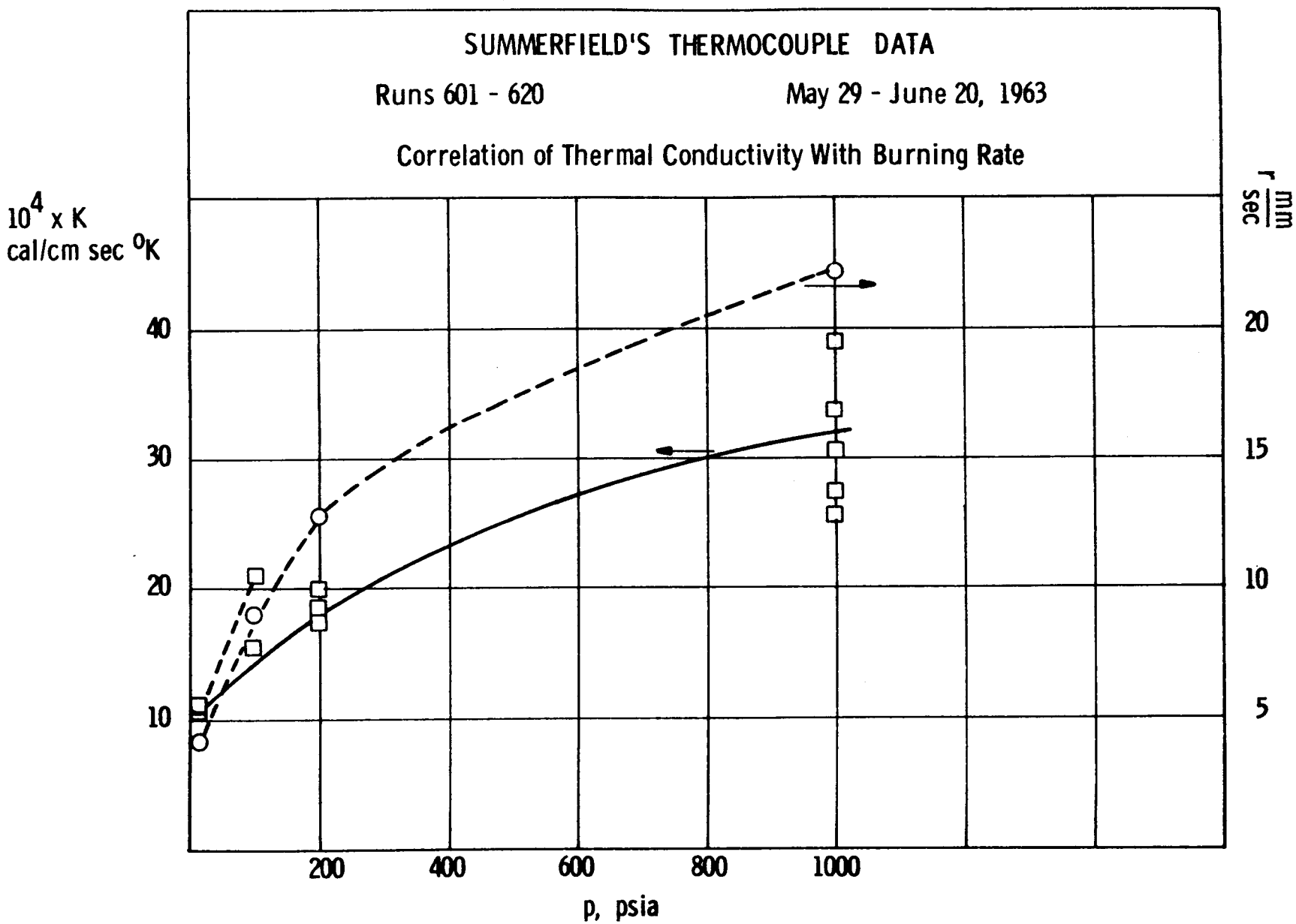
SUMMERFIELD'S THERMOCOUPLE DATA
Runs 601 - 620
May 29 - June 20, 1963
Correlation of Thermal Conductivity With Burning Rate
10^4 x K
cal/cm sec °K
r mm/sec
40
30
20
10
20
15
10
5
200
400
600
800
1000
p, psia

Figure 11

TEMPERATURE AND TRANSIENT OF PBD PROPELLANT

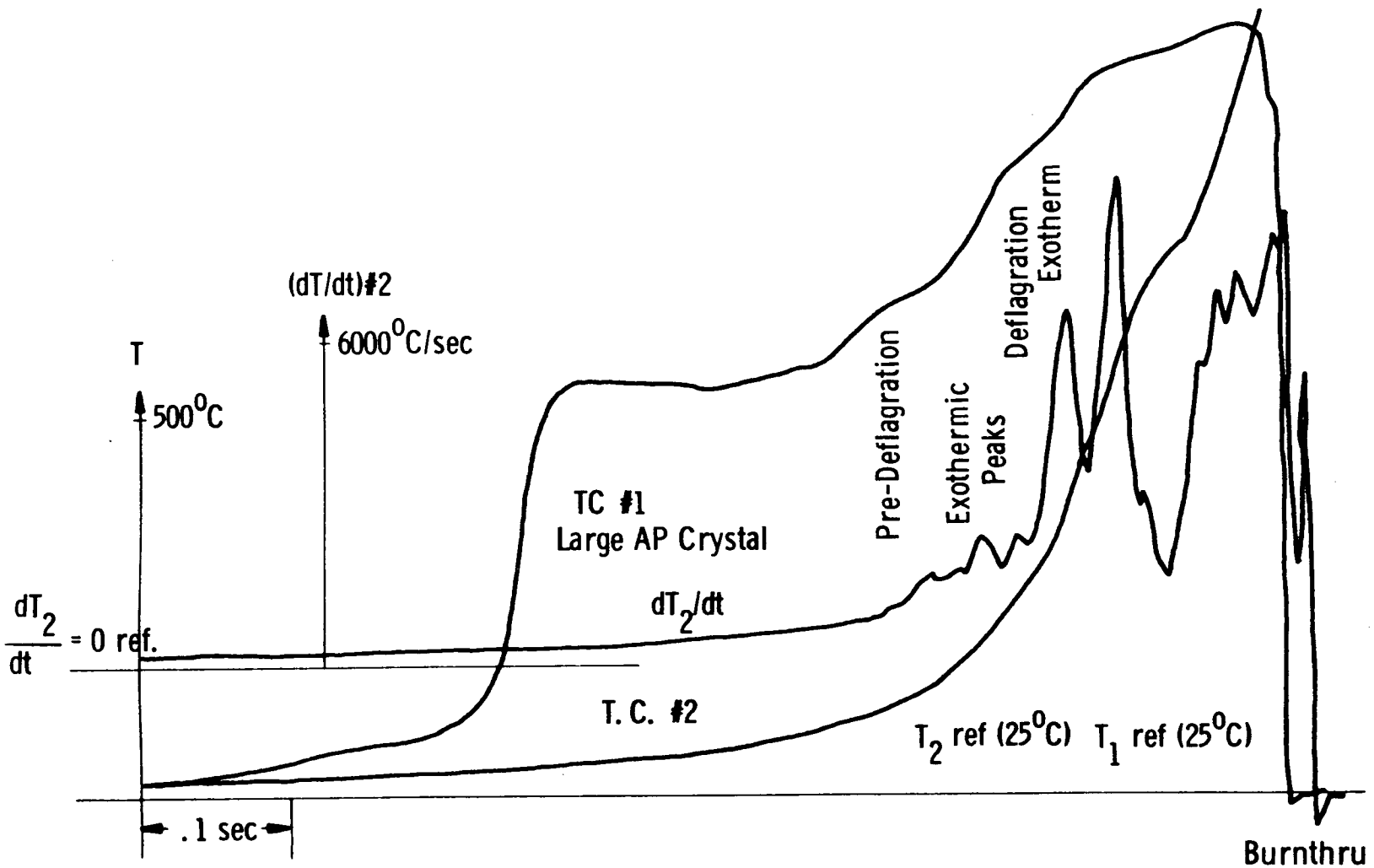

Figure 12

TEMPERATURE AND DERIVATIVE FOR MICROATOMIZED - AP POLYURETHANE PROPELLANT

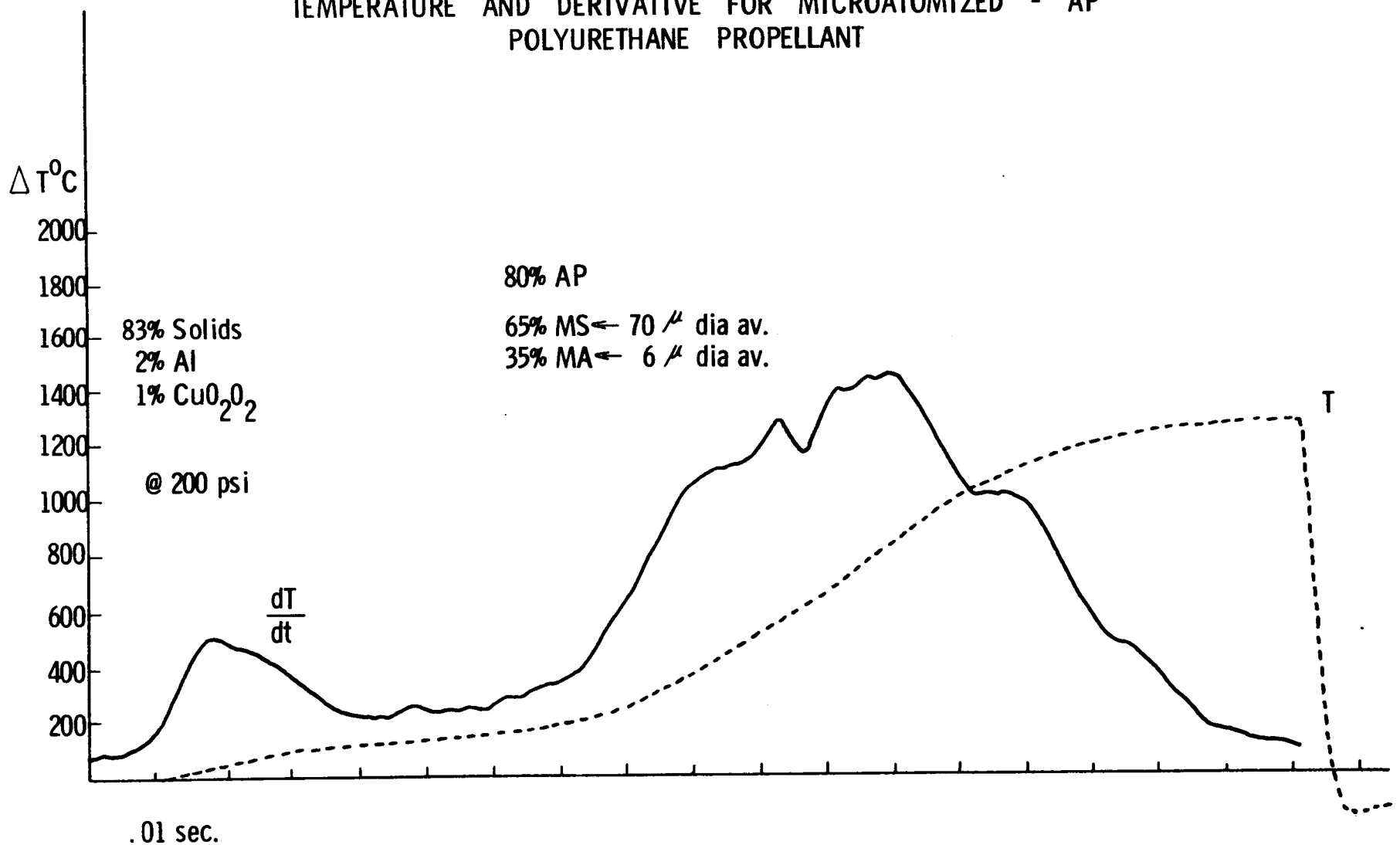

Figure 13

PHOTOCELL AND MONOCHROMETER VOLTAGES AS SEEN THROUGH PROPELLANT (AP, PU)

r = .05 in/sec

$\lambda = 1.45\mu$ T = 1120 °K
$\lambda = 2.2\mu$ = 1050 °K
960 °K
$\lambda = 4.0\mu$ = 740 °K

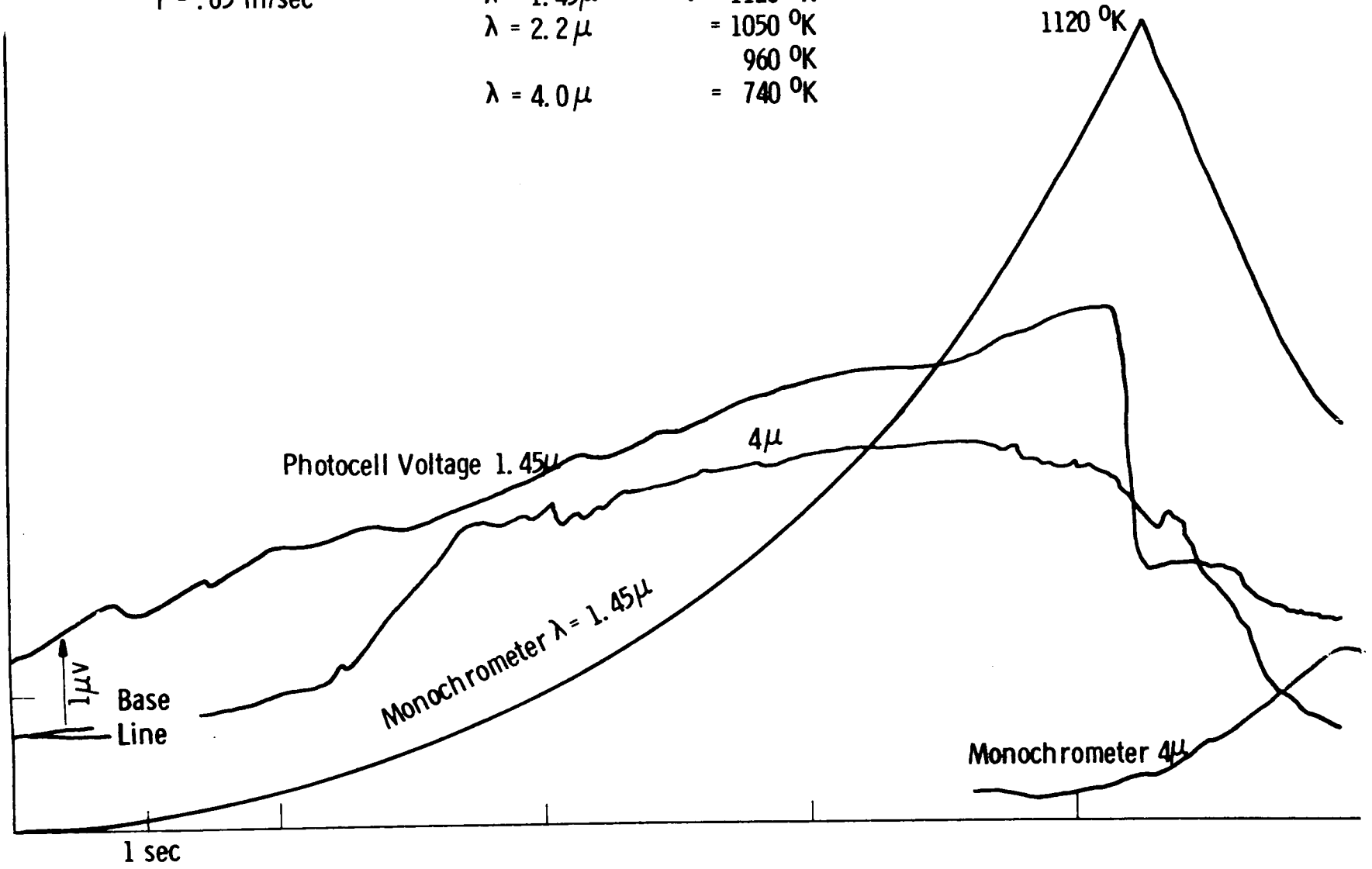

Figure 14

PEAK (SURFACE) VOLTAGES SEEN THROUGH PROPELLANT AS A FUNCTION OF WAVELENGTH

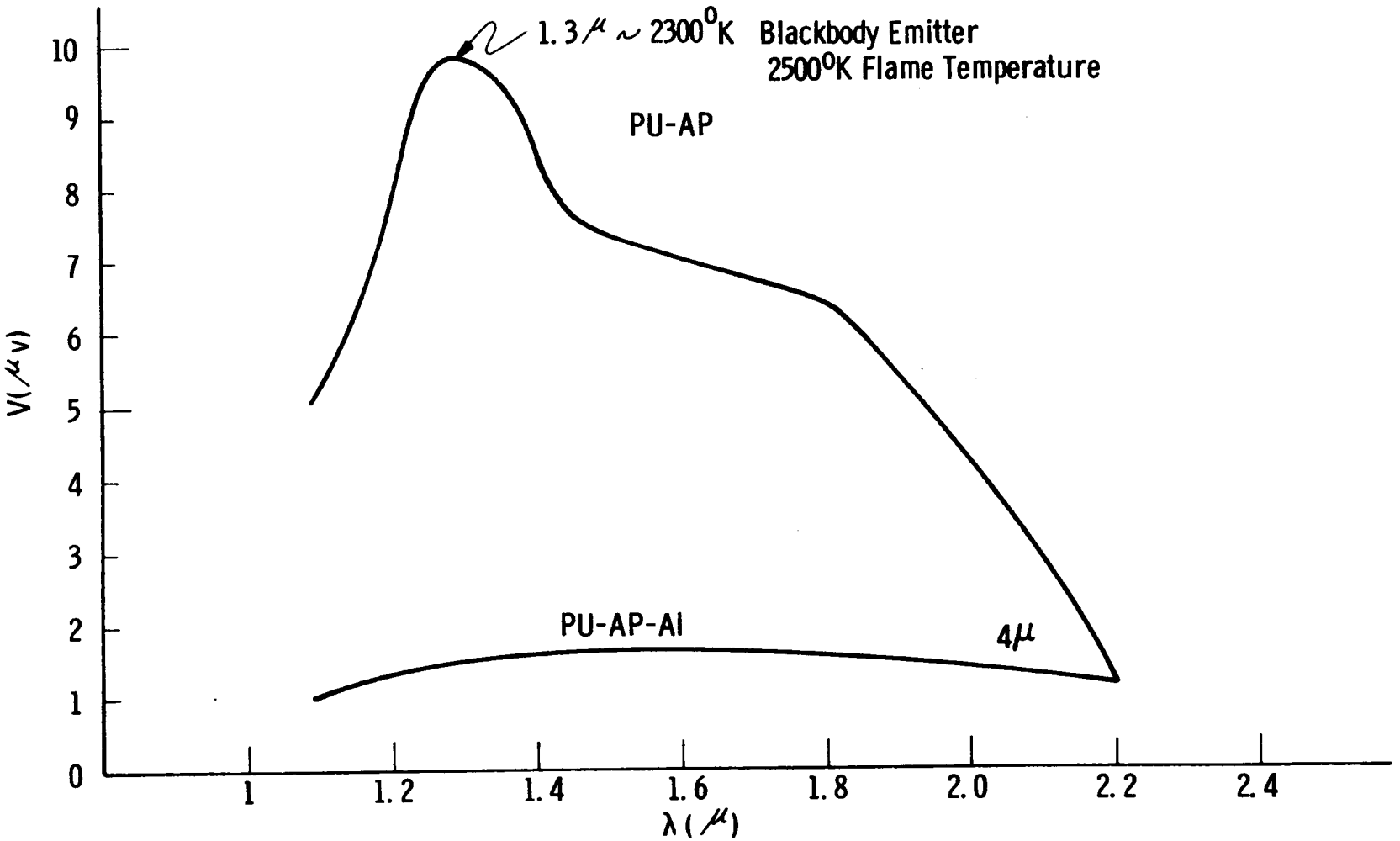

Figure 15

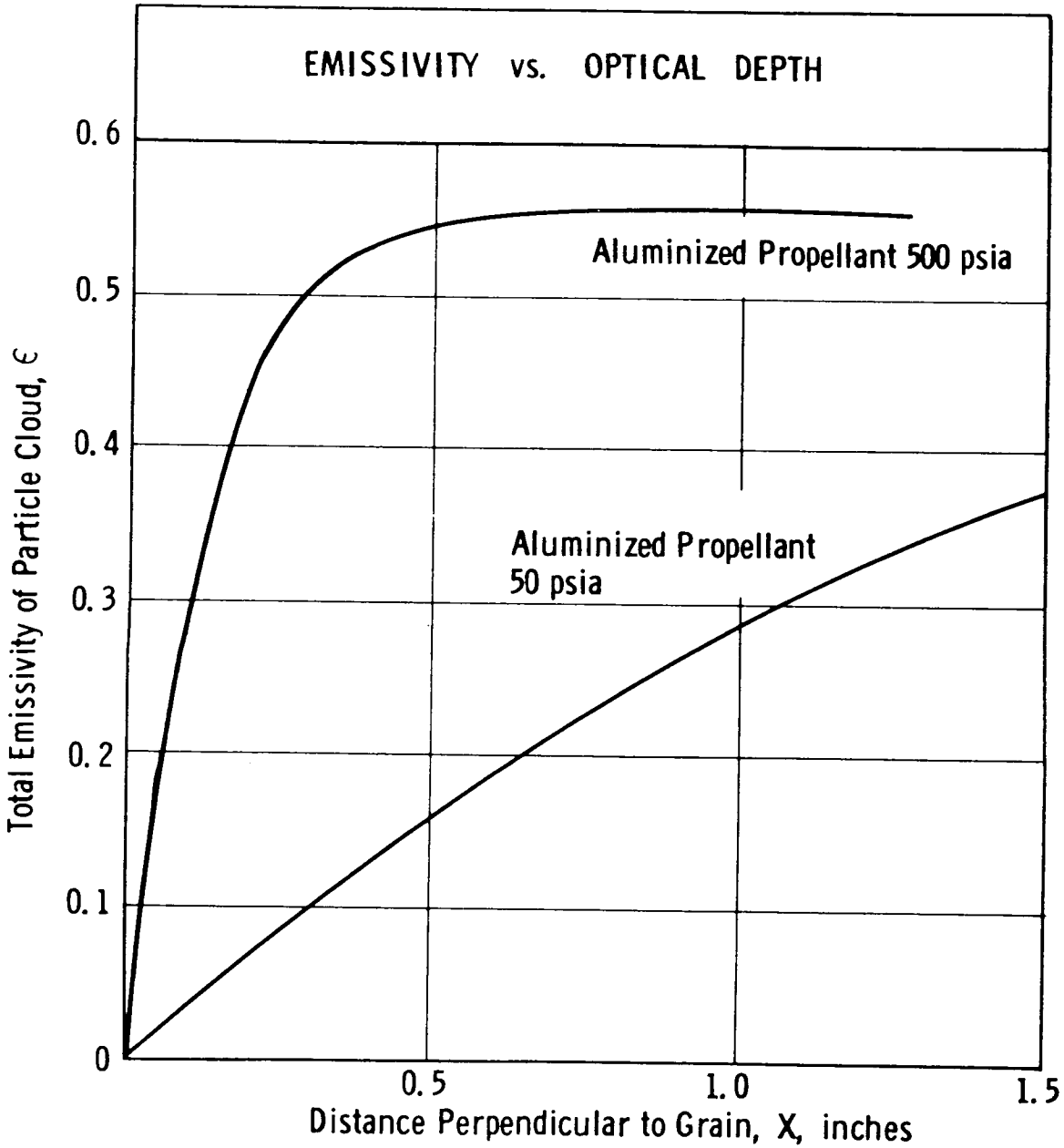
EMISSIVITY vs. OPTICAL DEPTH
Aluminized Propellant 500 psia
Aluminized Propellant
50 psia
Total Emissivity of Particle Cloud, ϵ
0.6
0.5
0.4
0.3
0.2
0.1
0
0.5
1.0
1.5
Distance Perpendicular to Grain, X, inches

Figure 16

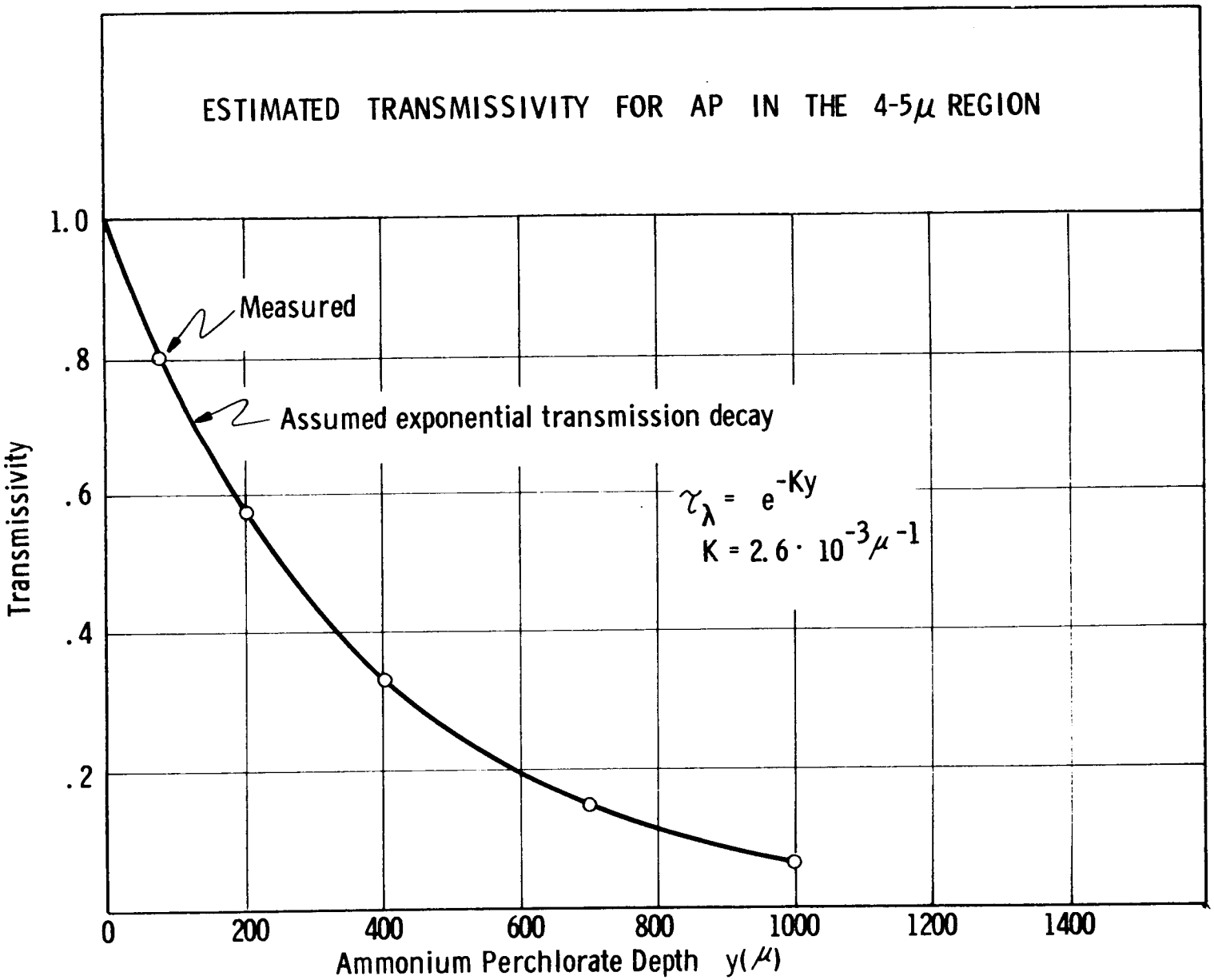
ESTIMATED TRANSMISSIVITY FOR AP IN THE 4-5μ REGION
1.0
.8
.6
.4
.2
Transmissivity
Measured
Assumed exponential transmission decay
$\tau_\lambda = e^{-Ky}$
$K = 2.6 \cdot 10^{-3} \mu^{-1}$
0
200
400
600
800
1000
1200
1400
Ammonium Perchlorate Depth y(μ)

Figure 17

SCHEMATIC OF EXPERIMENTAL SET-UP

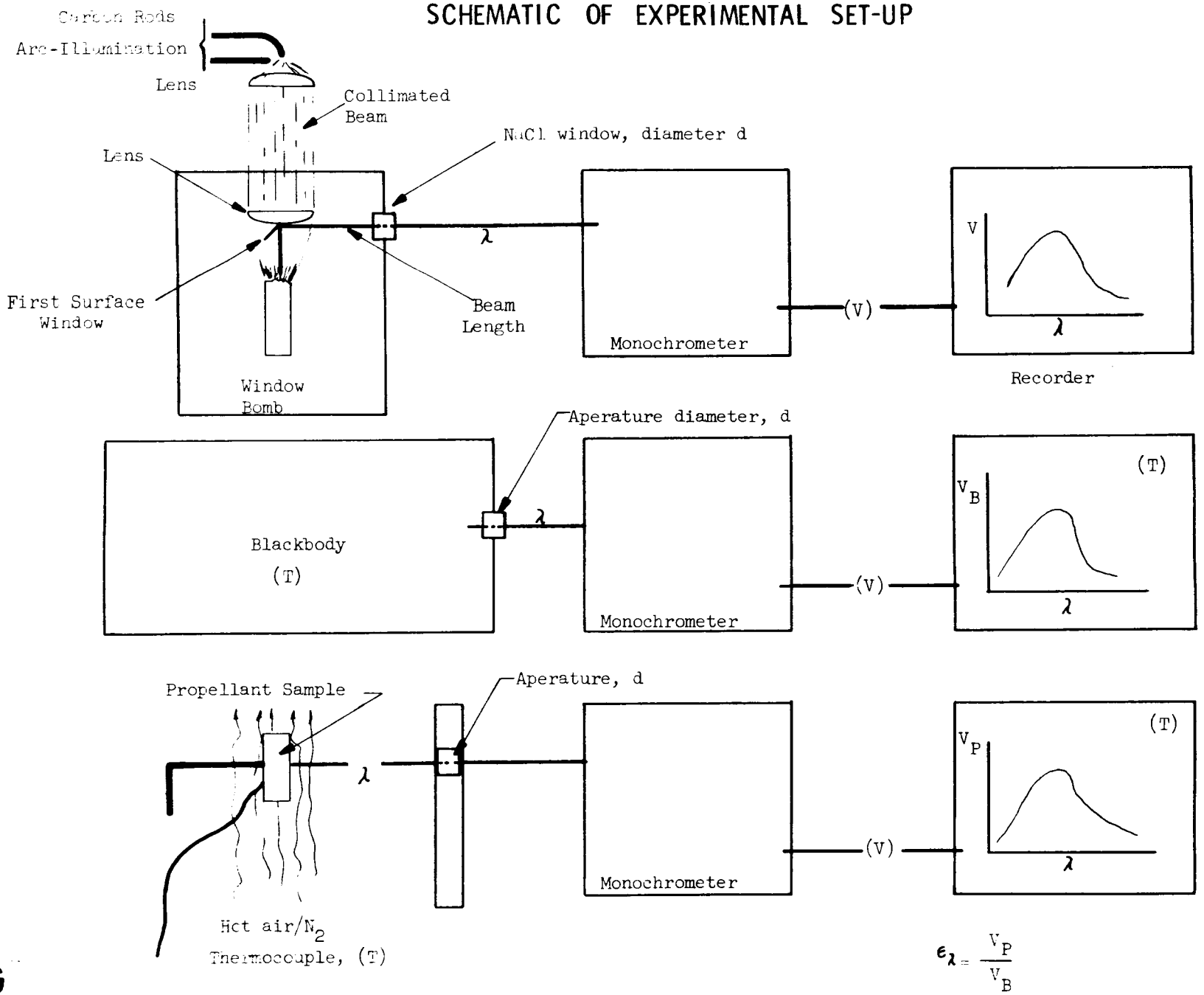

$$\epsilon_\lambda = \frac{V_P}{V_B}$$

Figure 18

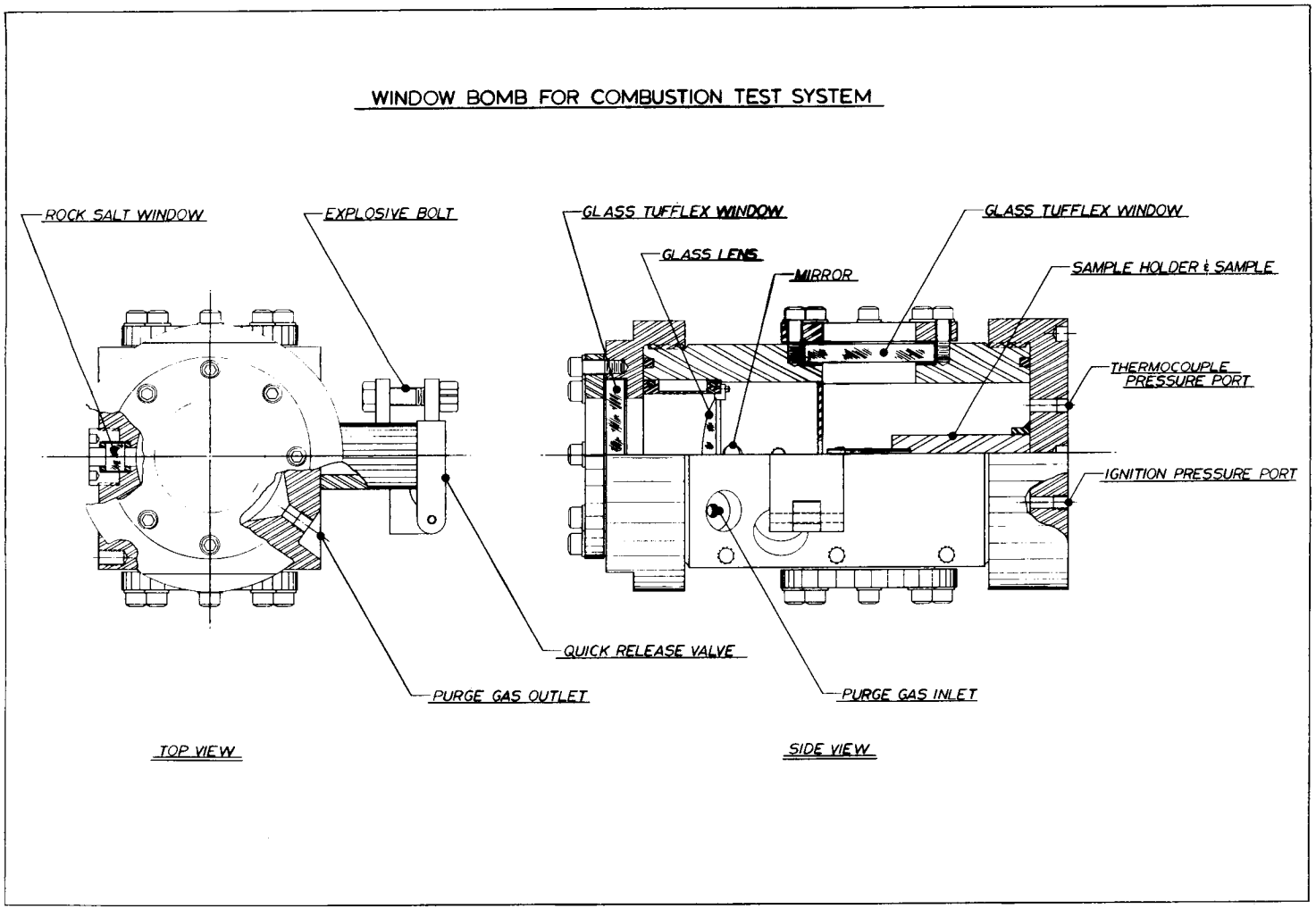
WINDOW BOMB FOR COMBUSTION TEST SYSTEM
ROCK SALT WINDOW
EXPLOSIVE BOLT
GLASS TUFFLEX WINDOW
GLASS TUFFLEX WINDOW
GLASS LENS
MIRROR
SAMPLE HOLDER & SAMPLE
THERMOCOUPLE PRESSURE PORT
IGNITION PRESSURE PORT
QUICK RELEASE VALVE
PURGE GAS OUTLET
PURGE GAS INLET
TOP VIEW
SIDE VIEW

Figure 19

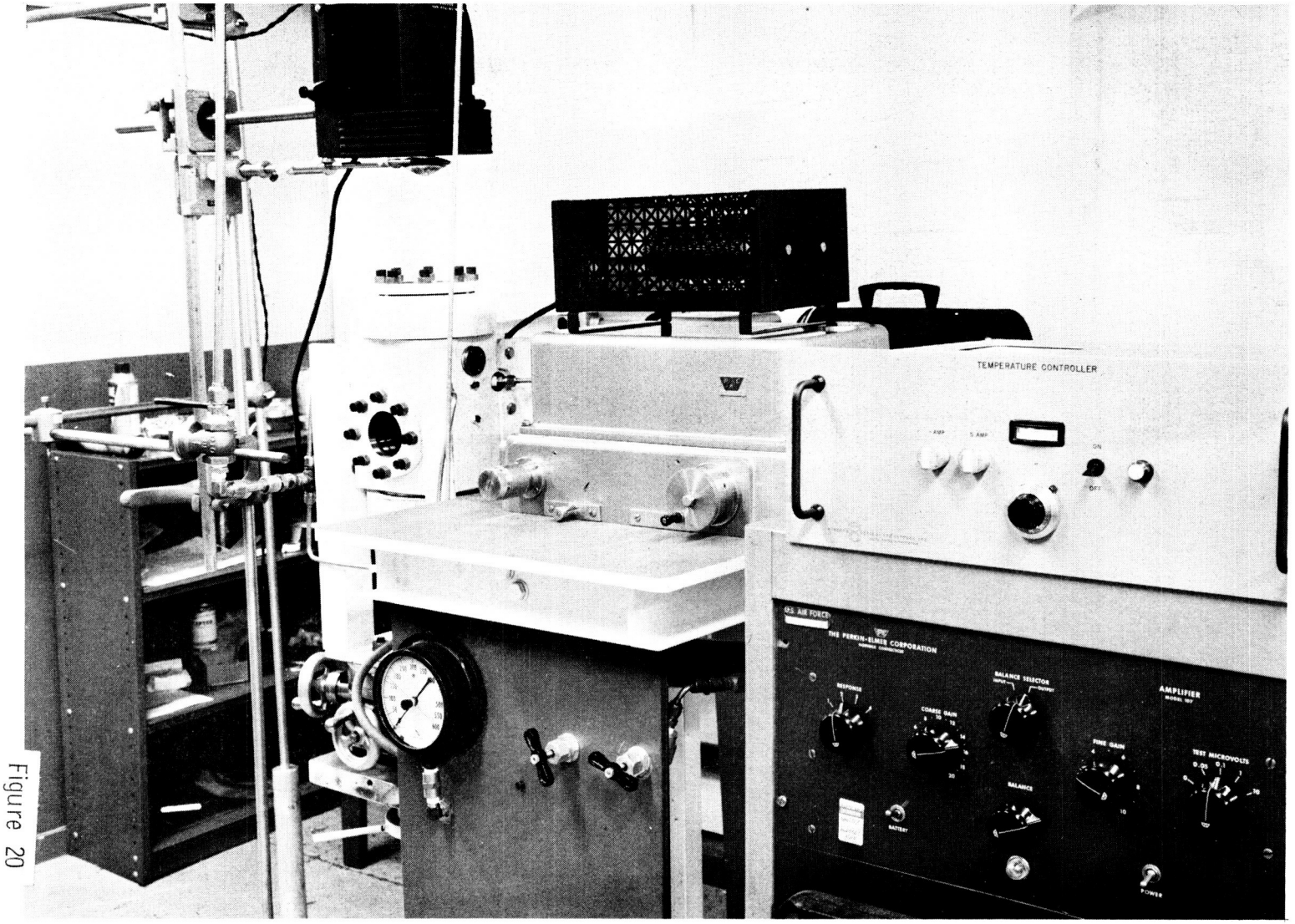
TEMPERATURE CONTROLLER
AMP
5 AMP
ON
OFF
U.S. AIR FORCE
THE PERKIN-ELMER CORPORATION
RESPONSE
COARSE GAIN
BALANCE SELECTOR
FINE GAIN
AMPLIFIER
TEST MICROVOLTS
BALANCE
BATTERY
POWER

Figure 20

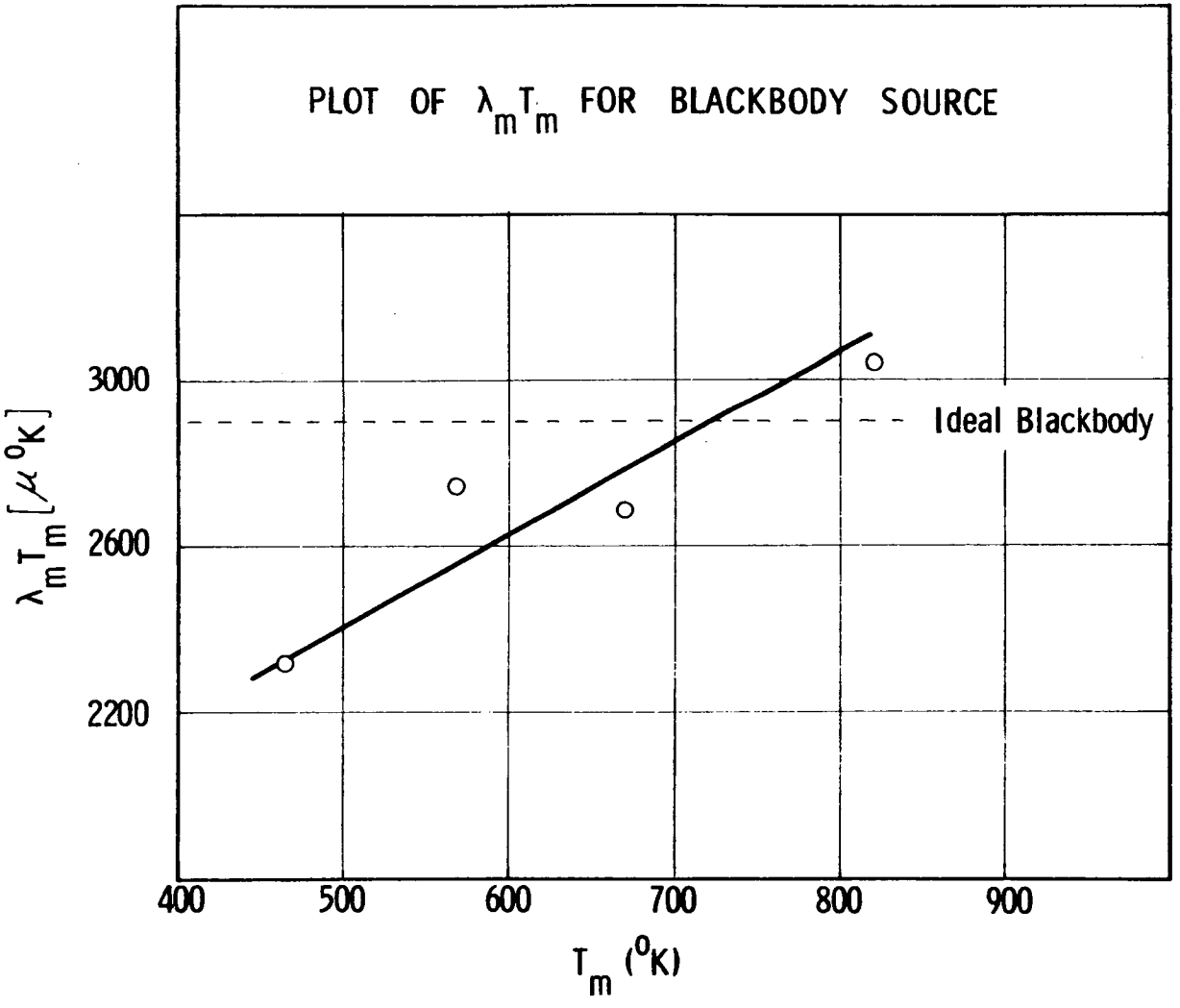
PLOT OF $\lambda_m T_m$ FOR BLACKBODY SOURCE
$\lambda_m T_m [\mu {}^0K]$
3000
2600
2200
Ideal Blackbody
400
500
600
700
800
900
T_m (^0K)

Figure 21

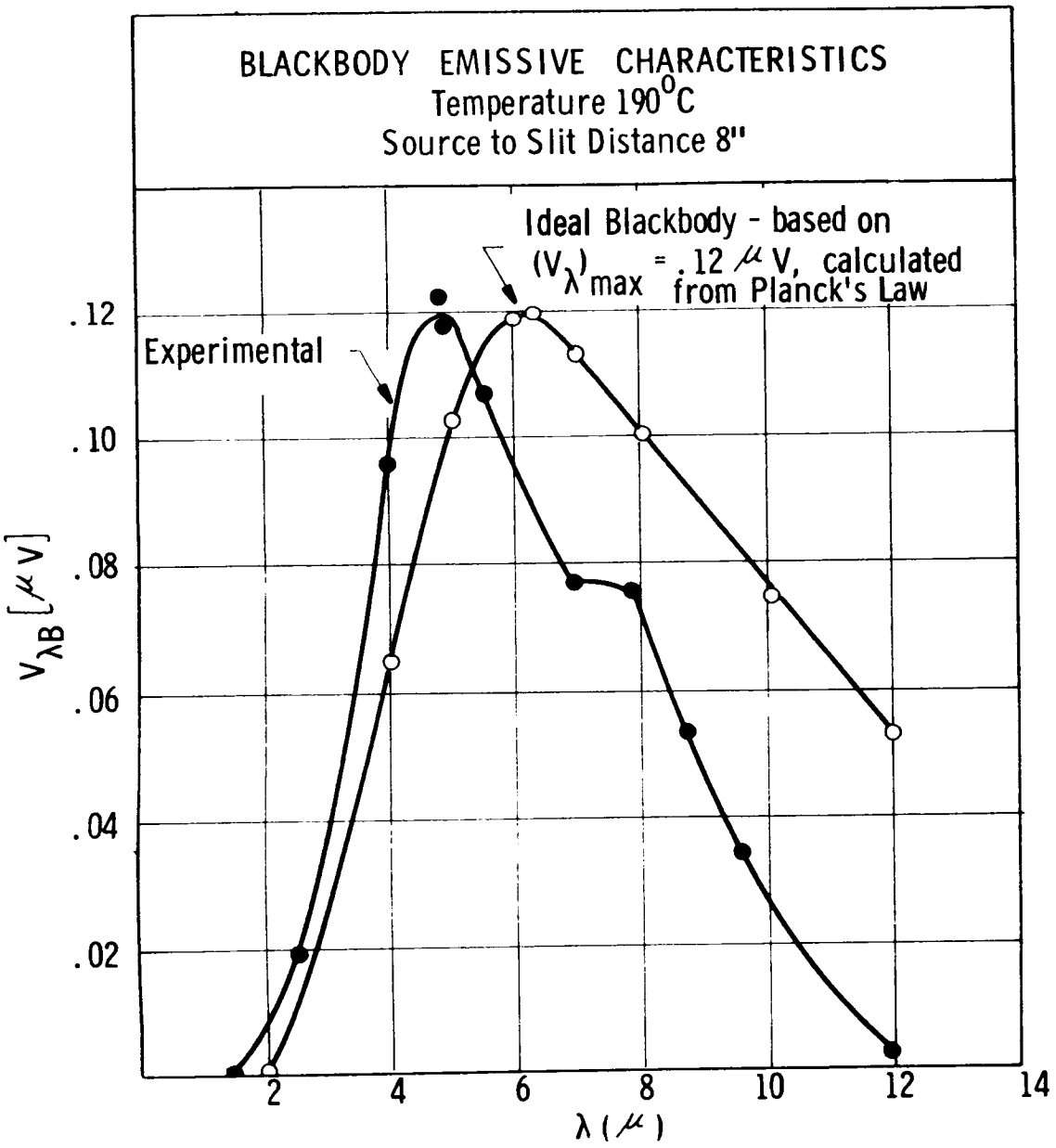
BLACKBODY EMISSIVE CHARACTERISTICS
Temperature 190°C
Source to Slit Distance 8"
Ideal Blackbody - based on
$(V_\lambda)_{max}$ = .12 μV, calculated
from Planck's Law
Experimental
$V_{\lambda B}$ [μV]
.12
.10
.08
.06
.04
.02
2
4
6
8
10
12
14
λ (μ)

Figure 22

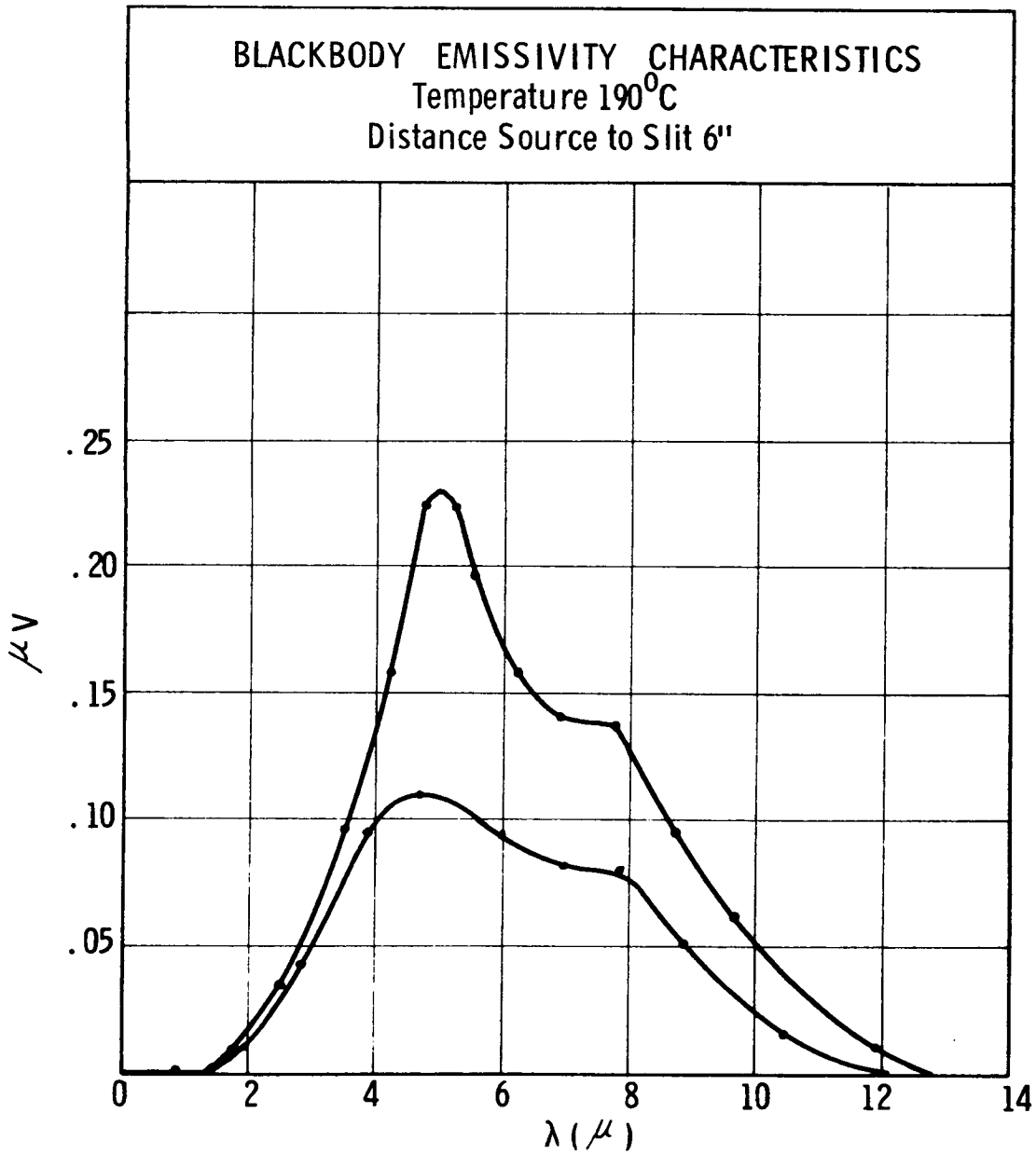
BLACKBODY EMISSIVITY CHARACTERISTICS
Temperature 190°C
Distance Source to Slit 6"
μV
.25
.20
.15
.10
.05
0
2
4
6
8
10
12
14
λ (μ)

Figure 23

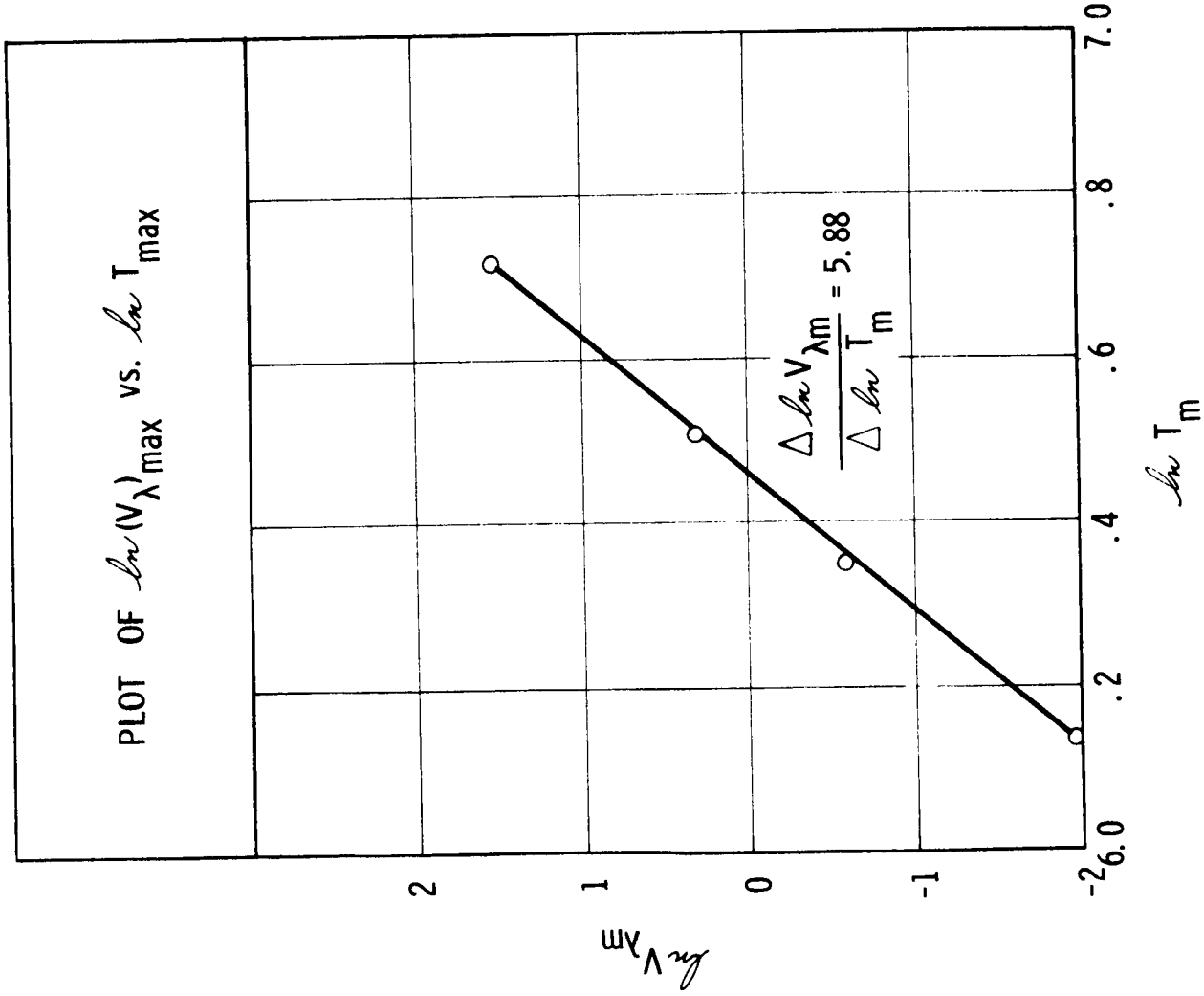
PLOT OF $ln(V_\lambda)_{max}$ vs. $ln\ T_{max}$
$\frac{\Delta ln V_{\lambda m}}{\Delta ln\ T_m} = 5.88$
$ln\ V_{\lambda m}$
$ln\ T_m$
2
1
0
-1
-2
6.0
.2
.4
.6
.8
7.0

Figure 24

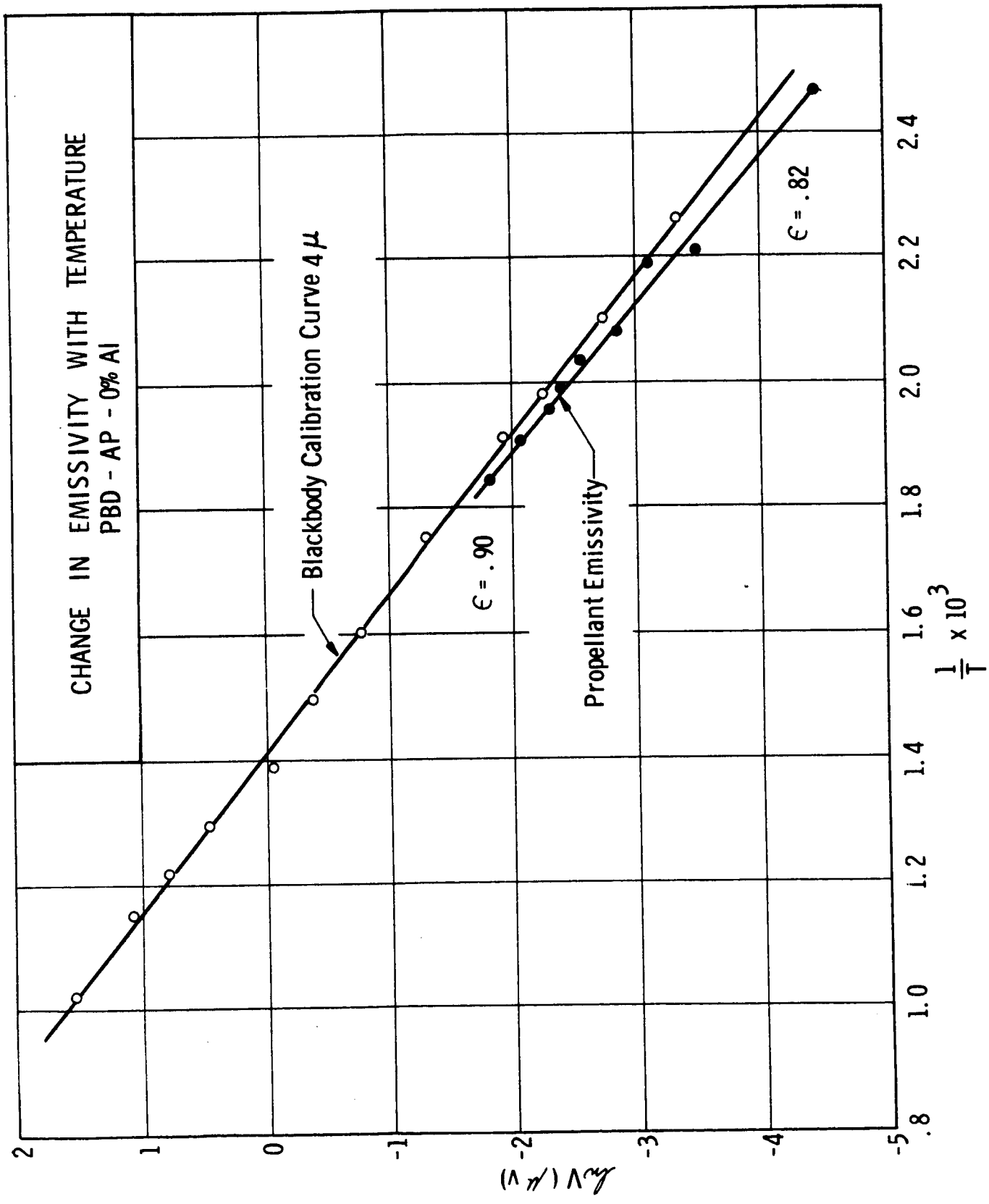
CHANGE IN EMISSIVITY WITH TEMPERATURE
PBD - AP - 0% Al
Blackbody Calibration Curve 4 μ
ε = .90
ε = .82
Propellant Emissivity
2
1
0
-1
-2
-3
-4
-5
.8
1.0
1.2
1.4
1.6
1.8
2.0
2.2
2.4
1/T x 10^3
Δ E_λ V (μ V)

Figure 25

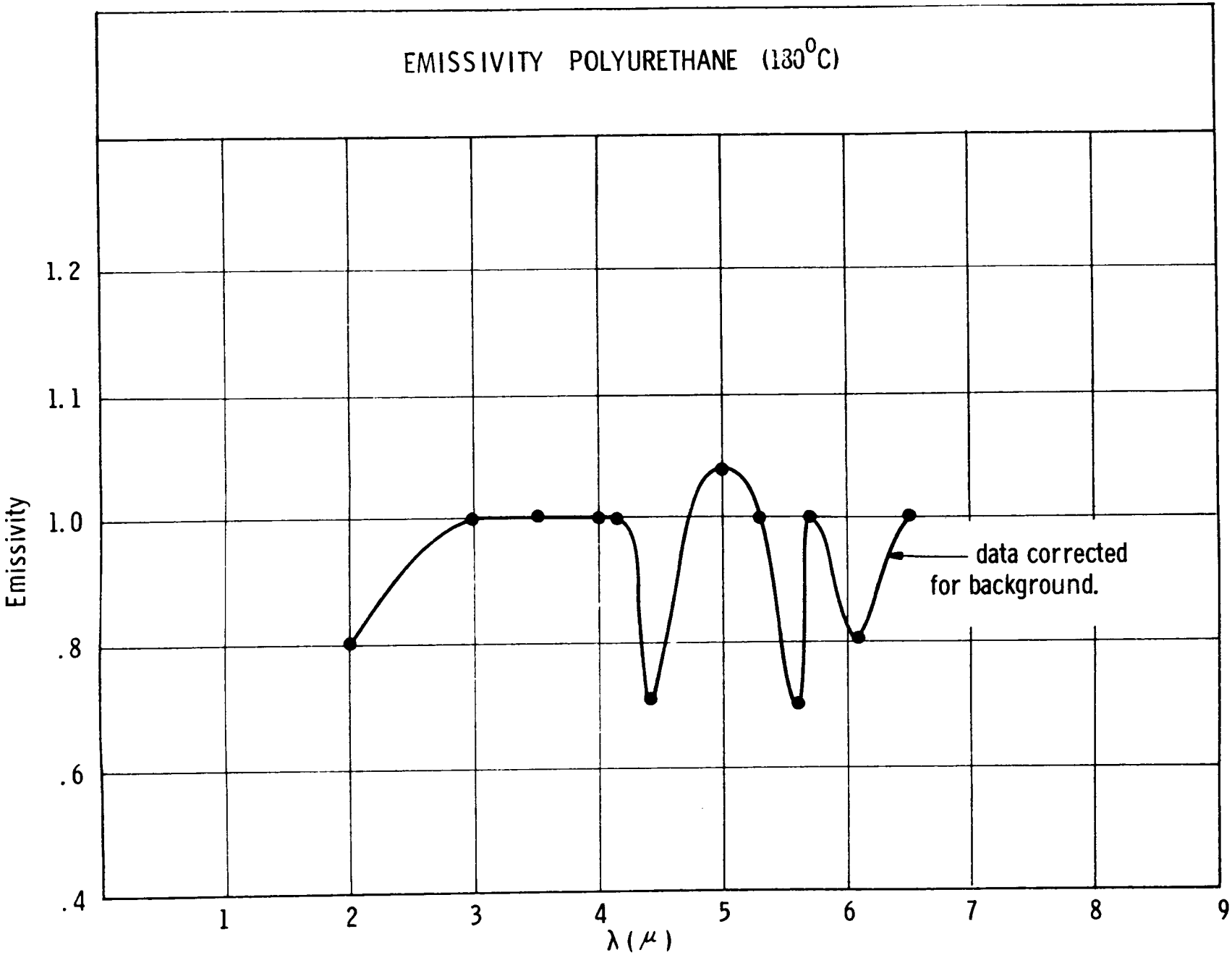
EMISSIVITY POLYURETHANE (130°C)
Emissivity
1.2
1.1
1.0
.8
.6
.4
1
2
3
4
5
6
7
8
9
λ (μ)
data corrected
for background.

Figure 26a

PBD-AP PROPELLANT

T = 178 °C

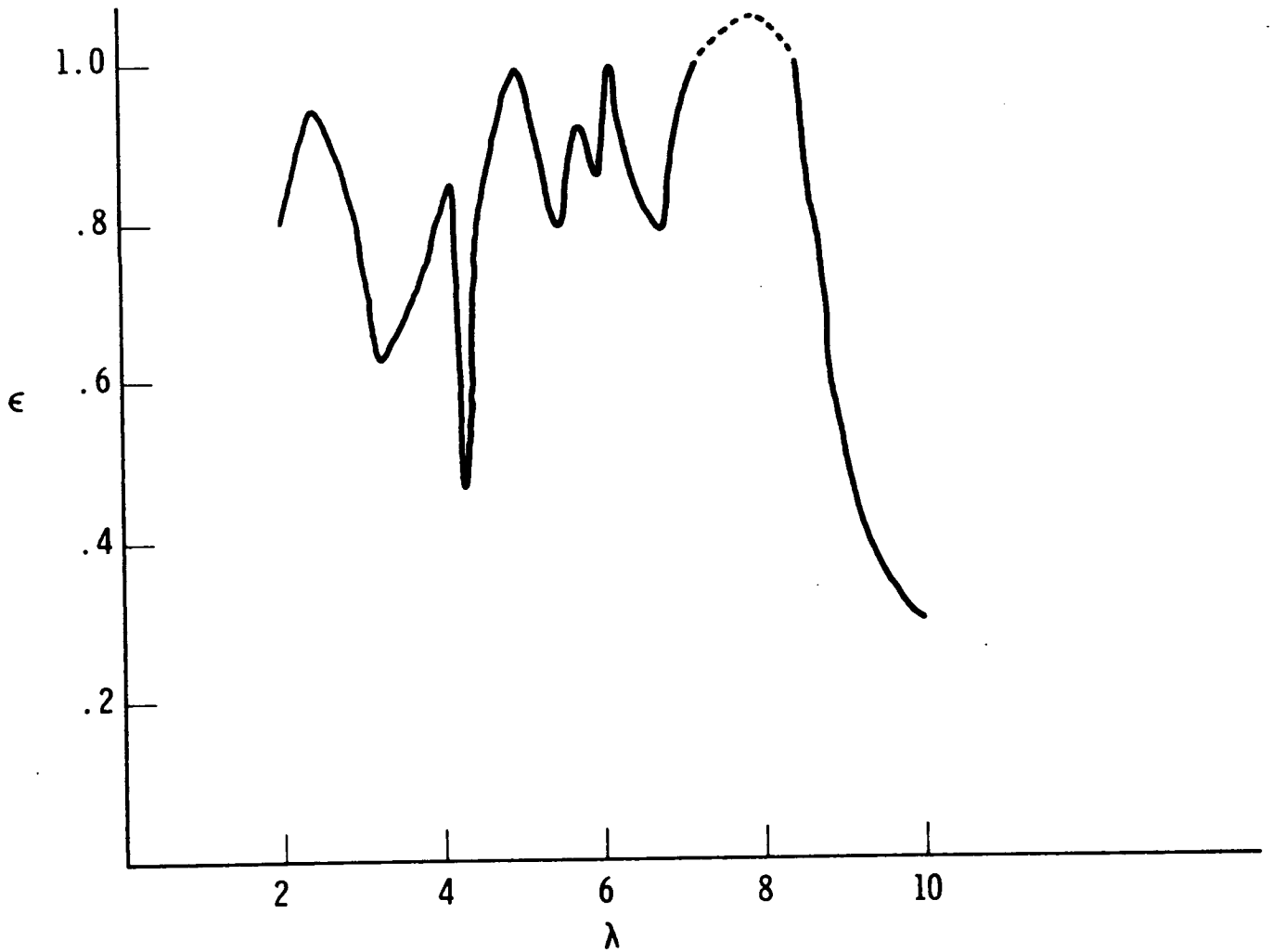

Figure 26 b

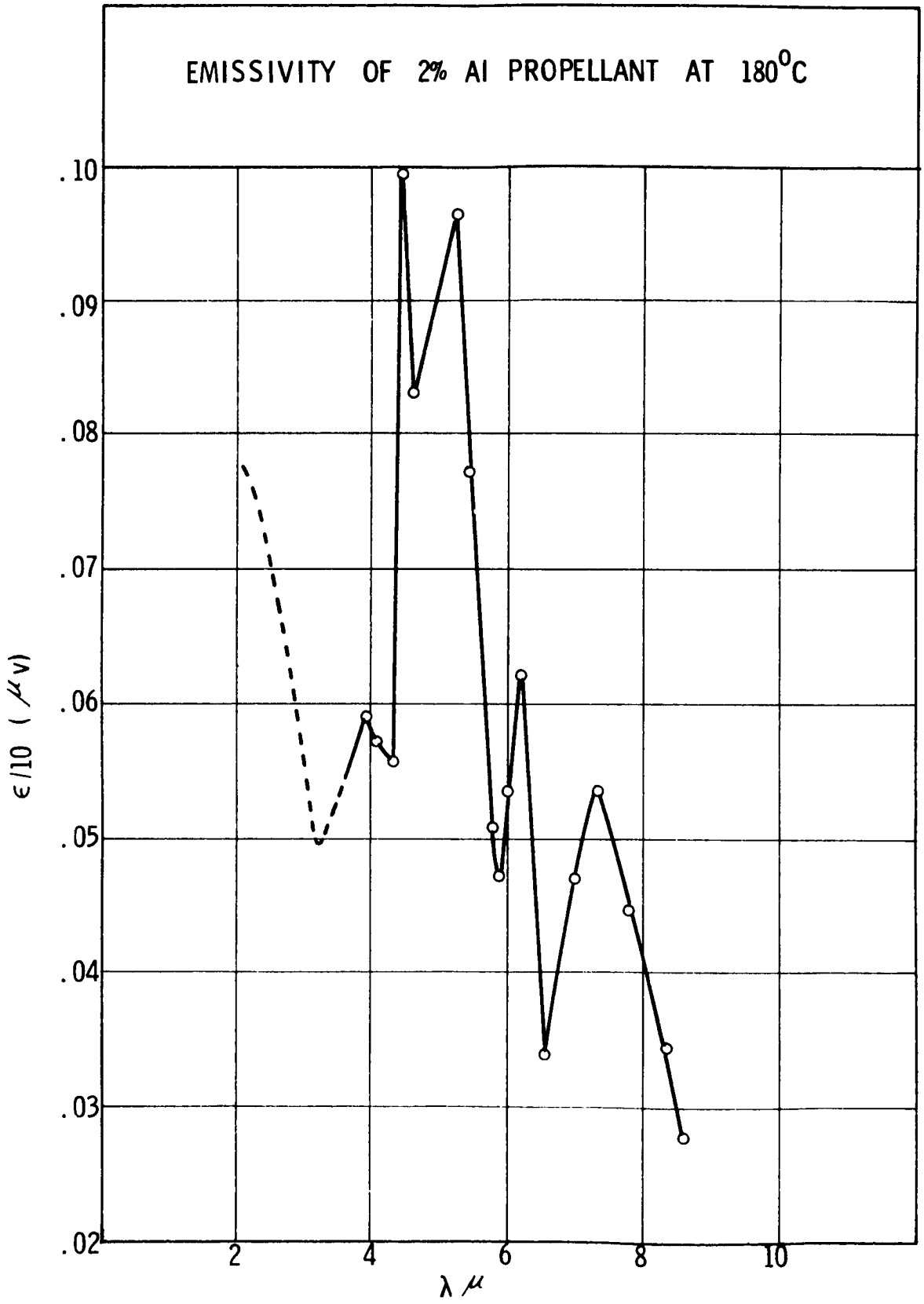
EMISSIVITY OF 2% Al PROPELLANT AT 180°C
.10
.09
.08
.07
.06
.05
.04
.03
.02
ε/10 (μv)
2
4
6
8
10
λ μ

Figure 26c

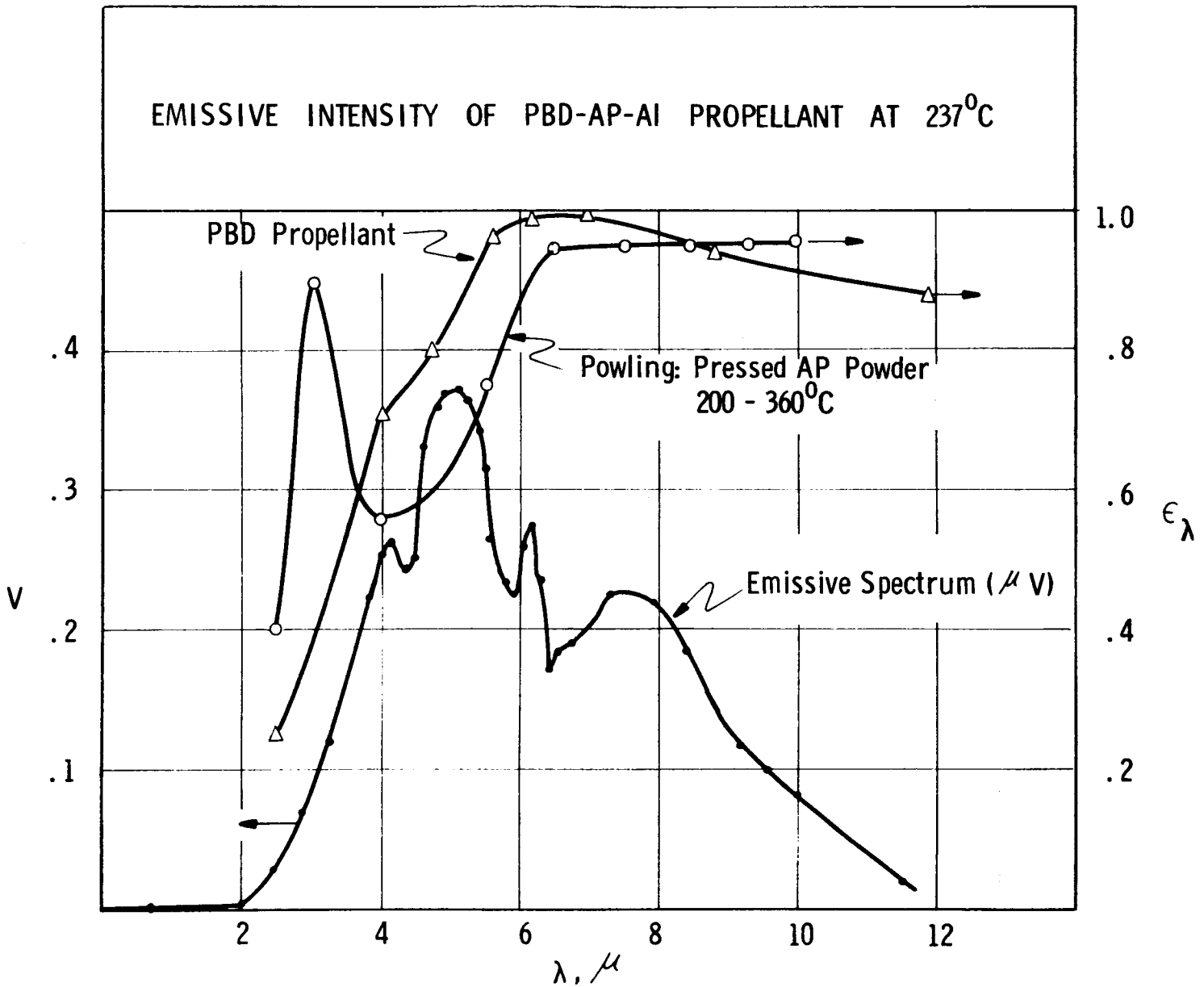
EMISSIVE INTENSITY OF PBD-AP-Al PROPELLANT AT 237°C
PBD Propellant
Powling: Pressed AP Powder
200 - 360°C
Emissive Spectrum (μ V)
V
.1
.2
.3
.4
1.0
.8
.6
.4
.2
ϵ_λ
2
4
6
8
10
12
λ, μ

Figure 27

DEPRESSURIZATION TEST WITH THERMOCOUPLE READING AND MONOCHROMATOR

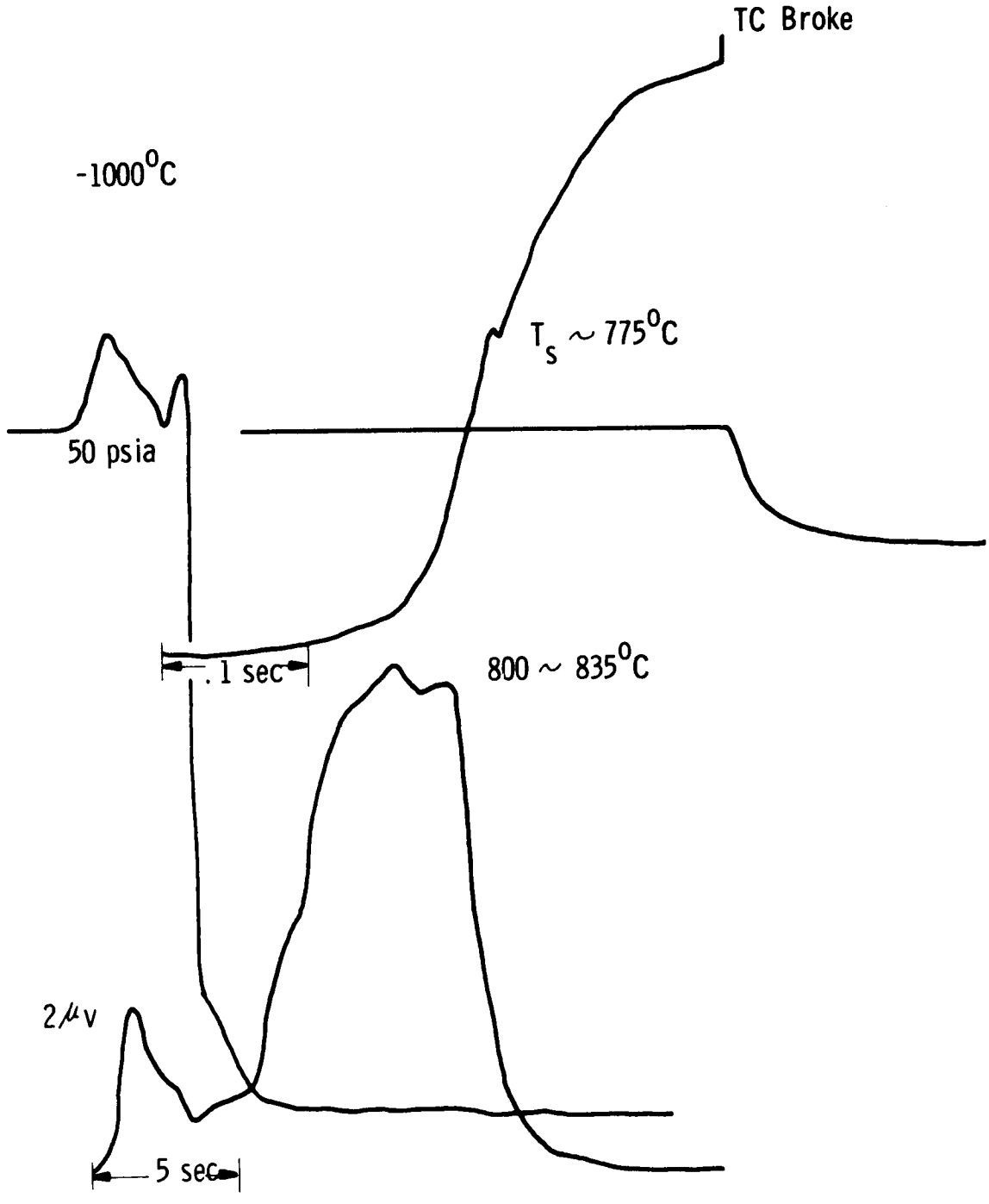

Figure 28

SCANNING PROFILE OF PU-AP

Figure 29

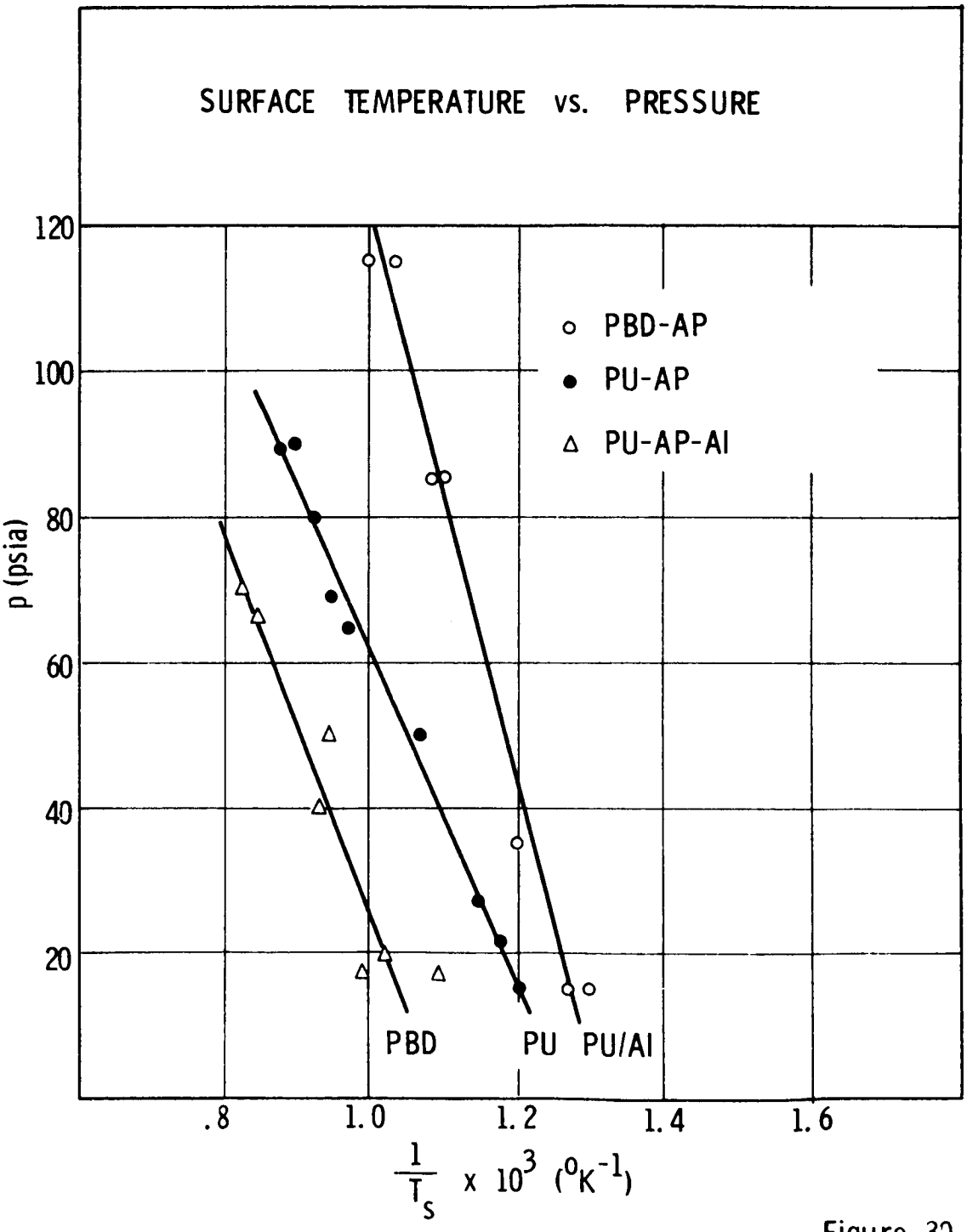
SURFACE TEMPERATURE vs. PRESSURE
120
100
80
60
40
20
p (psia)
PBD-AP
PU-AP
PU-AP-Al
PBD
PU
PU/Al
.8
1.0
1.2
1.4
1.6
$\frac{1}{T_s} \times 10^3$ ($^0K^{-1}$)

Figure 30

SURFACE TEMPERATURE DURING DEPRESSURIZATION
AP-PU-2% Aluminum Propellant

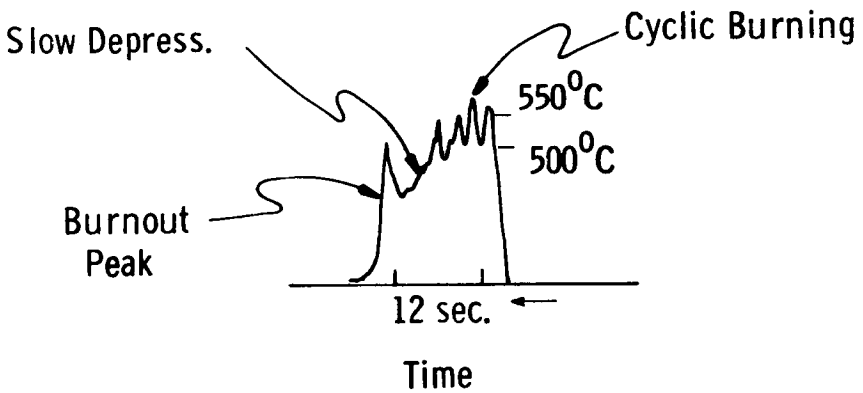

Figure 31

SURFACE TEMPERATURE RESPONSE DURING DEPRESSURIZATION

PBD-AP

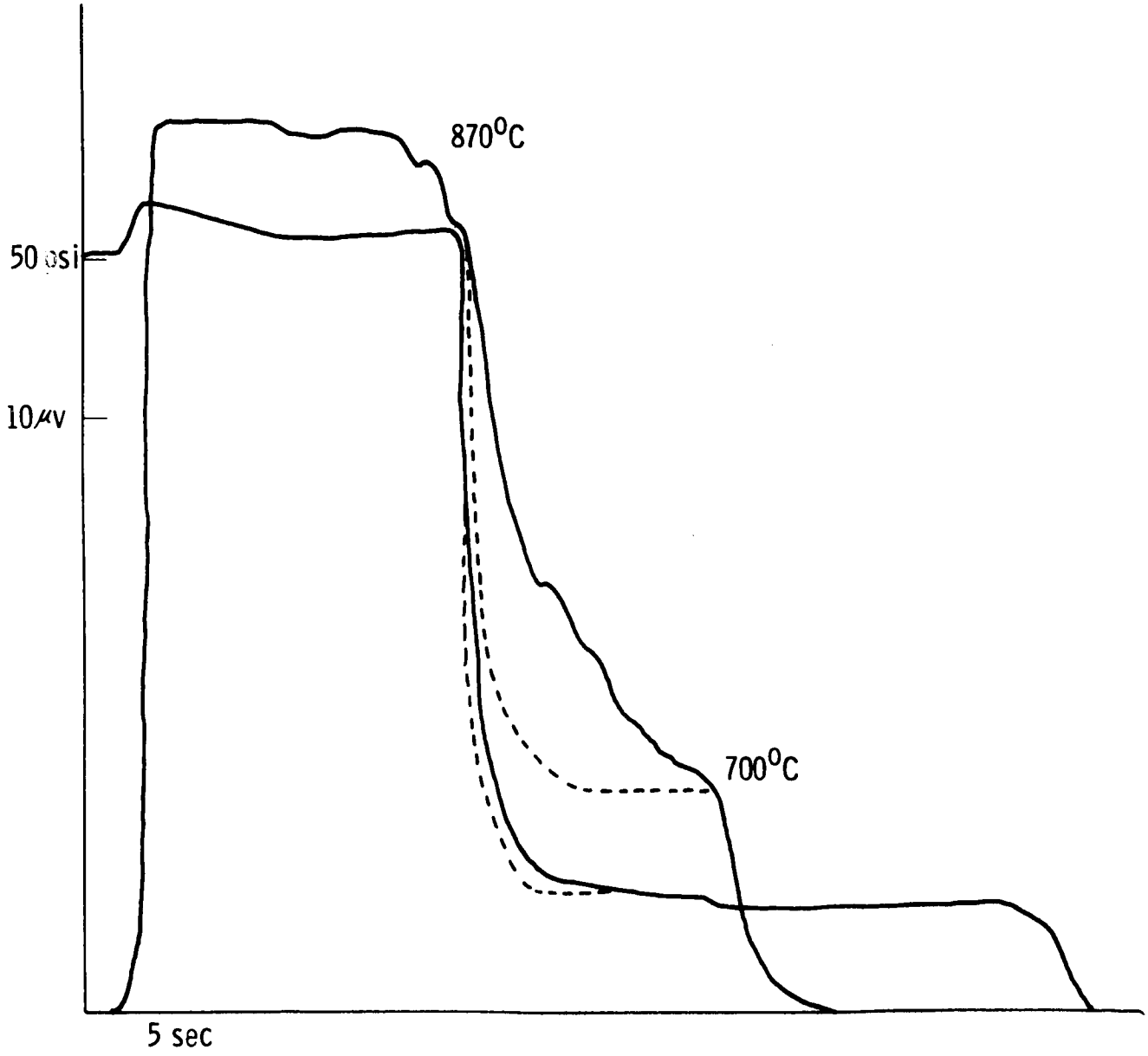

Figure 32

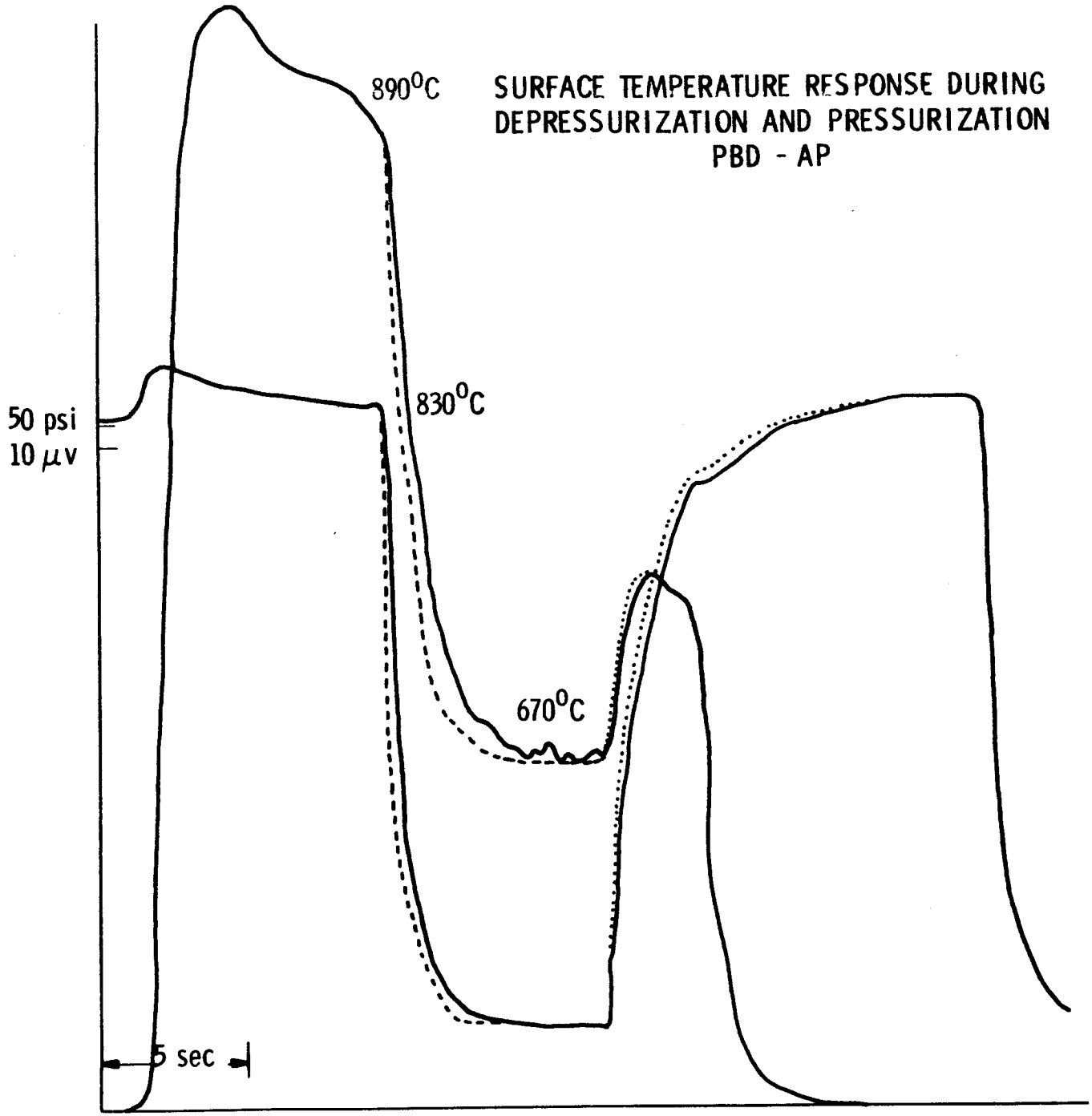
890°C
SURFACE TEMPERATURE RESPONSE DURING
DEPRESSURIZATION AND PRESSURIZATION
PBD - AP
830°C
50 psi
10 μv
670°C
5 sec

Figure 33

PU-AP DEPRESSURIZATION TEST

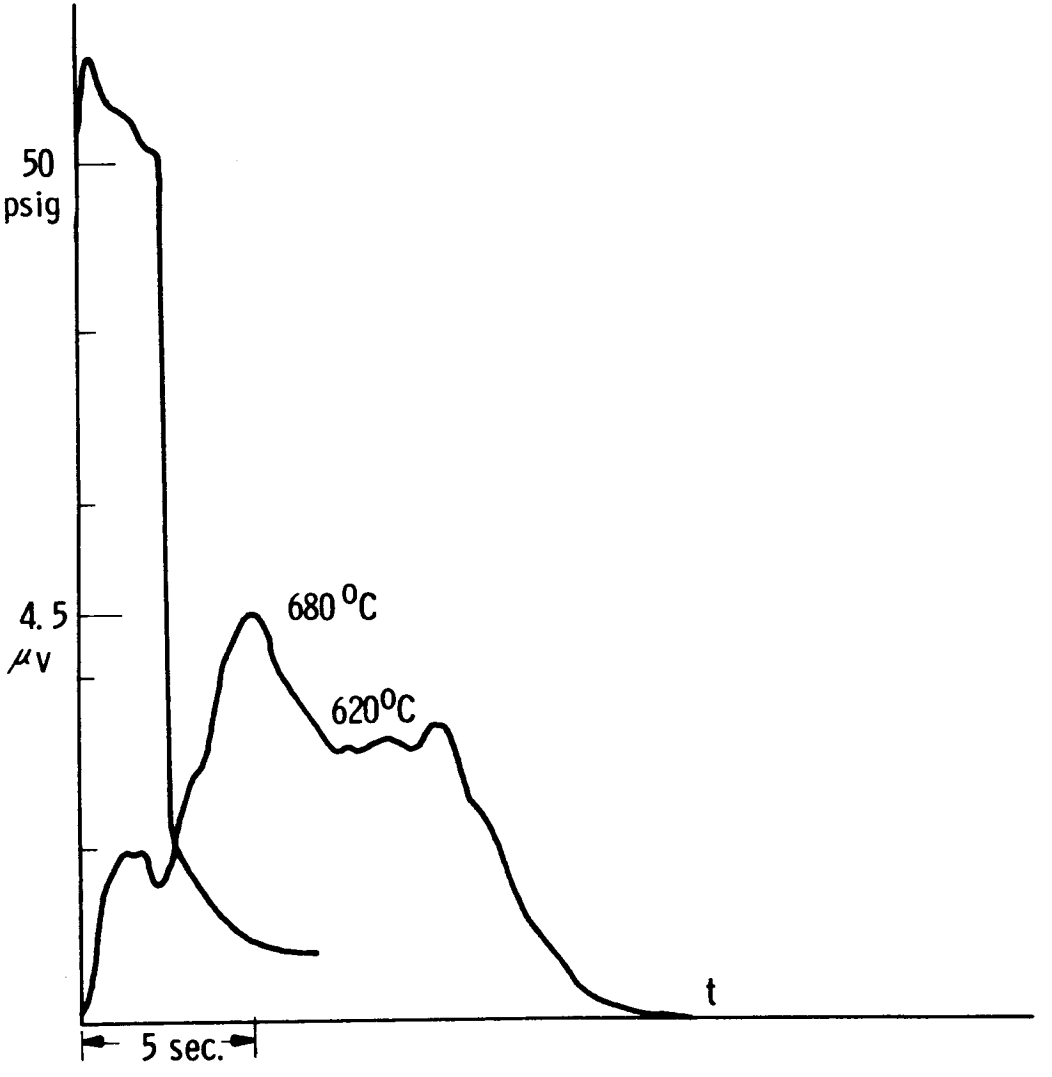

Note: Pressure leads monochrometer trace by .5 sec.

Figure 34

SURFACE TEMPERATURE CHANGES DURING PRESSURIZATION
FOR POLYURETHANE-AP PROPELLANT

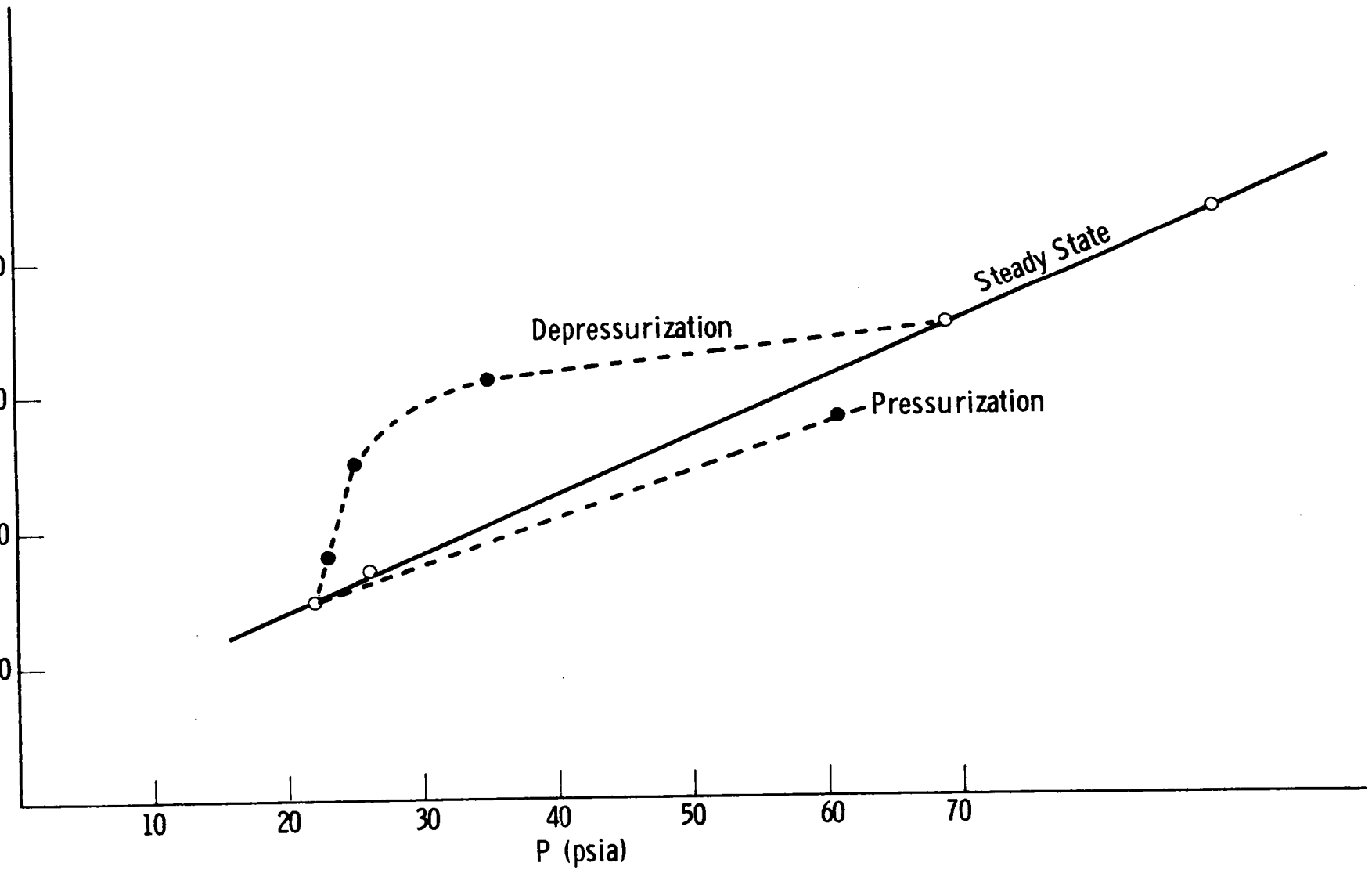

Figure 35

POLYBUTADIENE PROPELLANT
SURFACE TEMPERATURE CHANGES DURING PRESSURIZATION

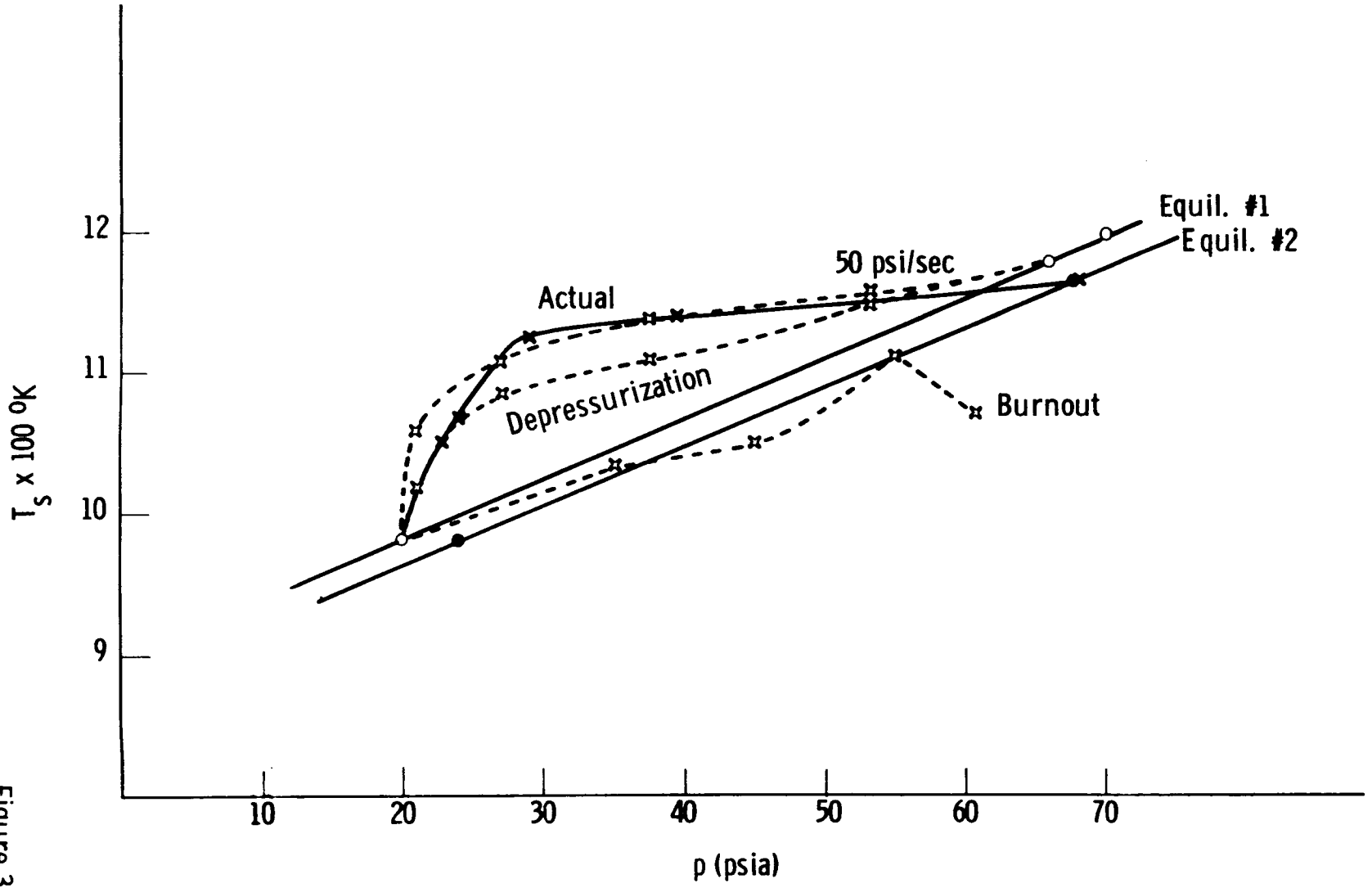

Figure 36

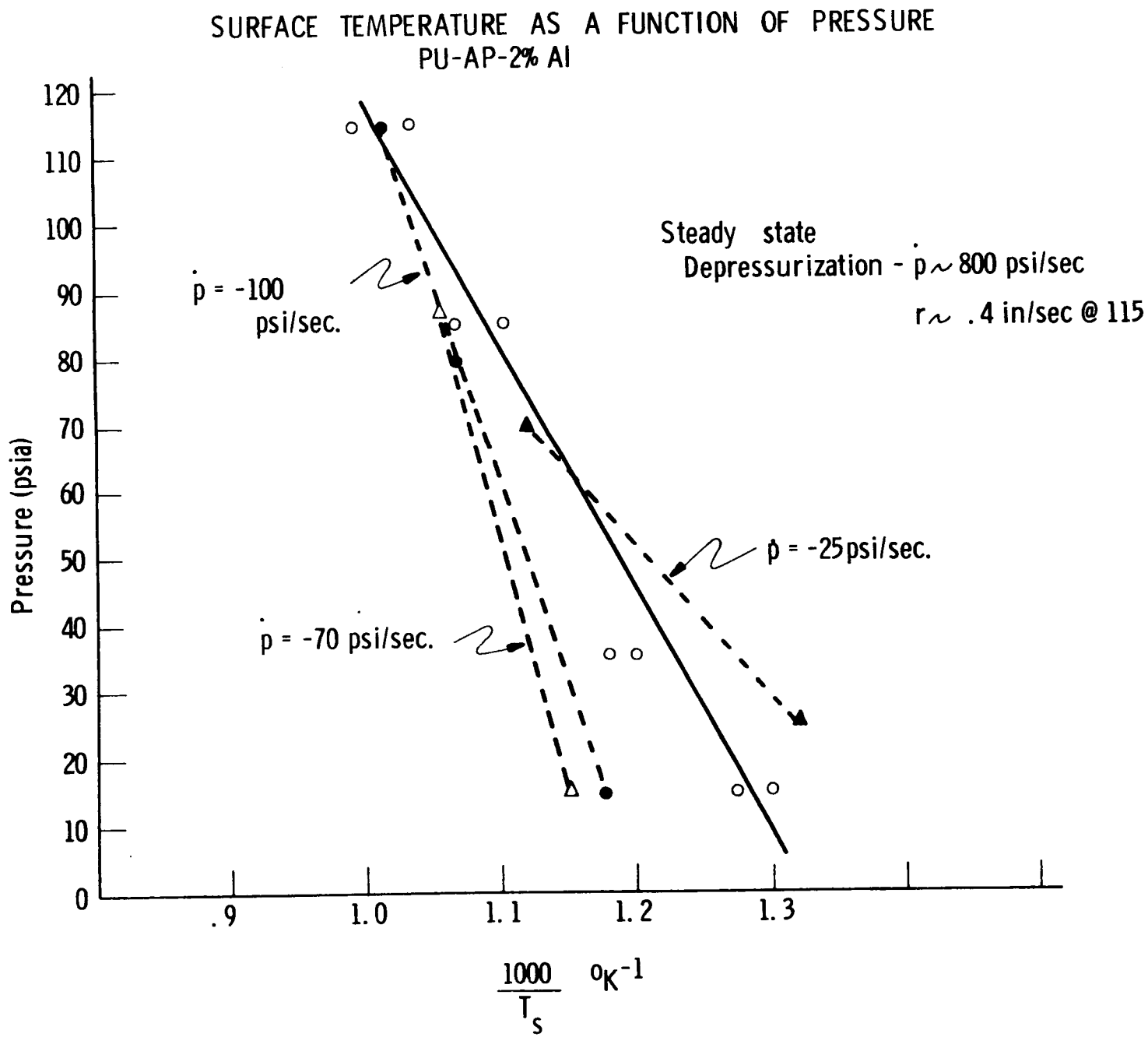
SURFACE TEMPERATURE AS A FUNCTION OF PRESSURE
PU-AP-2% Al
Pressure (psia)
120
110
100
90
80
70
60
50
40
30
20
10
0
.9
1.0
1.1
1.2
1.3
1000 / T_s °K^-1
Steady state
Depressurization - ṗ ~ 800 psi/sec
r ~ .4 in/sec @ 115
ṗ = -100 psi/sec.
ṗ = -25 psi/sec.
ṗ = -70 psi/sec.

Figure 37

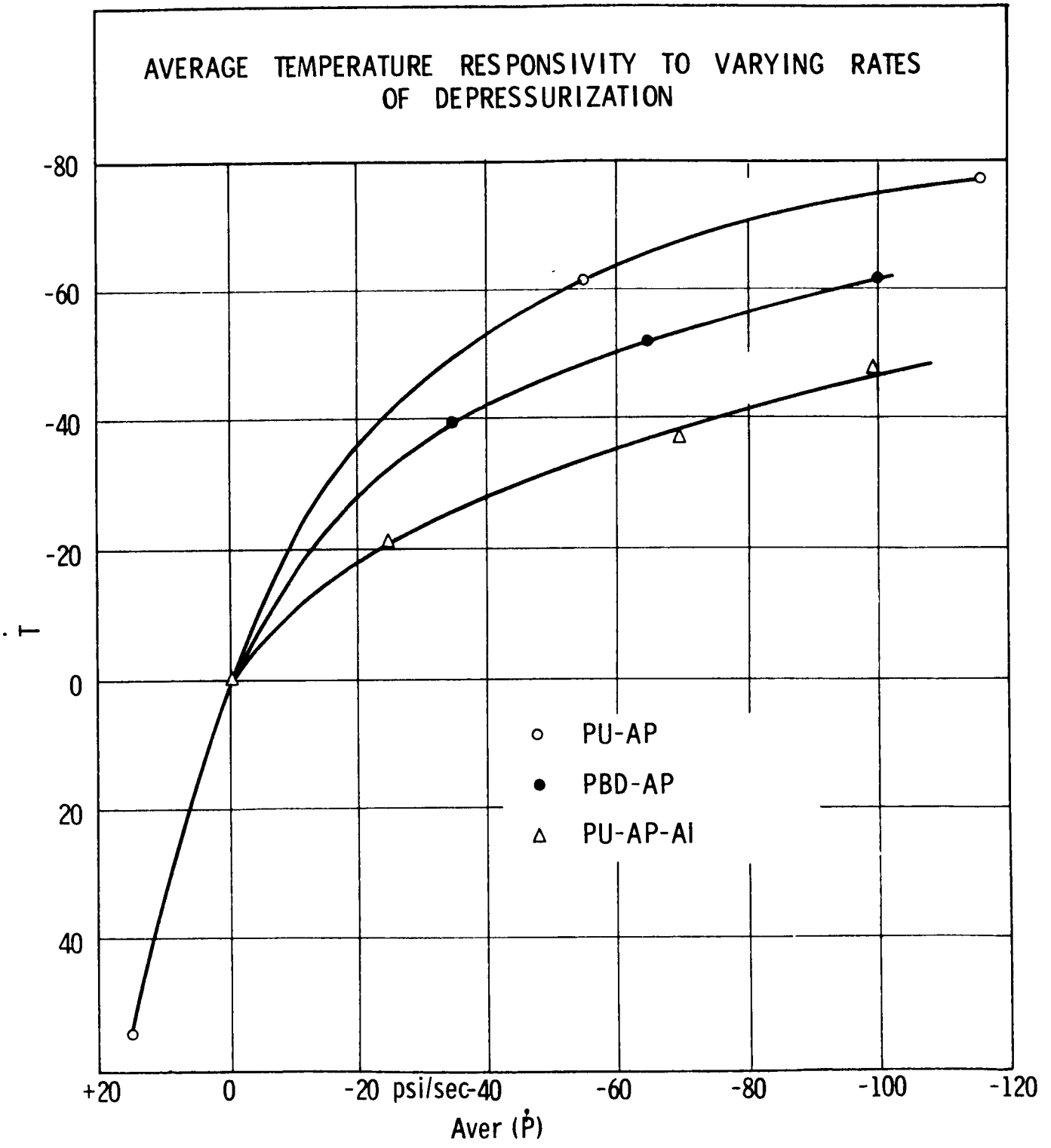
AVERAGE TEMPERATURE RESPONSIVITY TO VARYING RATES OF DEPRESSURIZATION
-80
-60
-40
-20
0
20
40
T
PU-AP
PBD-AP
PU-AP-Al
+20
0
-20
-40
-60
-80
-100
-120
psi/sec
Aver (Ṗ)

Figure 38

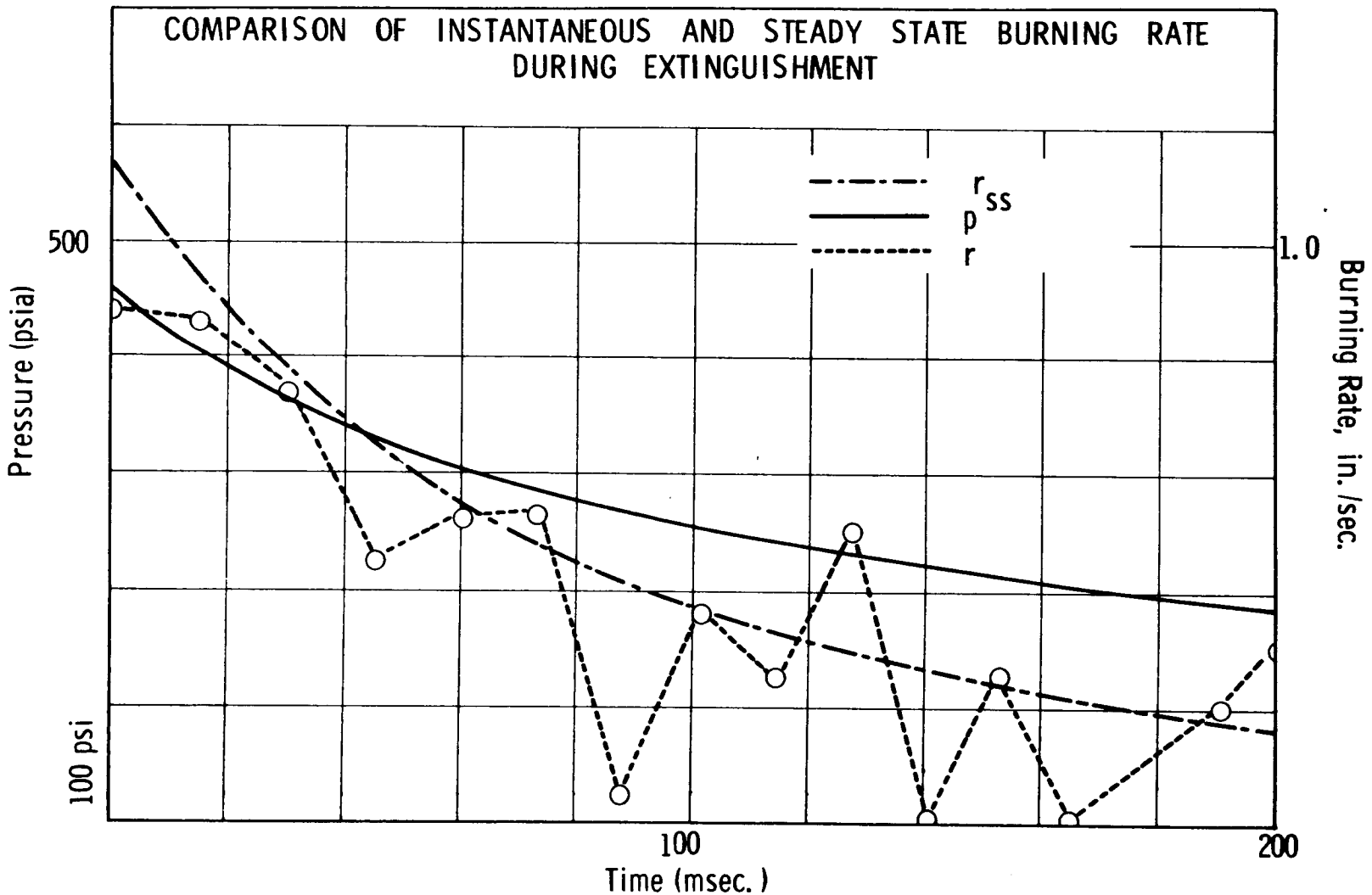
COMPARISON OF INSTANTANEOUS AND STEADY STATE BURNING RATE
DURING EXTINGUISHMENT
r_{ss}
p
r
500
100 psi
Pressure (psia)
1.0
Burning Rate, in./sec.
100
200
Time (msec.)

Figure 39

PROFILE RESPONSE AT 50μ BELOW SURFACE DURING DEPRESSURIZATION

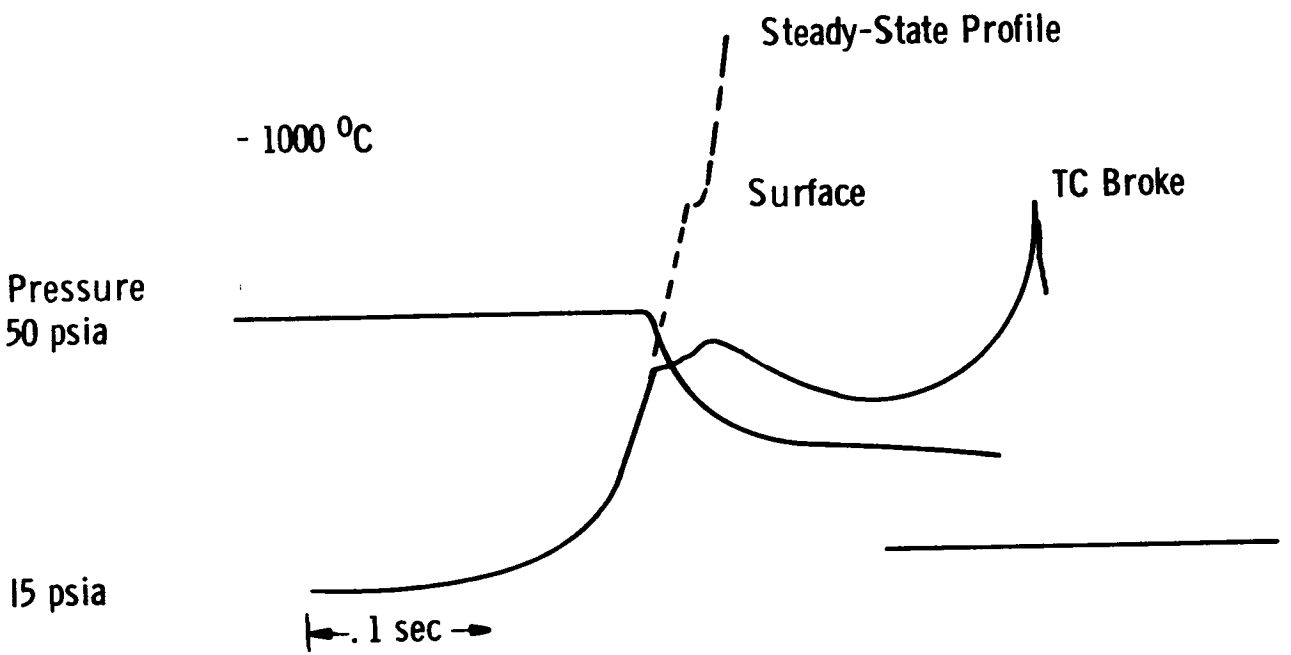

Figure 40

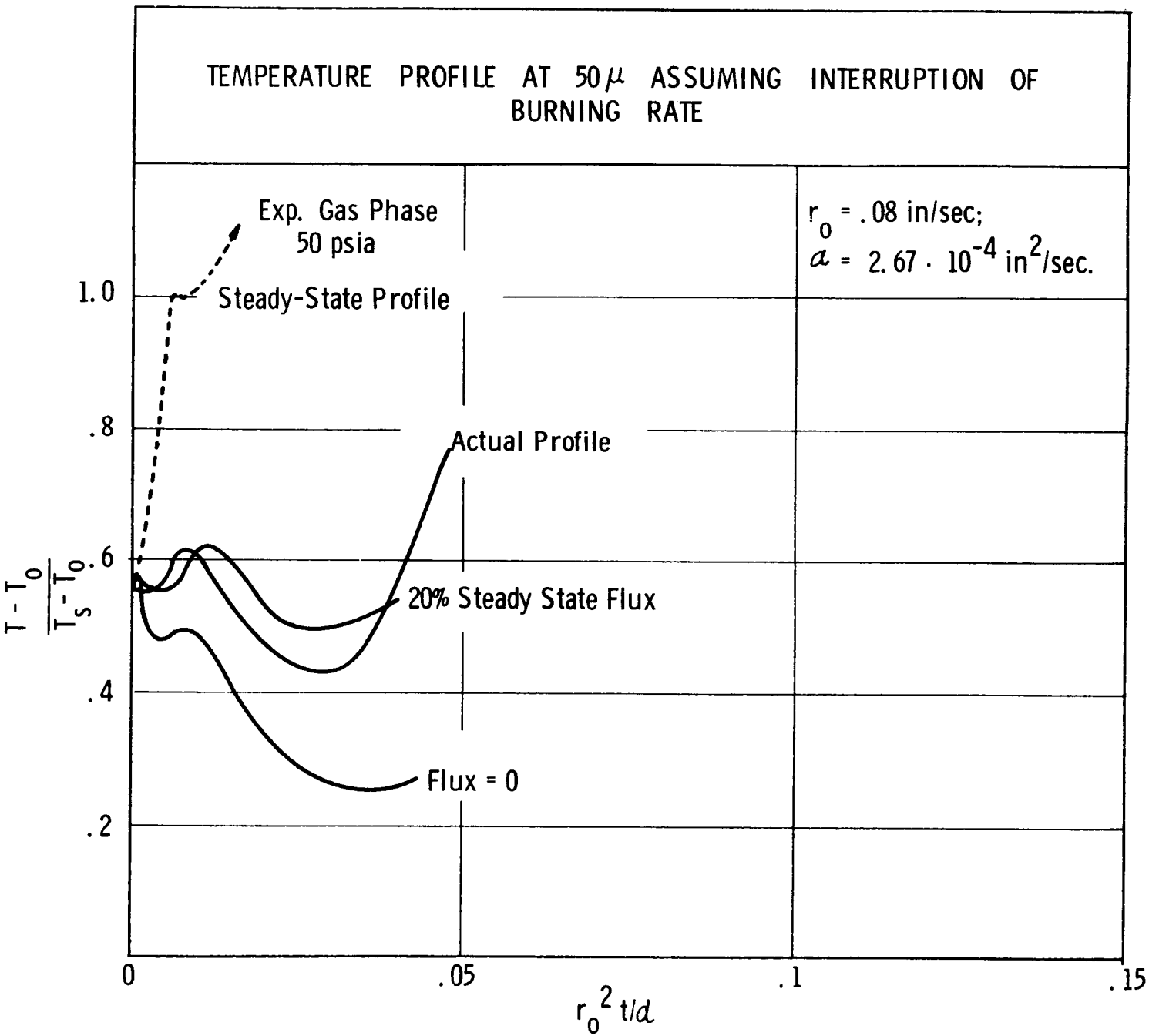
TEMPERATURE PROFILE AT 50 μ ASSUMING INTERRUPTION OF BURNING RATE
Exp. Gas Phase 50 psia
Steady-State Profile
r_0 = .08 in/sec;
α = 2.67 · 10^{-4} in^2/sec.
Actual Profile
20% Steady State Flux
Flux = 0
$\frac{T - T_0}{T_s - T_0}$
1.0
.8
.6
.4
.2
0
.05
.1
.15
r_0^2 t/d

Figure 41

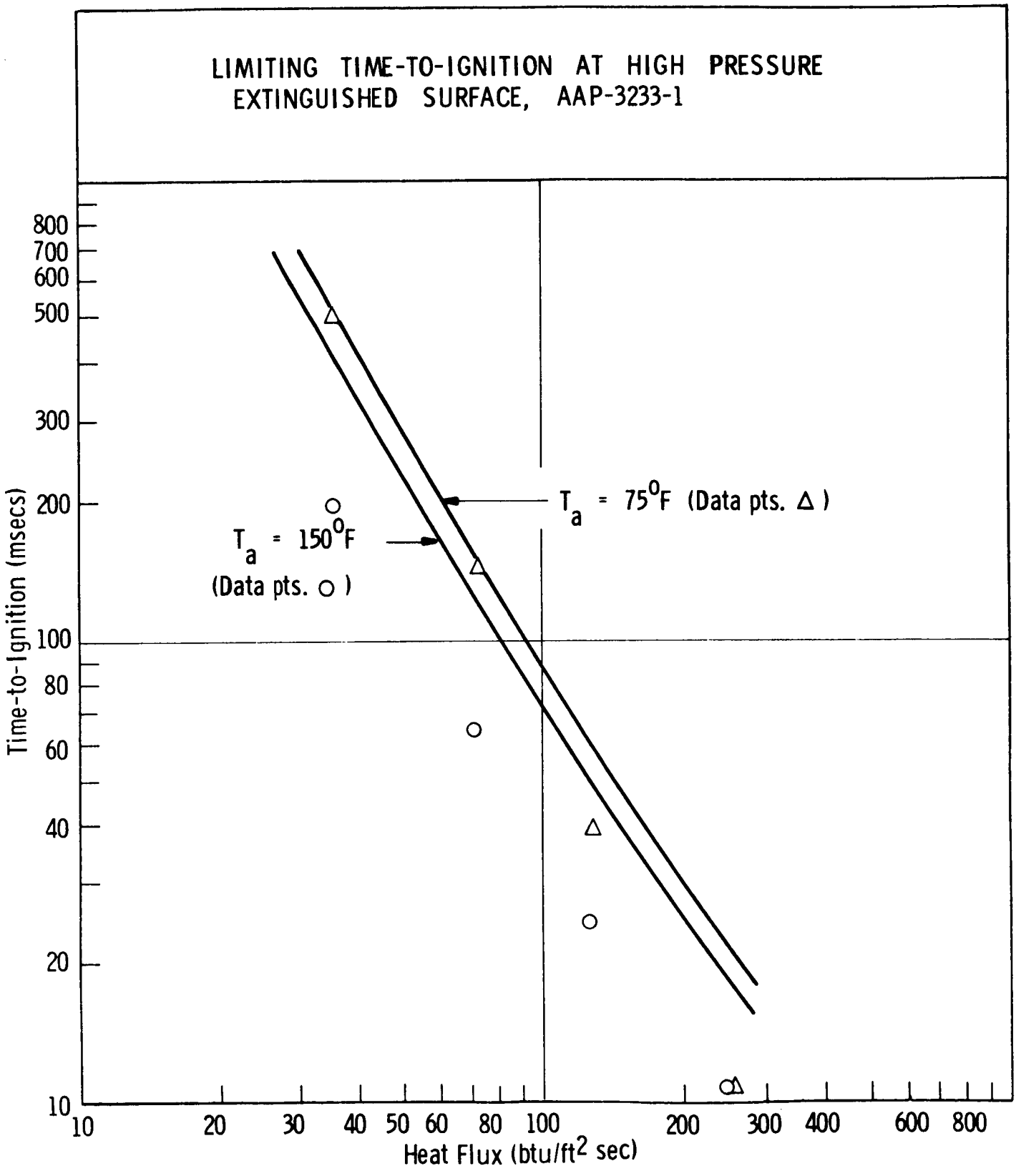
LIMITING TIME-TO-IGNITION AT HIGH PRESSURE
EXTINGUISHED SURFACE, AAP-3233-1
Time-to-Ignition (msecs)
800
700
600
500
300
200
100
80
60
40
20
10
T_a = 150°F
(Data pts. ○)
T_a = 75°F (Data pts. Δ)
10
20
30
40
50
60
80
100
200
300
400
600
800
Heat Flux (btu/ft² sec)

Figure 42

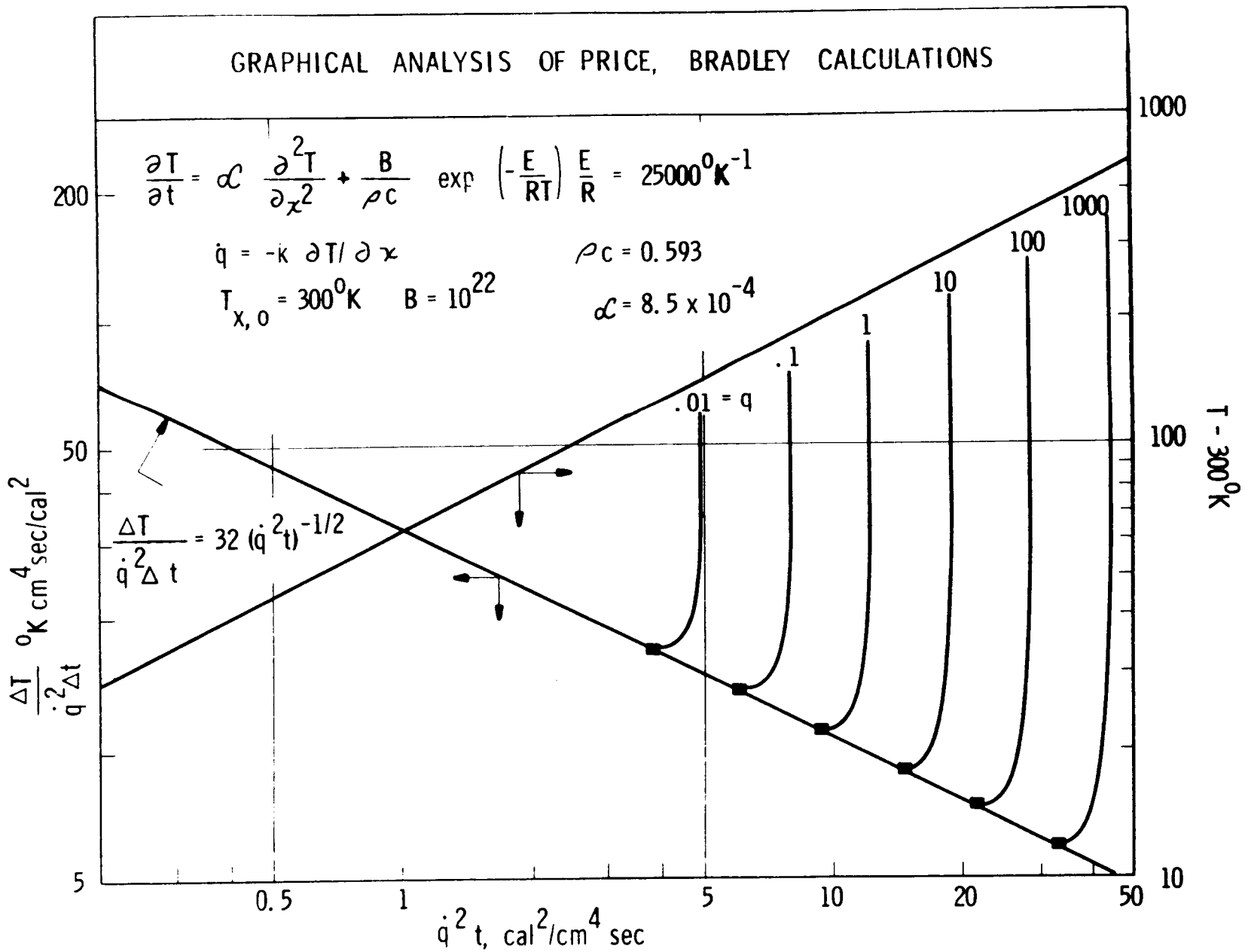
GRAPHICAL ANALYSIS OF PRICE, BRADLEY CALCULATIONS
$\frac{\partial T}{\partial t} = \alpha \frac{\partial^2 T}{\partial x^2} + \frac{B}{\rho c} \exp\left(-\frac{E}{RT}\right) \frac{E}{R} = 25000^{\circ}K^{-1}$
$\dot{q} = -k\, \partial T / \partial x$
$\rho c = 0.593$
$T_{x,0} = 300^{\circ}K$ $B = 10^{22}$
$\alpha = 8.5 \times 10^{-4}$
.01 = q
.1
1
10
100
1000
$\frac{\Delta T}{\dot{q}^2 \Delta t} = 32 (\dot{q}^2 t)^{-1/2}$
$\frac{\Delta T}{\dot{q}^2 \Delta t}$ $^{o}K\ cm^4 sec/cal^2$
200
50
5
0.5
1
5
10
20
50
$\dot{q}^2 t$, $cal^2/cm^4\ sec$
1000
100
10
T - 300°K

Figure 43

IGNITION BY RADIANT HEAT FLUX
COMPARISON OF THERMOCOUPLE AND MONOCHROMETER AT 2.2 μ

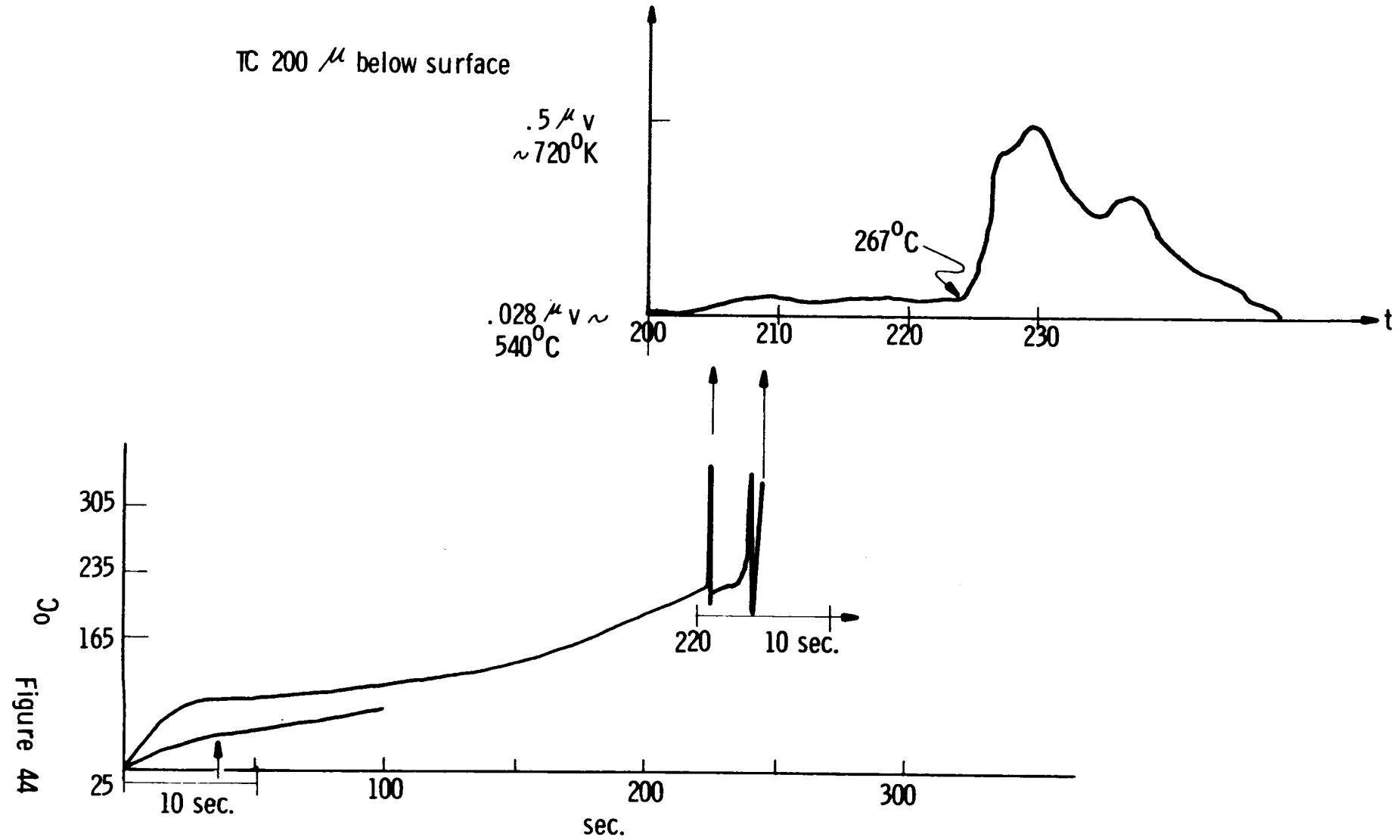

Figure 44

DTA OF EXTINGUISHED PROPELLANTS TAKEN FROM VARIOUS GRAIN DEPTHS
$\beta = 8^{o}$/min.

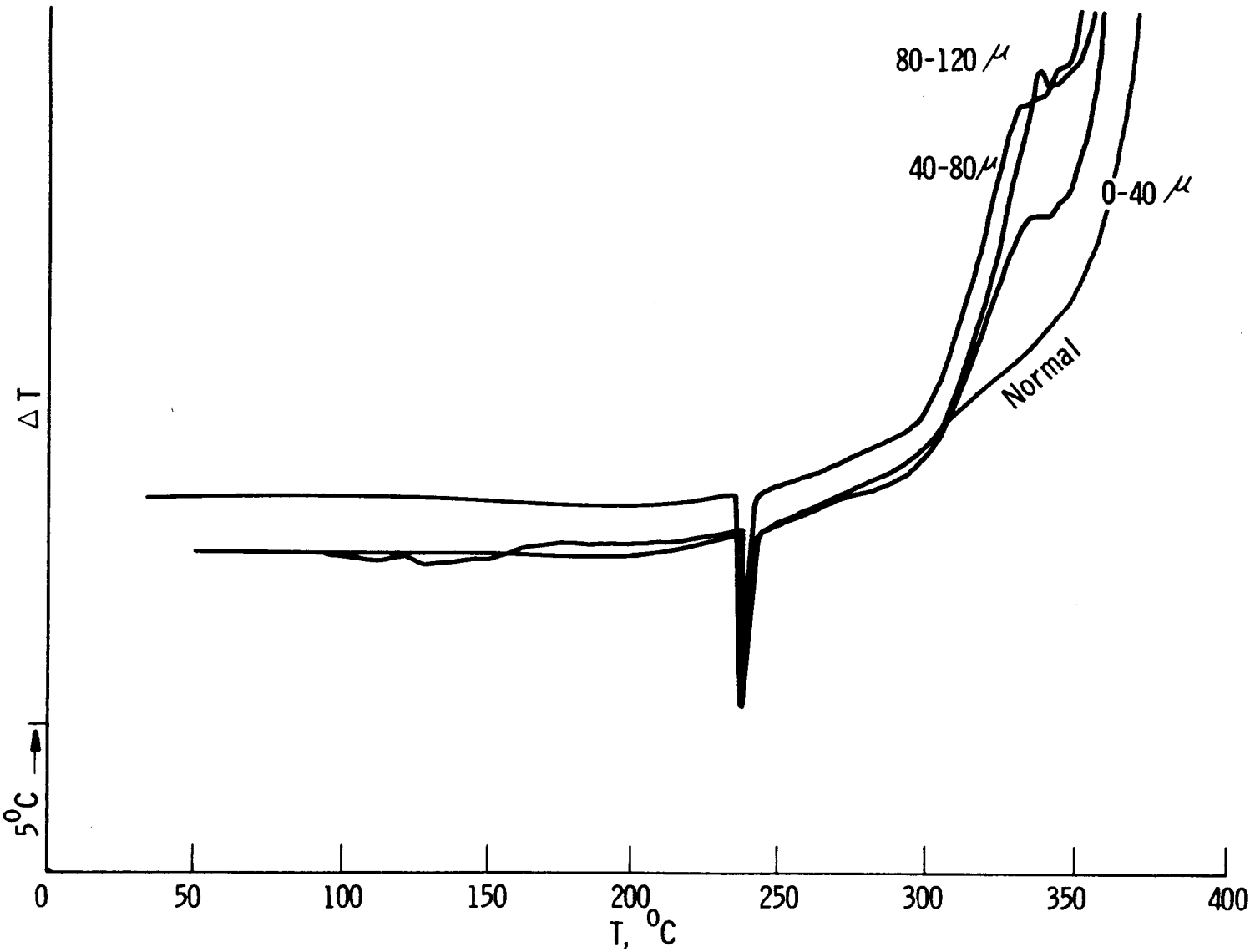

Figure 45

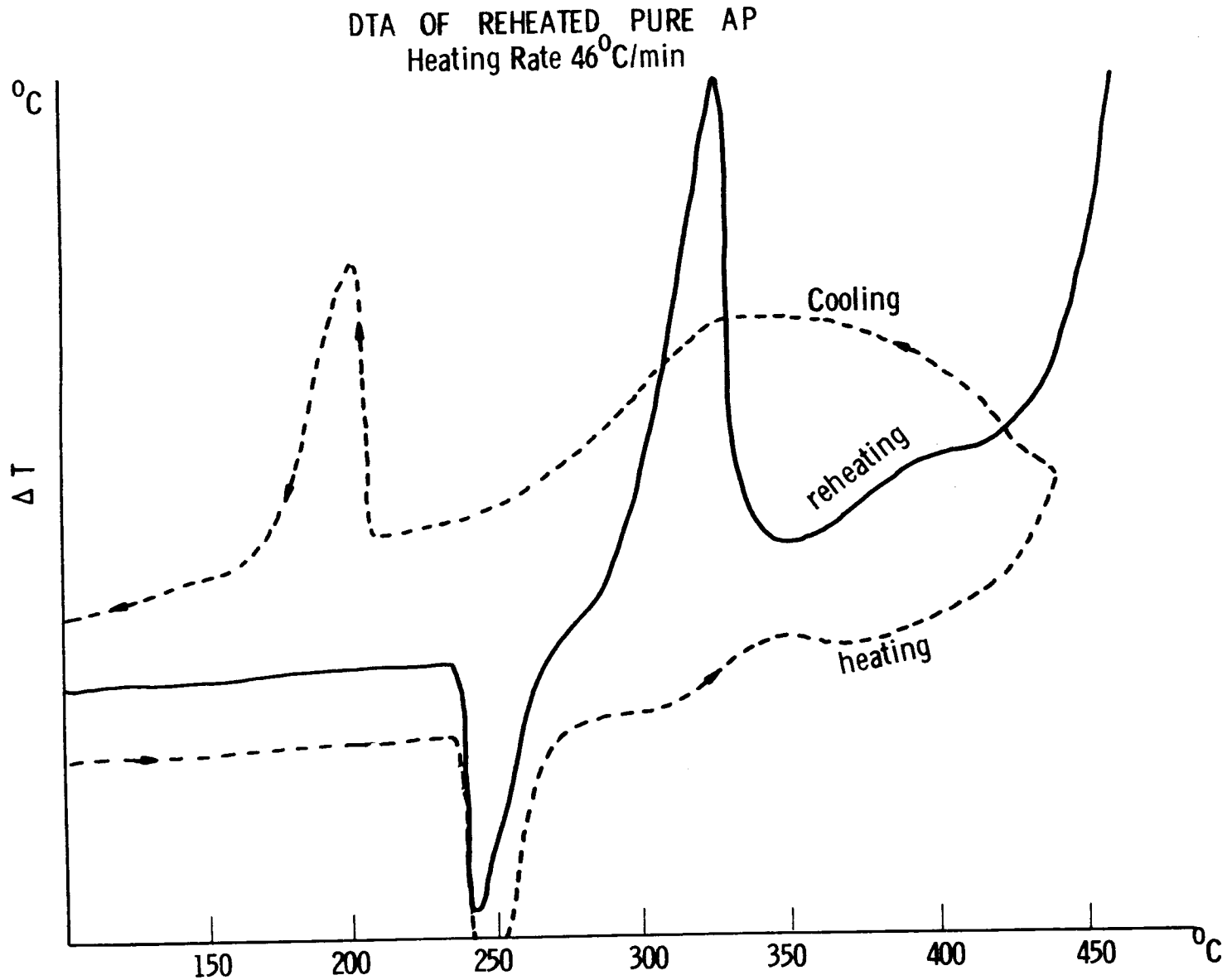
DTA OF REHEATED PURE AP
Heating Rate 46°C/min
°C
ΔT
Cooling
reheating
heating
150
200
250
300
350
400
450
°C

Figure 46

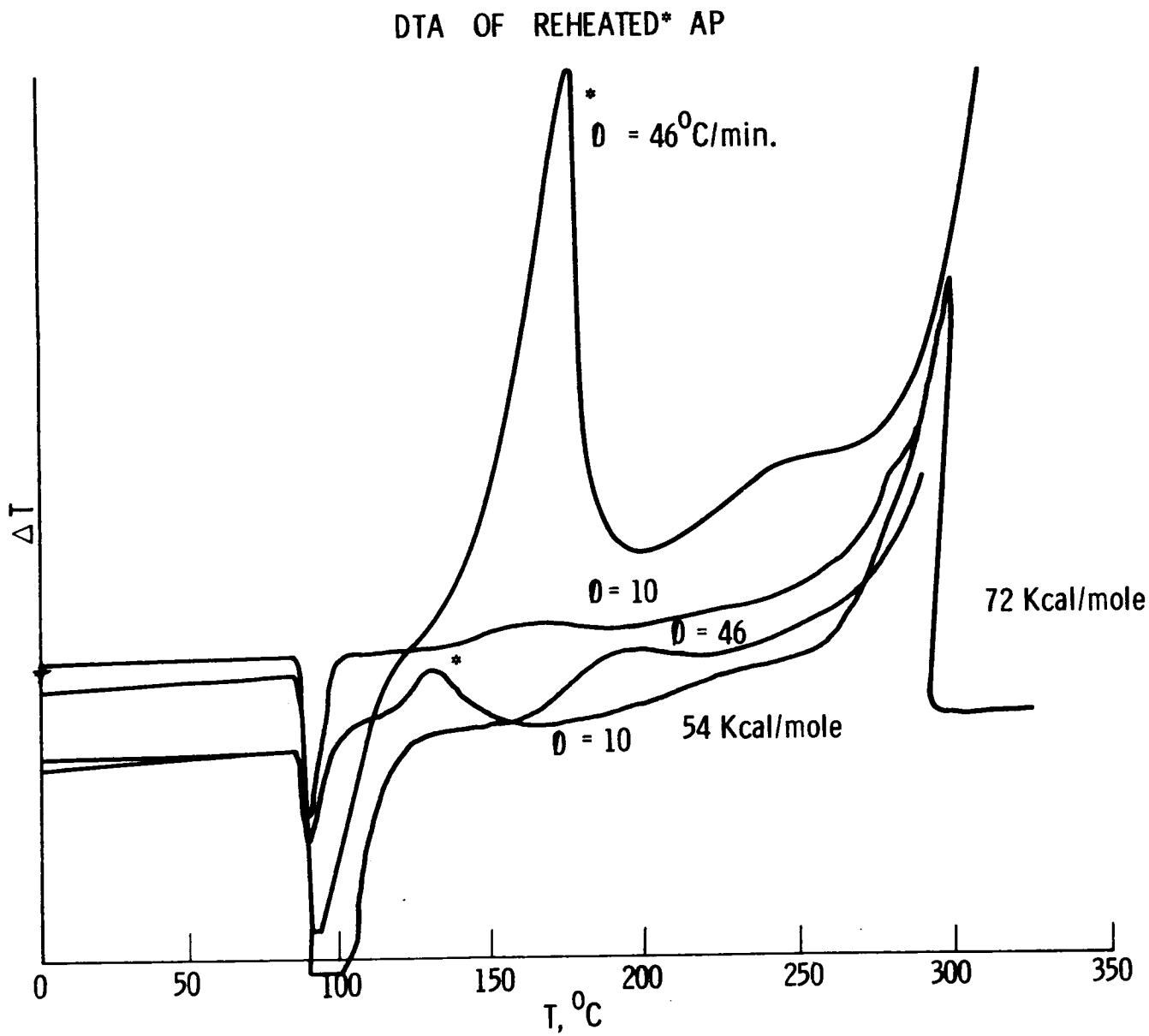
DTA OF REHEATED* AP
*
Ø = 46°C/min.
ΔT
Ø = 10
Ø = 46
72 Kcal/mole
*
Ø = 10
54 Kcal/mole
0
50
100
150
200
250
300
350
T, °C

Figure 46a

DTA PATTERN OF REHEATED PBD PROPELLANT

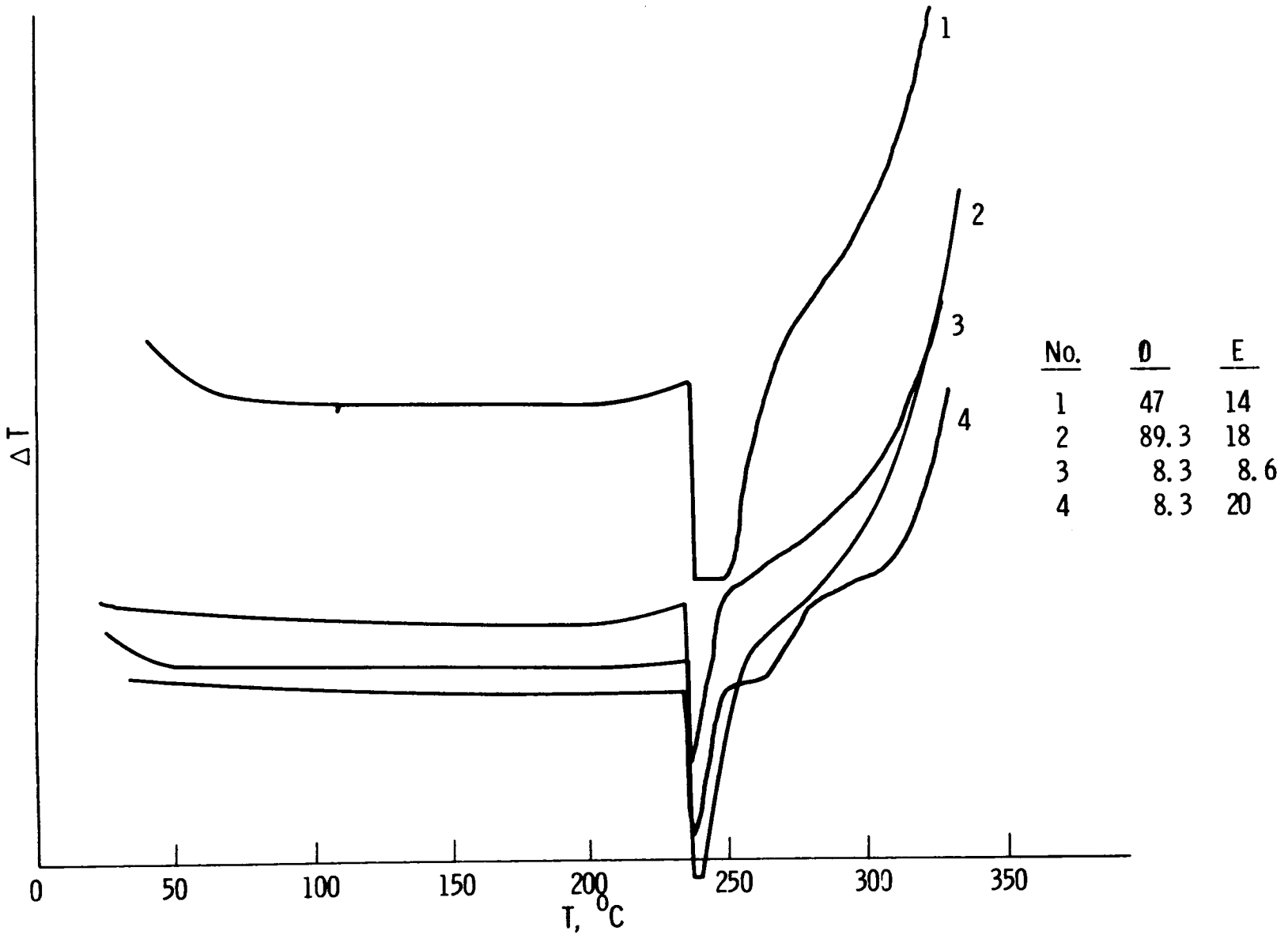

No.	D	E
1	47	14
2	89.3	18
3	8.3	8.6
4	8.3	20

Figure 46b

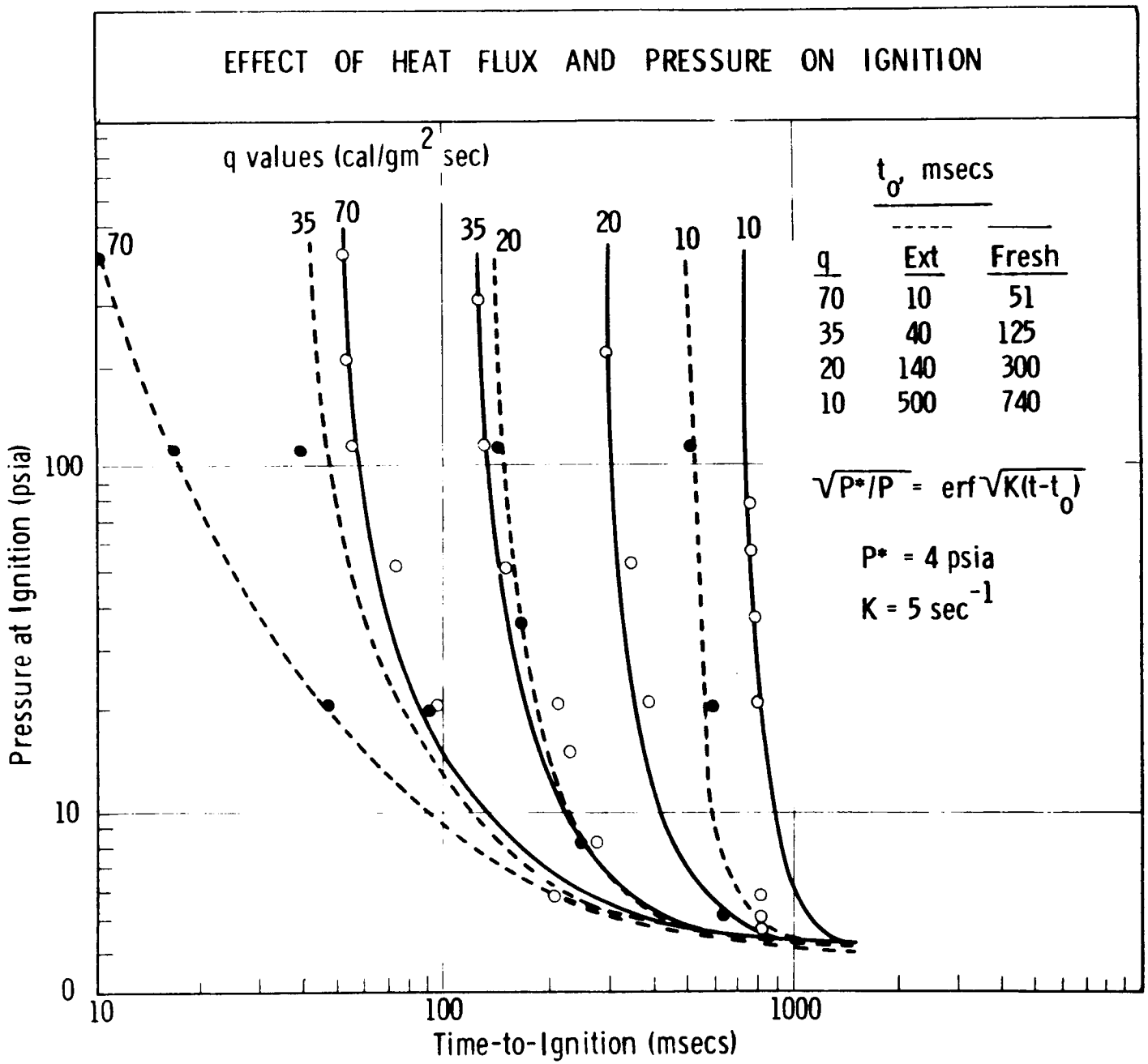
EFFECT OF HEAT FLUX AND PRESSURE ON IGNITION
q values (cal/gm^2 sec)
70
35
70
35
20
20
10
10
t_o, msecs
q | Ext | Fresh
70 | 10 | 51
35 | 40 | 125
20 | 140 | 300
10 | 500 | 740
$\sqrt{P^*/P} = \text{erf}\sqrt{K(t-t_o)}$
P* = 4 psia
K = 5 sec^{-1}
Pressure at Ignition (psia)
100
10
0
10
100
1000
Time-to-Ignition (msecs)

Figure 47

DTA OF PBD PROPELLANT
Heating Rate 1.65°/min.

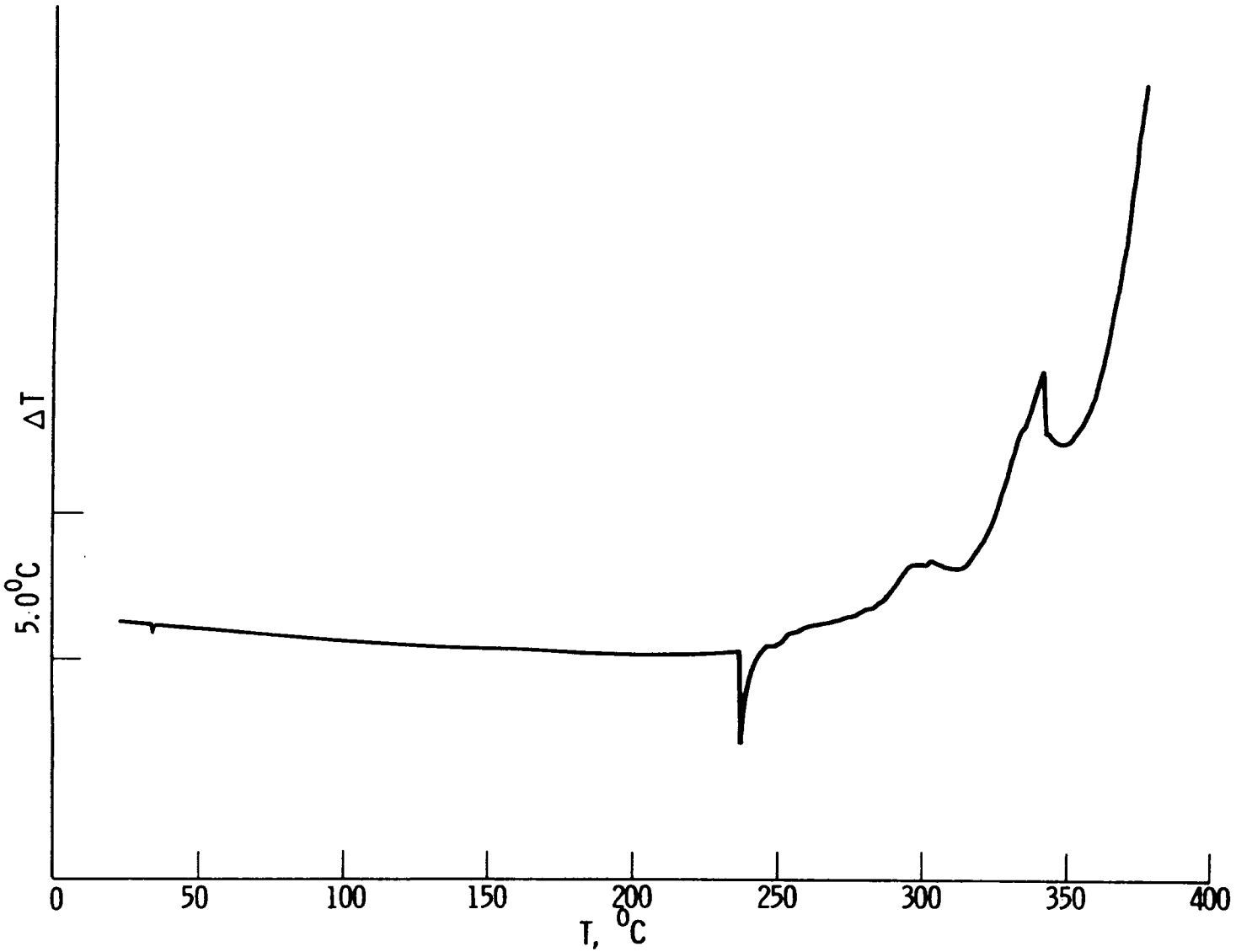

Figure 48

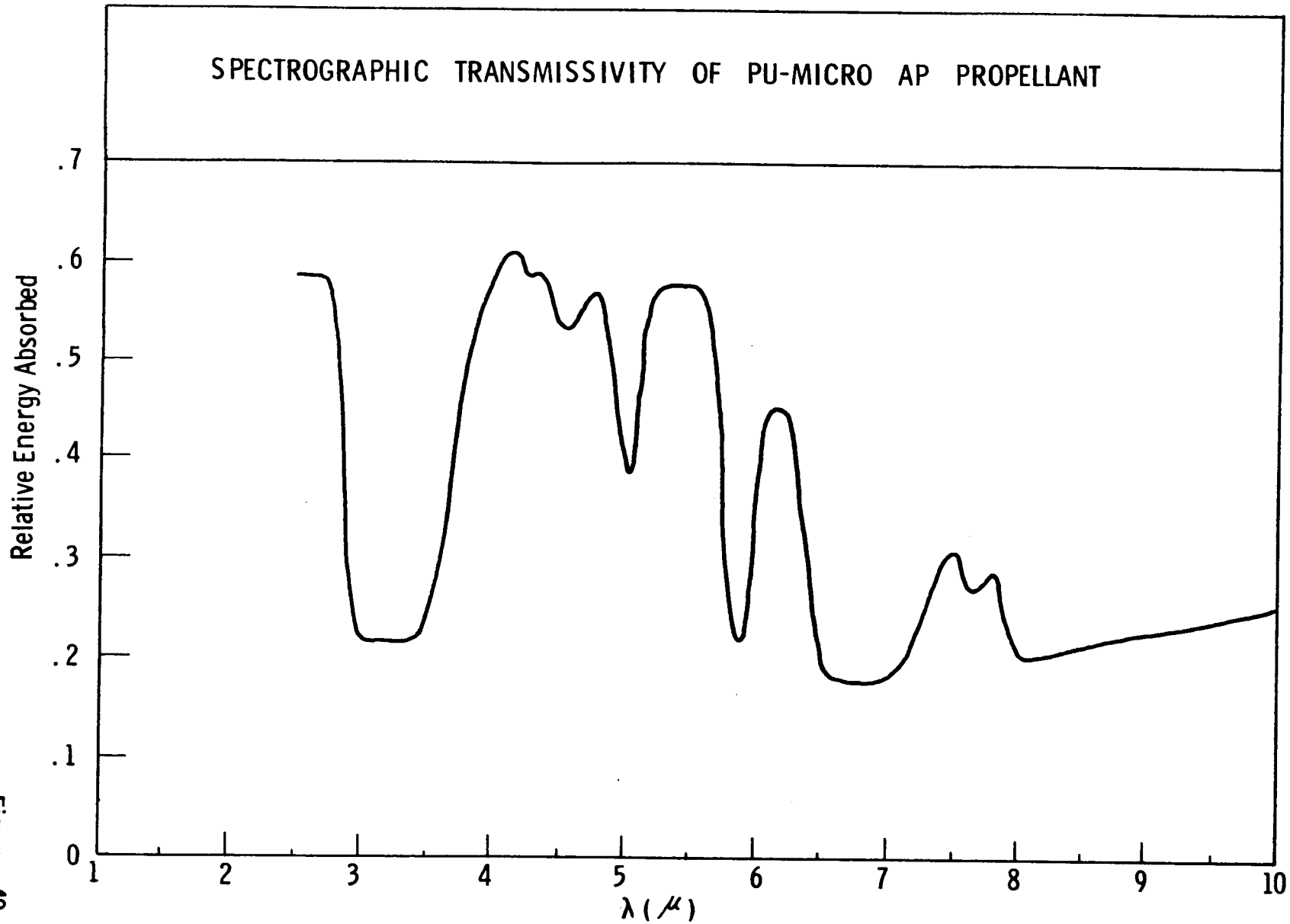
SPECTROGRAPHIC TRANSMISSIVITY OF PU-MICRO AP PROPELLANT
Relative Energy Absorbed
.7
.6
.5
.4
.3
.2
.1
0
1
2
3
4
5
6
7
8
9
10
λ (μ)

Figure 49